DISSERTATION

METALLOCENE-CATALYZED POLYMERIZATION OF FUNCTIONALIZED ALKENES WITHIN SILICATE NANOGALLERIES AND IN SOLUTION

Submitted by

Wesley R. Mariott

Department of Chemistry

In partial fulfillment of the requirements

For the Degree of Doctor of Philosophy

Colorado State University

Fort Collins, Colorado

Spring 2007

COLORADO STATE UNIVERSITY

December 12, 2006

WE HEREBY RECOMMEND THAT THE DISSERTATION PREPARED UNDER OUR SUPERVISION BY **WESLEY R. MARIOTT** ENTITLED **METALLOCENE-CATALYZED POLYMERIZATION OF FUNCTIONALIZED ALKENES WITHIN SILICATE NANOGALLERIES AND IN SOLUTION** BE ACCEPTED AS FULFILLING IN PART REQUIREMENTS FOR THE DEGREE OF DOCTOR OF PHILOSOPHY

Committee on Graduate Work

Peter K. Dorhout

Oren P. Anderson

C. Michael Elliott

Laurence A. Belfiore

Eugene Y.-X. Chen / Advisor

Anthony K. Rappé / Department Head/Director

ABSTRACT OF DISSERTATION

METALLOCENE-CATALYZED POLYMERIZATION OF FUNCTIONALIZED ALKENES WITHIN SILICATE NANOGALLERIES AND IN SOLUTION

The research presented herein studies the polymerization of functionalized alkenes such as (meth)acrylates and acrylamides catalyzed by early transition metallocenium complexes within layered silicate nanogalleries and in solution. Key findings of this study include: (a) the first *in situ* production of exfoliated silicate nanocomposites consisting of stereochemically controlled poly(methyl methacrylate) [P(MMA)] matrices using intergallery anchored metallocenium cations, (b) development of the novel, highly isospecific and living polymerization of acrylamides catalyzed by metallocenium enolate complexes, (c) identification of the chain transfer and termination processes occurring in the polymerization of acrylates by metallocene complexes that prevent the formation of high molecular weight polymer, and (d) the isolation and structural characterization of three new cationic and zwitterionic tantalocene complexes that are relevant to the polymerization of MMA and *N,N*-dimethylacrylamide (DMAA) by group(V) tantalocenes.

The broad focus of this dissertation concerns the mechanisms of the polymerization of polar vinyl monomers by highly reactive, electrodeficient, cationic metallocene complexes. In return, this dissertation work has also provided several advanced and potentially useful polymeric materials: exfoliated silicate/stereoregular P(MMA)

nanocomposites, stereo-defect free and high melting transition temperture isotactic P(DMAA), as well as the amphiphilic stereodiblock copolymer P(MMA)-*b*-P(DMAA).

Wesley R. Mariott
Chemistry Department
Colorado State University
Fort Collins, CO 80523
Spring 2007

TABLE OF CONTENTS

CHAPTER I

INTRODUCTION

This dissertation is written in a "journals-format" style that the Graduate School at Colorado State University allows and is based on five separate peer-reviewed publications appearing in American Chemical Society journals, including *Journal of the American Chemical Society*, *Macromolecules* and *Organometallics*. A level of consistency is achieved herein by (a) this introduction, (b) the use of bridging paragraphs at the beginning of each chapter, and (c) a final summary chapter. The general theme of this dissertation involves investigations into the metallocene catalyzed polymerization of functionalized alkenes, such as (meth)acrylates and acrylamides, within silicate nanogalleries and in solution, with a focus on the mechanistic details of these polymerization systems. A concise overview of each chapter's contents is presented below.

Chapter II examines the *in situ* stereospecific polymerization of methyl methacrylate (MMA) within silicate nanogalleries using both intergallery-anchored metallocenium cations as well as organo-Lewis acid intergallery-anchored silicate activators in combination with metallocene dimethyls of varied symmetries. Evidence supporting the formation of exfoliated poly(methyl methacrylate) [P(MMA)]-silicate

nanocomposites consisting of stereocontrolled P(MMA) matrices is presented.

Chapter III examines the living, isospecific polymerization of acrylamides, including *N*,*N*-dimethylacrylamide (DMAA), *N*,*N*-dimethylmethacrylamide (DMMA), and *N*-isopropylacrylamide (IPAA) using chiral *ansa*-zirconocenium ester and amide enolates. Mechanistic details of this polymerization system were elucidated via investigations into polymerization kinetics, polymer microstructure and chain-end groups, and block copolymerization behavior as well as modeling and isolation of the active propagating species.

Chapter IV studies the polymerization of *n*-butyl acrylate (*n*-BA) by the chiral *ansa*-zirconocenium ester enolate. This polymerization proceeds in an uncontrolled fashion to only moderate monomer conversions, producing poly(*n*-BA) with three types of chain structures—one major linear and two minor cyclic β-ketoester-terminated poly(*n*-BA) chains resultant from chain termination and transfer reactions. Mechanistic insight into the chain termination and transfer reactions in the acrylate polymerization were achieved through the combined polymerization, chain structure, and model reaction studies presented in this chapter.

Chapter V investigates the activation of tantalocene(V) alkyl and alkylidene complexes with strong organo-Lewis acids as well as their application to the polymerization of functionalized alkenes. This work reexamines the reaction of tantalocene trialkyls with strong organo-Lewis acids, investigates the activation of Schrock's alkylidene complex and employs the alkylidene complex for the polymerization of MMA and DMAA. This work also solves the structures of three new cationic and zwitterionic tantalocene complexes derived from this study.

Chapter VI is a brief summary of the material presented.

To keep a high level of consistency and focus, although the bulk of the 4½ years of work is included in this dissertation, the published work from several other projects that somewhat deviate from the main theme of this dissertation topic are not described here. For the convenience of the reader, Appendix A lists all publications during the dissertation work.

CHAPTER II

IN SITU POLYMERIZED, STEREOCONTROLLED P(MMA)–LAYERED SILICATE NANOCOMPOSITES

This dissertation chapter contains the manuscript of a communication published in the *Journal of the American Chemical Society* [Mariott, W. R.; Chen E. Y.-X. *J. Am. Chem. Soc.* **2003**, *125*, 15726–15727] as well as the subsequent studies for a full paper in preparation, describing the synthesis of *in situ* polymerized poly(methyl methacrylate) [P(MMA)]-silicate nanocomposites with stereocontrolled polymer matrices. Overall, it was found that the use of intergallery-anchored metallocenium cations allows for the synthesis of exfoliated P(MMA)-silicate nanocomposites, while the use of intergallery-anchored Lewis acid activators in combination with metallocene dimethyls produces intercalated P(MMA)-silicate nanocomposites. Significantly, we demonstrated the ability of these systems to modulate the tacticity of the resultant P(MMA) matrices on the basis of the catalyst structure, providing the first reported example of stereocontrolled P(MMA)-silicate nanocomposites. Access to such stereocontrolled P(MMA)-silicate nanocomposites led to investigations into the generation of P(MMA)-silicate nanocomposites with matrices of higher order, namely supramolecular stereocomplex P(MMA)-silicate nanocomposites.

Abstract

The synthesis of *in situ* polymerized silicate nanocomposites consisting of stereochemically controlled polymer matrixes has been explored. The protonolysis reaction of metallocene dimethyls of various symmetries and an organically modified layered silicate $Me(HT)_2NH^+$/MMT, a montmorillonite (MMT) clay with methyl bishydrogenated tallow alkyl ammonium as the intergallery cation, cleanly produces the intergallery-anchored metallocenium catalysts. Methyl methacrylate (MMA) polymerizations by these catalysts yield atactic (*at*-) poly(methyl methacrylate) [P(MMA)]-silicate nanocomposites ([*mr*] = 39.8%), isotactic (*it*-) P(MMA)–silicate nanocomposites ([*mm*] = 93.0%), and syndiotactic (*st*-) P(MMA)–silicate nanocomposites ([*rr*] = 72.0%) with exfoliated silicate morphologies. An alternative approach using alane-intercalated clay activators in combination with metallocene dimethyls of C_2 and C_S symmetry produces *it*-P(MMA)–silicate nanocomposites ([*mm*] = 96.3%) and *st*-P(MMA)–silicate nanocomposites ([*rr*] = 75.4%) nanocomposites, respectively, with intercalated silicate morphologies. Additionally, the stereocomplexation behavior of 2/1 blends of *st*-P(MMA)–silicate nanocomposites with *it*-P(MMA)–silicate nanocomposites has also been explored. Stereocomplexation via dilute solution crystallization allowed for novel stereocomplex P(MMA)–silicate nanocomposites with melting transition temperatures as high as 210 °C.

Introduction

While conventionally filled macro- and microcomposite polymers are commonplace in the industrial production of a large variety of plastics, a new emerging

class of polymer composites is making large strides in property enhancements (e.g. tensile modulus, strength, heat distortion temperatures, etc.) over conventionally filled polymers. These new classes of polymer composites such as polymer-layered silicate nanocomposites are defined by the nanoscale dispersion of the inorganic filler in a continuous polymer matrix. They have gained increased attention in both industry and academics due to their potentials for enhanced materials properties with only a few weight percent dispersion of the inorganic filler on the nanometer scale.[1]

Polymer-layered silicate nanocomposites made their debut to the scientific community in 1990 when a team of scientists at the Toyota Central Research and Development Laboratories announced the discovery of nylon 6-clay hybrid nanocomposites.[2] The nylon 6-clay hybrid nanocomposites showed a doubling in tensile modulus and strength without sacrificing impact resistance, as well as an increase in the heat distortion temperature by up to 100 °C with as little as 2 wt% inorganic filler. Since this discovery, a number of combinations of polymer matrixes with a variety of inorganic fillers have been researched.[1]

Some of the most prevalent layered inorganic fillers, as in the case of the nylon 6-clay hybrid, belong to a family of phyllosilicates (2:1 layered silicates) that consist of edge-shared octahedral sheets of alumina fused between two tetrahedral sheets of silica. On average, these individual layers maintain an overall negative charge as a result of isomorphic substitution within them. This results in a layered morphology with the intergallery spaces being occupied by alkali or alkali earth cations to counterbalance the charge. The individual layers have lateral dimensions that can range from 30 nanometers (nm) to several microns and a thickness of about 1 nm depending on the particular

layered silicate. Of interest to this study is the 2:1 layered silicate montmorillonite (MMT) with a general formula of $M_x(Al_{4-x}Mg_x)Si_8O_{20}(OH)_4$, where M is a monovalent cation and x is the degree of isomorphic substitution.

There are three main types of morphologies that can be accessed upon formation of polymer-layered silicate composites. The first of these can be described as a phase-separated composite in which the polymer matrix and the inorganic filler are immiscible, resulting in a conventionally filled composite. Of more importance are the two morphologies corresponding to the dispersion of the inorganic layered silicates within a continuous polymer matrix, resulting in either intercalated or exfoliated morphologies. Intercalated morphologies can be characterized by the maintained order of the layered silicates, while having single (or sometimes more) polymer chains intercalated into the gallery spaces, resulting in an increased basal spacing of the layered silicate. On the other hand, exfoliated silicate nanocomposites are a result of the homogeneous dispersion of silicate nanoplatelets in a continuous polymer matrix.

As an important member of such advanced materials, poly(methyl methacrylate) [P(MMA)]–silicate nanocomposites exhibit enhanced thermal stability and flame retardancy, increased storage modulus and T_g, and improved toughness and barrier properties.[3] However, the P(MMA) matrices present in the previous nanocomposites were essentially atactic and produced from various radical polymerization processes.[3] The physical and mechanical properties of a polymer having stereocenters in the repeating unit depend largely on its stereochemistry; stereoregular polymers typically have superior materials properties such as solvent resistance, modulus, impact strength, and fatigue resistance to their amorphous counterparts. Therefore, the study of

structure–property relationships of the nanocomposite using stereochemically controlled P(MMA) is of fundamental interest.

Although the stereospecific polymerization of MMA with group 4 metallocenes has been well documented,[4] the synthesis of P(MMA)–silicate nanocomposites using these catalysts remains unexplored. If such stereospecific metal complexes in their active form can be effectively anchored in the silicate galleries, subsequent polymerization should lead to P(MMA) with the desired stereo-microstructures. However, the challenge in catalyst intercalation lies in the incompatibility between these often highly sensitive metal catalysts and unprotected layered silicate galleries that often contain protic impurities and polar functionalities. Nevertheless, Cp_2ZrMe^+ was reported to directly ion-exchange into the galleries of the synthetic silicates after the internal surfaces were protected with methylalumoxane.[5] The more tolerant late metal (Pd)-based olefin polymerization catalyst was intercalated in the unprotected fluorohectorite galleries.[6] We communicate here the synthesis and characterization of intergallery-anchored metallocenium cations via a non cation-exchange approach involving protonolysis of the metallocene dimethyl with $Me(HT)_2NH^+$/MMT, a montmorillonite (MMT) clay modified by methyl bis(hydrogenated tallow alkyl) ammonium. These intercalated metallocene catalysts allow for the first synthesis of *in situ* polymerized nanocomposites comprising delaminated silicate nano-platelets dispersed in the atactic, isotactic, or syndiotactic P(MMA) matrices.

Experimental

Materials and Methods. All syntheses and manipulations of air- and moisture-

sensitive materials were carried out in flamed Schlenk-type glassware on a dual-manifold Schlenk line, a high-vacuum line (10^{-5} to 10^{-7} Torr), or in an argon-filled glovebox (<1.0 ppm oxygen and moisture). NMR-scale reactions (typically in a 0.02 mmol scale) were conducted in Teflon-valve-sealed J. Young-type NMR tubes. HPLC grade organic solvents were sparged with nitrogen during filling of the solvent reservoir and then dried by passage through activated alumina (for THF, and CH_2Cl_2) followed by passage through Q-5-supported copper catalyst (for toluene and hexanes) stainless steel columns. Toluene used for polymerizations was further dried over sodium/potassium alloy and filtered before use. Benzene-d_6 and toluene-d_8 were dried over sodium/potassium alloy and vacuum-distilled or filtered, whereas C_6D_5Br, $CDCl_3$, CD_2Cl_2, and *o*-dichlorobenzene were dried over activated Davison 4-Å molecular sieves. NMR spectra were recorded on either a Varian Inova 300 (FT 300 MHz, ^1H; 75 MHz, ^{13}C; 282 MHz, ^{19}F) or a Varian Inova 400 spectrometer. Chemical shifts for ^1H and ^{13}C spectra were referenced to internal solvent resonances and are reported as parts per million relative to tetramethylsilane, whereas ^{19}F NMR spectra were referenced to external $CFCl_3$. Elemental analyses were performed by Desert Analytics, Tucson, AZ.

The MMT clays Closite® 93A and 30B were purchased from Southern Clay Products, Inc., Gonzales, TX. Closite® 93A, with a cation exchange capacity (CEC) of 90meq/100 g, is an organically modified montmorillonite with methyl bishydrogenated tallow alkyl ammonium [$Me(HT)_2NH^+$/MMT, where the hydrogenated tallow consists of approximately 65% C_{18}, 30% C_{16}, and 5% C_{14}] as the intergallery cation. Closite® 30B, with a CEC of 90 meq/100 g, is an organically modified MMT with methyl bis(2-hydroxyethyl) tallow alkyl ammonium [$Me(T)N(C_2H_4OH)_2^+$/MMT, where the tallow

consists of approximately 65% C_{18}, 30% C_{16}, and 5% C_{14}] as the intergallery cation. The organically modified MMT clays were further dried at 60 °C under high vacuum (10^{-6}–10^{-7} Torr) for 8 h.

Methyl methacrylate (MMA) was purchased from Aldrich Chemical Co.; the monomer was first degassed and dried over CaH_2 overnight, followed by vacuum distillation; final purification of MMA involved titration with neat tri(*n*-octyl)aluminum to a yellow end point[7] followed by distillation under reduced pressure. The purified monomer was stored in a brown bottle in a –30 °C freezer inside the glovebox.

Tris(pentafluorophenyl)borane, $B(C_6F_5)_3$, was obtained as a research gift from Boulder Scientific Co. and further purified by recrystallization from hexanes at –35 °C. Tris(pentafluorophenyl)alane $Al(C_6F_5)_3$, as a 0.5 toluene adduct $Al(C_6F_5)_3 \cdot (C_7H_8)_{0.5}$ based on elemental analysis of the vacuum-dried sample, was prepared by the ligand exchange reaction of $B(C_6F_5)_3$ and $AlMe_3$ in a 1:3 toluene/hexanes solvent mixture in quantitative yield;[8] this is the modified synthesis based on literature procedures.[9] *Extra caution should be exercised when handling this material, especially the unsolvated form, because of its thermal and shock sensitivity.* Literature procedures were employed for the preparation of the following compounds and metallocene complexes: Cp_2ZrMe_2 (Cp = η^5-C_5H_5),[10] (EBI)H_2 [EBI = $C_2H_4(Ind)_2$],[11] *rac*-(EBI)$ZrMe_2$,[12] and CGC$TiMe_2$ (CGC = $Me_2Si(Me_4C_5)$(*t*-BuN)).[13]

Synthesis of Intergallery-Anchored Metallocenium Catalysts. To a stirred suspension of Closite® 93A (0.500 g, CEC = 90 meq/100 g) in 10 mL of toluene at ambient temperature was added Cp_2ZrMe_2 (0.126 g, 0.50 mmol) in 11% stoichiometric excess. The reaction mixture was allowed to stir at ambient temperature overnight. The

solid was filtered off, washed with 3 × 5 mL of toluene followed by 5 mL of hexanes (to remove any residual Cp_2ZrMe_2), and dried *in vacuo* to afford Cp_2ZrMe^+/MMT (**A**) in quantitative yield. *rac*-(EBI)$ZrMe^+$/MMT (**B**) and CGCTiMe^+/MMT (**C**), both obtained in quantitative yields, were synthesized in the same manners as for the preparation of **A**.

After removing the volatiles, the filtrate residue from the reaction of Closite® 93A and *rac*-(EBI)$ZrMe_2$ consisted of the discharged neutral amine ($Me(HT)_2N$) and the recovered excess *rac*-(EBI)$ZrMe_2$ in a 9:1 ratio by ^1H NMR spectroscopy. This ratio and the 10% of the recovered metallocene dimethyl strongly suggest the protonolysis reaction followed by the neutral amine discharge was quantitative (this was further confirmed by the XPS analysis of the intercalated catalysts) and that decomposition or side reactions (e.g., surface absorption) involving the metallocene dimethyl was negligible.

Synthesis of Alane-Intercalated Clay Activator. To a stirred suspension of the dried Closite® 30B (0.500 g) in 10 mL of toluene was added $Al(C_6F_5)_3$•0.5 toluene (0.287 g, 0.50 mmol) at ambient temperature. The reaction mixture was allowed to stir at this temperature for 10 h. The solid was filtered off, washed with 3 × 5 mL of toluene followed by 5 mL of hexanes (to remove any residual $Al(C_6F_5)_3$ and the co-product C_6F_5H), and dried under vacuum to produce the alane-intercalated clay $Me(T)N[C_2H_4OAl(C_6F_5)_2]_2^+$/MMT (**D**) in quantitative yield. After removing the volatiles of the filtrate, the small amount of residue showed the presence of only C_6F_5H by ^{19}F NMR.

Synthesis of TMA-Pretreated Alane-Intercalated Clay Activator. To a stirred suspension of the dried Closite® 30B (0.500 g) in 10 mL of toluene at ambient temperature was added TMA (1.00 mmol). The reaction mixture was allowed to stir at

this temperature for 10 h. The solid was filtered off, washed with 3 × 5 mL of toluene followed by 5 mL of hexanes, and dried under vacuum. To this TMA-treated clay was added $B(C_6F_5)_3$ (0.256 g, 0.50 mmol) and 10 mL toluene. The reaction mixture was allowed to stir at ambient temperature for 10 h. Using the same work-up procedure as the first step of this reaction, the alane-intercalated clay $Me(T)N[C_2H_4OalMe(C_6F_5)]_2^+$/MMT (**E**) was isolated in quantitative yield. After removing the volatiles of the filtrate, the ^{19}F NMR of the residue showed the presence of excess $B(C_6F_5)_3$ as the major species, plus traces of $MeB(C_6F_5)_2$ and $Me_2B(C_6F_5)$.

Polymerization of MMA using Intergallery-Anchored Metallocenium Catalysts. All polymerizations were carried out in an argon-filled glovebox (< 1.0 ppm oxygen and moisture). In a typical procedure 50 mg of the intergallery-anchored metallocenium cation was suspended in 5 mL of toluene. MMA (1.0 mL, 9.35 mmol) was added to the suspension and the reaction mixture was allowed to stir for the desired time period. The products were precipitated into 100 mL of methanol, stirred for 30 min, filtered, washed with methanol, and dried in a vacuum oven at 50 °C overnight to a constant weight. The P(MMA)–silicate nanocomposites are white powdery materials.

Polymerization of MMA using Alane-Intercalated Clay Activators. Polymerizations were carried out in an argon-filled glovebox at ambient temperature. In a typical procedure, 50 mg of the alane-intercalated clay activator was suspended in 3 mL of toluene. MMA (1.0 mL, 9.35 mmol) was added to the suspension, and the mixture was allowed to stir for 30 min before a solution of a metallocene dimethy initiator (23.4 μmol) in 2 mL of toluene was quickly added. After the reaction mixture was stirred for 24 h, the products were precipitated into 100 mL of methanol, stirred for 30 min, filtered, washed

with methanol, and dried in a vacuum oven at 50 °C overnight to a constant weight. The P(MMA)–silicate nanocomposites obtained are white powdery materials.

In efforts to eliminate any side reactions or polymerization caused by catalyst leeching, an alternate procedure was used to isolate the active intercalated species for the polymerization of MMA. This procedure involved suspending 50 mg of the alane-intercalated clay initiator in a 5 mL toluene solution containing the metallocene dimethyl initiator (23.4 μmol) and allowing them to stir for a period of 2 hrs before the solid was filtered off, washed with 3 × 5 mL of toluene followed by 5 mL of hexanes, and dried under vacuum. The solid was then suspended in 5 mL of toluene and MMA (1.0 mL, 9.35 mmol) was added to the stirred suspension. After the desired time interval, the polymerization products were precipitated into 100 mL of methanol, stirred for 30 min, filtered, washed with methanol, and dried in a vacuum oven at 50 °C overnight to a constant weight.

Supramolecular Stereocomplex P(MMA)–Silicate Nanocomposite Synthesis. The solution crystallization stereocomplex synthesis involved preparing separate 1 wt% solutions of the *st*-P(MMA)–silicate nanocomposite (prepared by **C**) and *it*-P(MMA)–silicate nanocomposite (prepared by **B**) in THF (complexing solvent). The homogeneous solutions were combined in a 2/1 ratio of *st*-/*it*- and allowed to stand undisturbed for one week after initial mixing of the solutions. The solution was precipitated into excess methanol, stirred for 30 min, filtered, washed with methanol, and dried in a vacuum oven at 50 °C overnight. The resulting polymer was then suspended in THF and the uncomplexed polymer was extracted from the sample before it was dried in a vacuum oven at 50 °C overnight to a constant weight.

Materials Characterization. Powder X-ray diffraction (XRD) analyses were performed on powder samples with a Scintag X2 Advanced Diffraction System using Cu Kα (λ = 1.5418 Å) radiation and a Peltier detector on the diffracted beam side. Measurements were performed using a step size of 0.02° with 2.0 seconds per step. Peak fittings were done with the Split-Pearson VII function using DMNST version 1.37 software.[14]

X-ray photoelectron spectroscopy (XPS) analyses was performed on a 2000 Physical Electron 5800 ultra-high vacuum XPS-Auger spectrometer using a monochromatic Al Kα x-ray source (hν = 1486.6 eV), a hemispherical analyzer, and a multi-channel detector. A low energy (30 eV) electron gun was used for charge neutralization on the non-conducting samples. The binding energy scales for the samples were referenced to the C 1*s* peak at 284.8 eV.[15] High resolution Ti 2*p*, Zr 3*d*, Al 2*p*, F 1*s*, and C 1*s* spectra were acquired at an analyzer pass energy of 23.5 eV with a 0.1 eV step size and an x-ray spot size of 800 μm. All XPS analyses were performed at a photoelectron takeoff angle of 45°. A Gaussian/Lorentzian function was used to fit all peaks and the fitting was performed until a minimum for the χ^2 value was achieved.

Specimen preparations for transmission electron microscopy (TEM) analyses of the P(MMA)–silicate nanocomposites involved embedding the powdery polymer samples in a low viscosity "Spurr" epoxy resin (Electron Microscopy Sciences) and allowing them to cure at 70 °C for 16 h. The epoxy block was then trimmed to form a block face of approximately 0.5 mm × 0.5 mm for microtoming. Ultrathin sections (70-100 nm) were cut at room temperature using a Reichert Ultracut E ultramicrotome equipped with either a glass or a diamond knife. The ultrathin sections were floated onto water after cutting.

The sections were then collected on uncoated copper TEM grids (hexagonal 200 mesh) and fully dried on filter papers at room temperature. Transmission electron micrographs were obtained using a JEOL JEM-2000EXII transmission electron microscope operating at an accelerating voltage of 100 kV.

Glass transition (T_g) temperatures of the polymer samples were measured by differential scanning calorimetry (DSC) on a DSC 2920 (TA Instruments). The P(MMA)–silicate nanocomposite samples were first heated to 180 °C at 20 °C/min, equilibrated at this temperature for 4 min, and then cooled to -25 °C at 20 °C/min. After being held at this temperature for 4 min, the samples were reheated to 180 °C at 10 °C/min. All T_g values were obtained from the second scan, after removing the thermal history. Maximum rate decomposition temperatures (T_{max}) and decomposition onset temperatures (T_{onset}) were measured by thermogravimetric analysis (TGA) on a TGA 2950 (TA Instruments). P(MMA)–silicate nanocomposite samples were heated from ambient temperature to 550 °C at a rate of 10 °C/min. Values for T_{max} were obtained from derivative (wt%/°C) *versus* temperature (°C) plots while T_{onset} values (initial and end temperatures) were obtained from wt% *versus* temperature (°C) plots.

Gel permeation chromatography (GPC) analyses of the extracted polymers (Soxhlet extraction with the BHT-stabilized THF for 24 h) from P(MMA)–silicate nanocomposite samples was carried out at 40 °C and a flow rate of 1.0 mL/min, with THF as the eluent, on a Waters University 1500 GPC instrument that was calibrated using 10 P(MMA) standards. Chromatograms were processed with Waters Empower software (2002); number-average molecular weight and polydispersity of polymers are given relative to

PMMA standards. ^{1}H NMR spectra for the analysis of P(MMA) microstructures were recorded in $CDCl_3$ and analyzed according to literature procedures.[16]

Results and Discussion

Synthesis and Characterization of Intergallery-Anchored Metallocenium Catalysts. The reactions of the pre-dried $Me(HT)_2NH^+$/MMT with C_{2v}-symmetric Cp_2ZrMe_2, C_2-symmetric *rac*-(EBI)$ZrMe_2$ (EBI = $Et(Ind)_2$), and C_s-symmetric $CGCTiMe_2$ (CGC = $Me_2Si(Me_4C_5)(t\text{-BuN})$) proceed quantitatively to generate the intercalated metallocenium catalysts Cp_2ZrMe^+/MMT (**A**), *rac*-(EBI)$ZrMe^+$/MMT (**B**), and $CGCTiMe^+$/MMT (**C**), respectively (Scheme 1), after elimination of methane and discharge of the resulting neutral amine. A slight excess of the metallocene dimethyl and the discharged neutral amine were effectively removed by extensive washing with toluene and hexanes followed by drying under vacuum, as monitored by ^{1}H NMR spectra of the filtrate residue, which showed the filtrate residue from the reaction of $Me(HT)_2NH^+$/MMT and *rac*-(EBI)$ZrMe_2$ consisted of the discharged neutral amine ($Me(HT)_2N$) and the recovered excess *rac*-(EBI)$ZrMe_2$ in a 9:1 ratio, consistent with the 10% excess of the metallocene dimethyl employed in the reaction. In addition to the ^{1}H NMR evidence, the X-ray photoelectron spectroscopy (XPS) analysis of the synthesized zirconocenium cation-intercalated silicates showed the absence of any N peaks, strongly suggesting that the protonolysis reaction followed by the neutral amine discharge was quantitative, and that decomposition or side reactions (e.g., surface absorption) involving the metallocene dimethyl was negligible.

Scheme 1. Synthesis of intergallery-anchored metallocenium cations and their corresponding high-resolution XPS spectra.

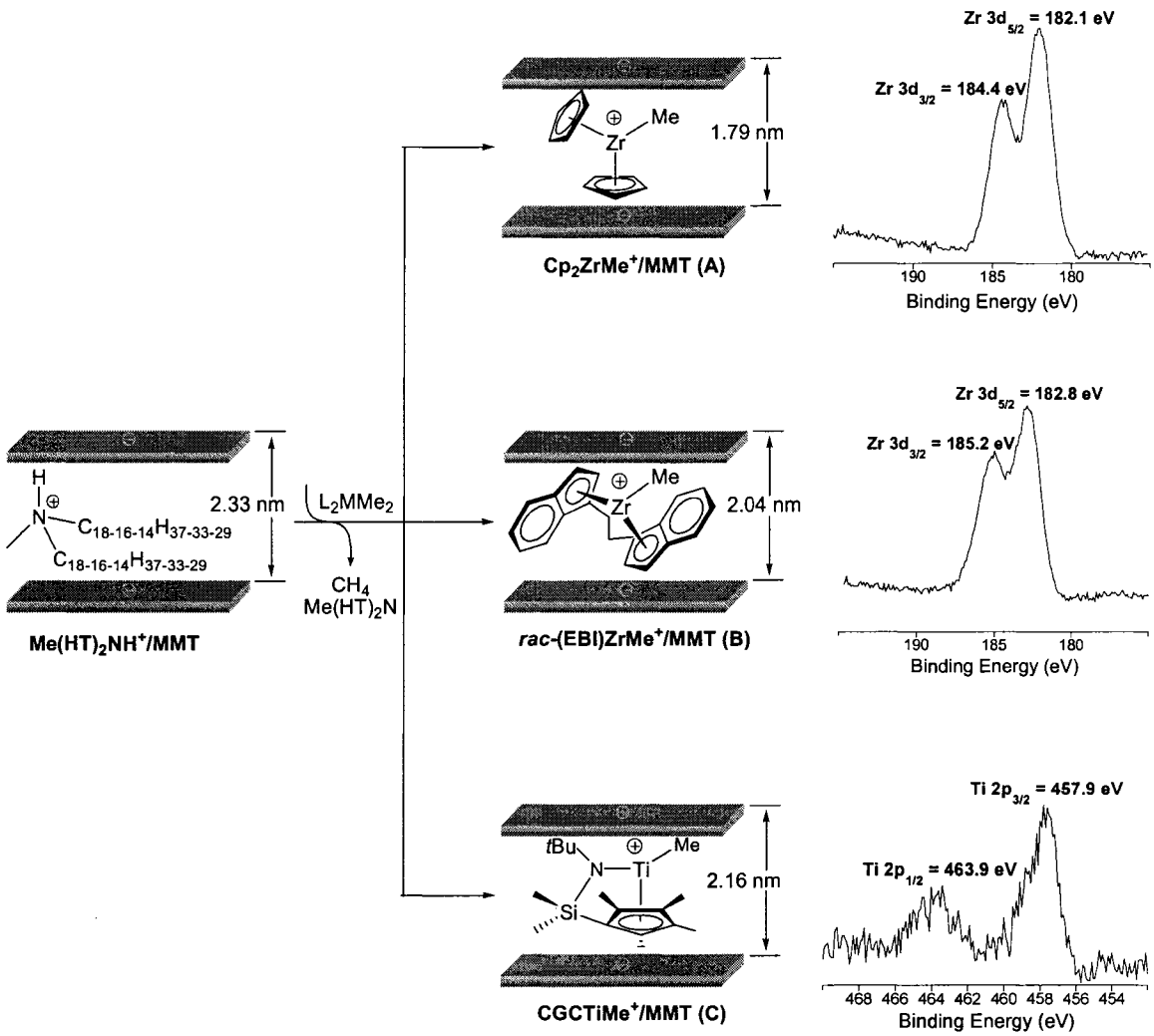

On the basis of the powder X-ray diffraction (XRD) analysis, the basal spacings for the synthesized **A**, **B**, and **C** are 1.79 nm, 2.04 nm, and 2.16 nm, respectively (Scheme 1, Figure 1), all of which differ substantially from that of precursor $Me(HT)_2NH^+$/MMT (2.33 nm). The increased *d* spacing on going from **A** to **B** is consistent with the relative molecular dimensions of the zirconocenium cations; however, **C** has the largest *d* spacing in this series, presumably reflecting the weaker coordination between the titanocenium cation and the anionic silicate sheets.

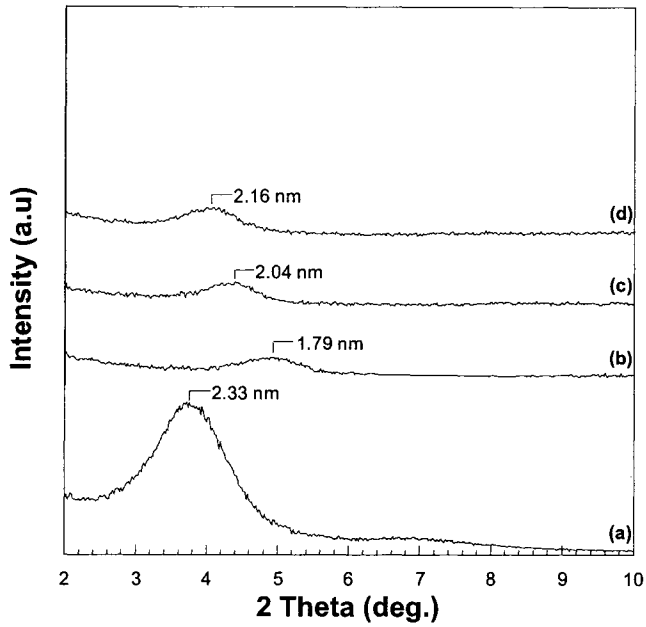

Figure 1. Overlay of XRD plots for $Me(HT)_2NH^+$/MMT (**a**), Cp_2ZrMe^+/MMT (**b**), *rac*-(EBI)$ZrMe^+$/MMT (**c**), and CGCTiMe^+/MMT (**d**).

The formation of the metallocenium cations is further confirmed by the high-resolution XPS analyses. Consistent with the binding energy for Cp_2ZrMe^+ (generated by mixing Cp_2ZrMe_2 with methylalumoxane) obtained by Gassman,[17] the measured Zr $3d_{5/2}$ binding energy for **A** is 182.1 eV (Scheme 1), which is 1.4 eV higher than that of Cp_2ZrMe_2. Likewise, the measured Zr $3d_{5/2}$ binding energy for **B** is 182.8 eV, which is 0.8 eV higher than that of *rac*-(EBI)$ZrCl_2$[18] and estimated to be ~1.8 eV higher than that of *rac*-(EBI)$ZrMe_2$, after considering the fact that dimethyl zirconocene has ~1.0 eV lower binding energy that of the dichloride derivative.[17] Finally, the measured Ti $2p_{3/2}$ binding energy for **C** is 457.9 eV; this value is 1.0 eV higher than that of CGCTiMe_2. These results strongly suggest that the metallocene complexes anchored inside the galleries of MMT are in their cationic forms.

Synthesis of Alane-Intercalated Clays. The synthesis of alane-intercalated clay activators was achieved through two different pathways (Scheme 2). The first was the

reaction of $Me(T)N(C_2H_4OH)_2^+$/MMT with $Al(C_6F_5)_3$ to produce the alane-intercalated clay **D**, after elimination of C_6F_5H. The second approach involves the ligand exchange reaction between the $AlMe_3$ capped terminal alcohols of $Me(T)N(C_2H_4OH)_2^+$/MMT, giving the intermediate $Me(T)N[C_2H_4OAlMe_2]_2^+$/MMT, with $B(C_6F_5)_3$ to produce the alane-intercalated clay activator **E**. The solution-phase model for the ligand exchange reaction between $AlMe_3$ and $B(C_6F_5)_3$ is known.[19]

Scheme 2. Synthesis of alane-intercalated clay activators

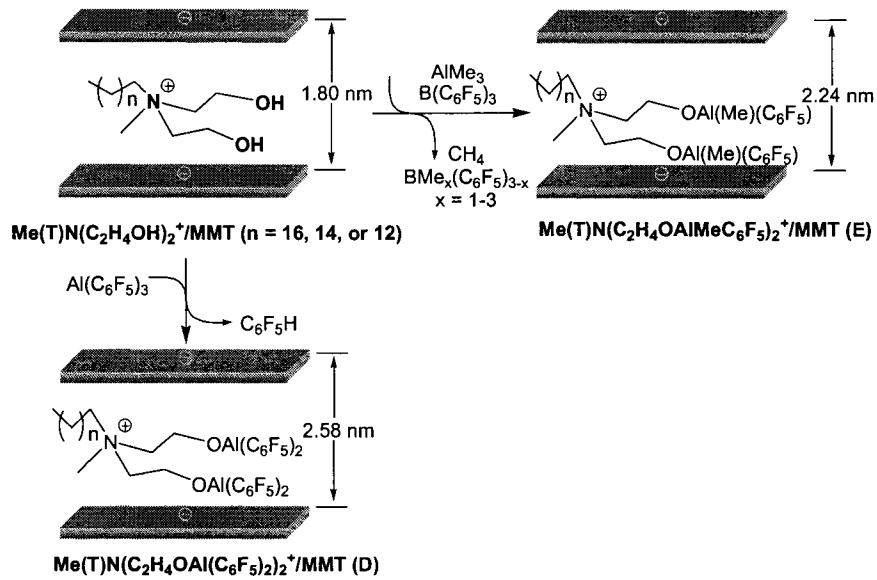

Evidence supporting the proposed alane-intercalated clay activator structure was derived from three key diagnostic tools: elemental analyses (measured by ICP), high-resolution XPS, and powder XRD. Elemental analysis results showed the presence of fluorine and significantly increased amounts of Al as compared to the precursor $Me(T)N(C_2H_4OH)_2^+$/MMT. Further evidence consistent with this finding, obtained from high-resolution XPS analyses, showed the presence of fluorine in the alane-intercalated clay activators that is absent in the precursor MMT. Another interesting feature was the presence of a new type of aluminum with a ~1.0 eV higher Al 2*p* binding energy than

that of the precursor MMT, which is attributed to the pentafluorophenyl substituted Al centers of the supported activators (Figures 2 and 3).

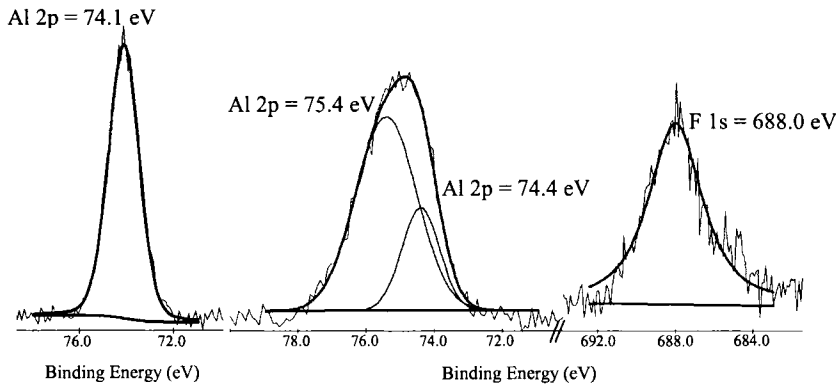

Figure 2. High-resolution XPS spectra for $Me(T)N(C_2H_4OH)_2^+$/MMT (Al 2*p* region, left) and clay activator **D** (Al 2*p* region, middle; F 1*s* region, right).

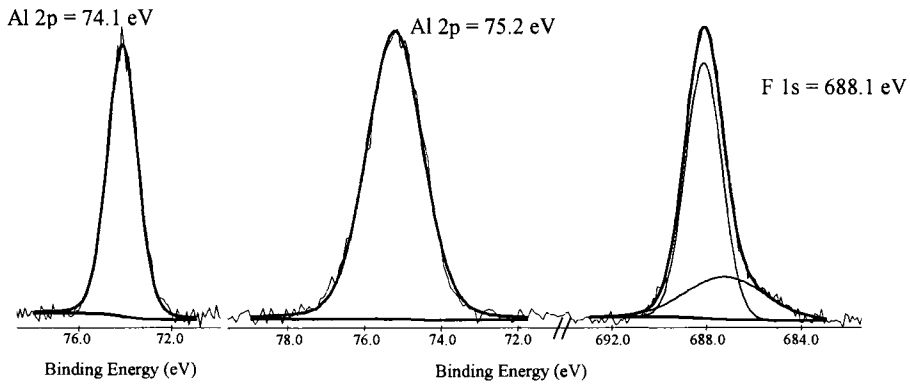

Figure 3. High resolution XPS spectra for $Me(T)N(C_2H_4OH)_2^+$/MMT (Al 2*p* region, left) and clay activator **E** (Al 2*p* region, middle; F 1*s* region, right).

Powder XRD analyses of the alane-intercalated clay activators yielded weak and broad diffraction peaks corresponding to *d* spacings of 2.58 nm and 2.24 nm for **D** and **E** (Figures 4), respectively, both of which are significantly larger than the *d* spacing of the precursor MMT (1.80 nm), providing further evidence supporting the proposed alane-intercalated clay activator structure.

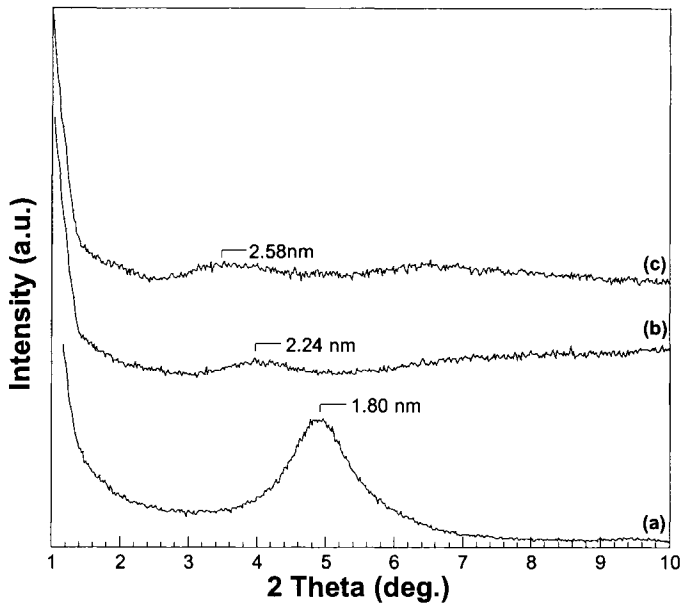

Figure 4. Overlay of XRD plots for $Me(T)N(C_2H_4OH)_2^+$/MMT (**a**), **D** (**b**), and **E** (**c**).

Synthesis of *in situ* Polymerized P(MMA)–Silicate Nanocomposites. The *in situ* polymerization of MMA catalyzed by the intergallery-anchored metallocenium cations **A**, **B**, and **C** afforded atactic ([*mr*] = 39.8%), isotactic ([*mm*] = 93.0%), and syndiotactic ([*rr*] = 72.0%) P(MMA)–silicate nanocomposites, respectively (Table 1; Scheme 3). One of the most interesting properties of these nanocomposites is the ability to modulate T_g's of the resultant P(MMA)–silicate nanocomposites based on the polymer matrix stereochemistry. As can be seen in Table 1, *st*-P(MMA)–silicate nanocomposite (T_g = 128 °C), *at*-P(MMA)–silicate nanocomposite (T_g = 103 °C), and *it*-P(MMA)–silicate nanocomposite (T_g = 64 °C) have significantly different T_g's depending on the polymer matrix stereochemistry. The powder XRD analyses of the stereochemically controlled P(MMA)–silicate nanocomposites showed the absence of significant diffraction peaks (over 2θ = 2 to 10°), providing evidence for a predominantly exfoliated nanocomposite morphology (Figure 5).

Table 1. Results of MMA Polymerizations using Intergallery-Anchored Metallocenium Cations and Properties of P(MMA)–Silicate Nanocomposites[a]

entry	catalyst	time (h)	yield (%)	M_n[b] (kg/mol)	PDI[b] (M_w/M_n)	T_g[c] (°C)	T_{max}[d] (°C)	$T_{int,\ end}$[e] (°C)	[mm][f] (%)	[mr][f] (%)	[rr][f] (%)
1	**A**	24	38	45.1	1.46	103	371	325, 393	24.5	39.8	35.7
2	**B**	3	80	102	1.58	64	371	328, 405	93.0	4.7	2.3
3	**C**	24	36	98.9	1.47	128	367	323, 388	4.8	23.2	72.0
4[g]	**C**	24	44	130	1.29	126	370	320, 392	3.9	25.0	71.1
5	**C**	24	85	182	1.37	126	368	328, 392	2.9	23.9	73.2

[a]Carried out in an argon-filled glovebox (oxygen and moisture < 1.0 ppm) at room temperature and in toluene (entries 1-4) or DCB (*o*-dichlorobenzene, entry 5); intergallery-anchored metallocenium loading vs monomer: 5wt%. [b]Number-average molecular weight (M_n) and polydispersity index (PDI) determined by GPC relative to PMMA standards using THF as eluent. [c]Glass transition temperature determined by DSC from second scans. [d]dwt%/dT peak max (maximum rate decomposition temperature) determined by TGA. [e]Decomposition onset temperatures determined by TGA. [f]Methyl triads determined by ^{1}H NMR spectroscopy. [g]The catalyst was preswelled by stirring in toluene overnight before the addition of MMA.

Scheme 3. *in situ* polymerization of MMA using intergallery-anchored metallocenium cations.

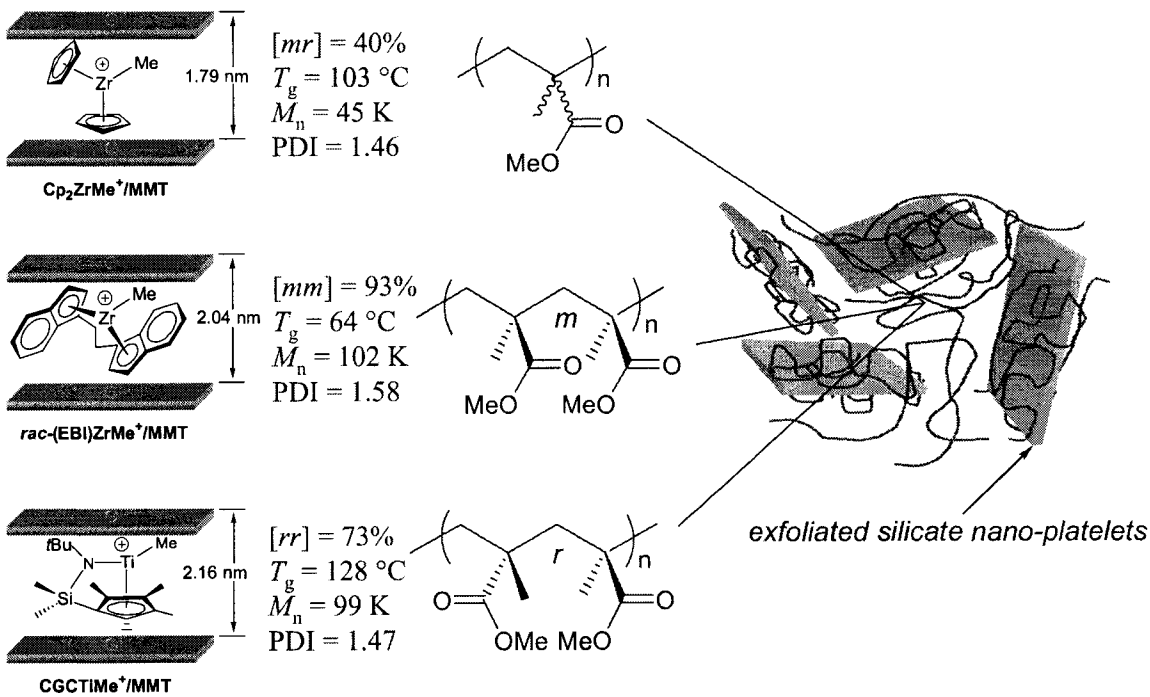

To further confirm the morphology of the P(MMA)–silicate nanocomposites produced, *it*-P(MMA)–silicate nanocomposite (produced by **B**) was examined by TEM. The TEM micrographs obtained clearly demonstrate both the homogeneous dispersion

and the exfoliated morphology of the silicate sheets within the polymer matrix (Figure 6).

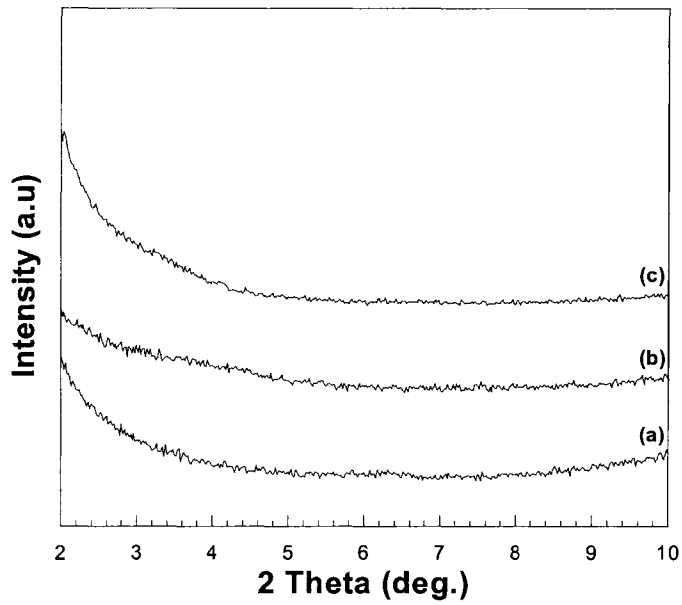

Figure 5. Overlay of XRD plots for *at*-P(MMA)–silicate nanocomposite by **A** (**a**), *it*-P(MMA)–silicate nanocomposite by **B** (**b**), and *st*-P(MMA)–silicate nanocomposite by **C** (**c**).

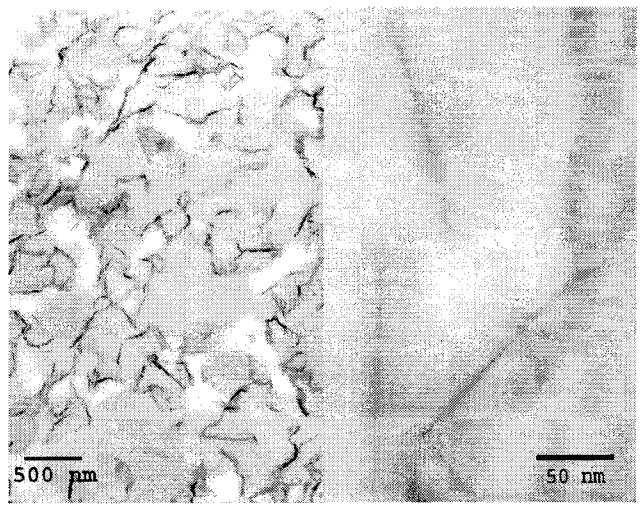

Figure 6. TEM images of *it*-P(MMA)–silicate nanocomposite produced by **B**.

The *in situ* polymerization of MMA using alane-intercalated clay activators in combination with a series of group 4 metallocene dimethyls was also examined. Control experiments using the clay activators **D** or **E** alone showed no activity for MMA polymerization; however, when suspended in a toluene-MMA solution, followed by

addition of a metallocene dimethyl initiator, the stereochemically controlled polymerization of MMA was affected. As in the case of the intergallery-anchored metallocenium cations, the resulting P(MMA) matrix stereochemistry can be modulated by the symmetry of the metallocene catalyst precursor. While the combination of **D** with the metallocene dimethyls Cp_2ZrMe_2 and *rac*-(EBI)$ZrMe_2$ resulted in syndiotactic ([*rr*] = 66.8%) and isotactic ([*mm*] = 60.2%) P(MMA)–silicate nanocomposites, respectively, the combination of **E** with Cp_2ZrMe_2, $CGCTiMe_2$, and *rac*-(EBI)$ZrMe_2$ afforded syndiotactic ([*rr*] = 60.8% and 75.4%) and isotactic ([*mm*] = 86.5%) P(MMA)–silicate nanocomposites, respectively (Table 2).

Table 2. Results of MMA Polymerizations using Alane-Intercalated Clay Activators in Combination with Metallocene Dimethyls and Properties of P(MMA)–Silicate Nanocomposites[a]

entry	catalyst (initiator)	yield (%)	M_n[b] (kg/mol)	PDI[b] (M_w/M_n)	T_g[c] (°C)	T_{max}[d] (°C)	$T_{int,\ end}$[e] (°C)	[*mm*][f] (%)	[*mr*][f] (%)	[*rr*][f] (%)
1	**D** (Cp_2ZrMe_2)	93	58.0	1.23	126	382	350, 411	2.3	30.9	66.8
2	**D** (*rac*-EBIZrMe_2)	96	36.0	1.89	71	379	350, 410	60.2	16.3	23.6
3	**E** (Cp_2ZrMe_2)	96	49.2	1.29	124	387, 417	358, 425	2.8	36.4	60.8
4	**E** (*rac*-EBIZrMe_2)	97	52.4	1.81	64	380	349, 410	86.5	5.8	7.7
5	**E** ($CGCTiMe_2$)	65	-	-	126	385	357, 401	2.3	23.0	74.7
6[g]	**E** ($CGCTiMe_2$)	>99	-	-	113	382	352, 400	2.5	22.1	75.4

[a]All polymerizations were carried out in 5 mL of toluene (unless otherwise noted) for 24 h in an argon-filled glovebox (< 1.0 ppm oxygen and moisture) at ambient temperature; 50 mg of modified MMT; 23.4 μmol of initiator; 9.35 mmol MMA. [b]Number-average molecular weight (M_n) and polydispersity index (PDI) determined by GPC relative to PMMA standards using THF as eluent. [c]Glass transition temperature determined by DSC from second scans. [d]dwt%/dT peak max (maximum rate decomposition temperature) determined by TGA. [e]Decomposition onset temperatures determined by TGA. [f]Methyl triads determined by ^{1}H NMR spectroscopy. [g]Reaction carried out in 5mL of DCB.

Powder XRD analyses of the stereochemically controlled P(MMA)–silicate nanocomposites produced by alane-intercalated clay activators in combination with

metallocene dimethyls showed weak, broad diffraction peaks (over 2θ = 2 to 10°) indicative of an intercalated morphology (Figure 7). The intercalated morphology of the nanocomposites was further confirmed by TEM analyses (Figure 8).

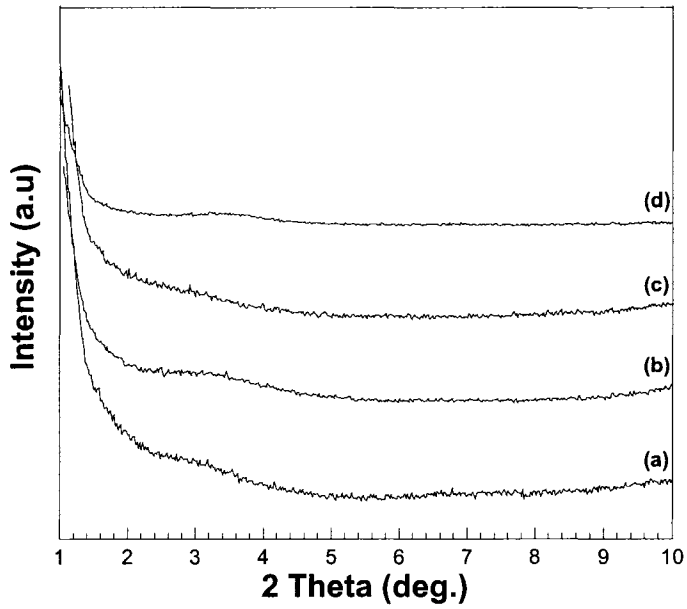

Figure 7. Overlay of XRD plots for *st*-P(MMA)–silicate nanocomposite by **D**/Cp_2ZrMe_2 (**a**), *it*-P(MMA)–silicate nanocomposite by **D**/*rac*-(EBI)$ZrMe_2$ (**b**), *it*-P(MMA)–silicate nanocomposite by **E**/*rac*-(EBI)$ZrMe_2$ (**c**), and *st*-P(MMA)–silicate nanocomposite by **E**/(CGC)$TiMe_2$ in DCB.

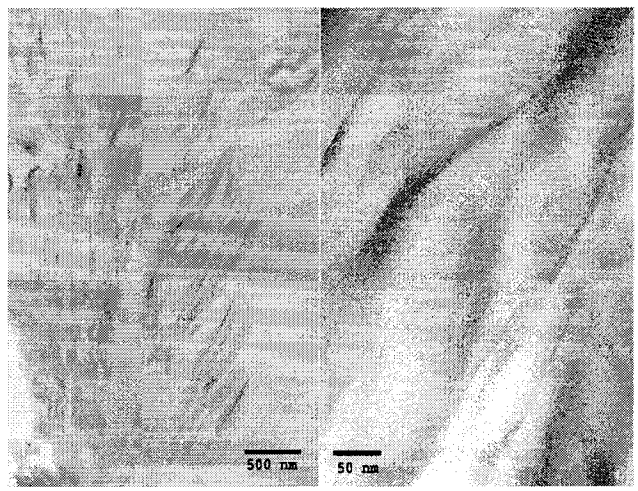

Figure 8. TEM images of the intercalated *st*-P(MMA)–silicate nanocomposite produced by clay activator **E** and (CGC)$TiMe_2$ in DCB.

Supramolecular Stereocomplex P(MMA)–Silicate Nanocomposites. With the successful synthesis of exfoliated P(MMA)–silicate nanocomposites incorporating stereocontrolled polymer matrices prepared by intergallery-anchored metallocenium cations established, we next turned our attention to the generation of P(MMA)–silicate nanocomposites with matrices of higher order. Specifically, this demonstrated ability to generate stereocontrolled P(MMA) matrices prompted us to investigate the accessibility of supramolecular stereocomplex P(MMA)–silicate nanocomposites. For pristine homopolymer P(MMA) (with no inorganic filler present), it has been demonstrated that a stereocomplex—by definition, a crystalline polymer complex between a pair of diastereomeric macromolecules—can be formed between highly *st*- and *it*-P(MMA) blends in certain ratios (typically 2/1) either in the solid state, when annealed, or in suitable solvents.[20] This self-assembled, double-stranded helical complex exhibits enhanced physical and mechanical properties when compared to the individual tactic polymers. To this end, we further examined the use of our stereocontrolled P(MMA)–silicate nanocomposites for the preparation of supramolecular stereocomplex P(MMA)–silicate nanocomposites.

The synthesis of 2/1 syndiotactic/isotactic (*st*-/*it*-) P(MMA)–silicate nanocomposite stereocomplexes was achieved to varying degrees through various strategies involving thermal crystallization, solvent casting, and solution crystallization methods; however, under our condition, the best results were obtained using a dilute solution crystallization method. The solution crystallization stereocomplex synthesis involved preparing separate 1 wt% solutions of the *st*-P(MMA)–silicate nanocomposite (produced by **C**) and *it*-P(MMA)–silicate nanocomposite (produced by **A**) in THF (a complexing solvent). The

homogeneous solutions were combined in a 2/1 ratio of *st-*/*it-* and allowed to stand undisturbed for one week after initial mixing of the solutions. The products isolated by precipitation into excess methanol followed by drying under vacuum at 50 °C overnight. Final treatment involved extracting the uncomplexed polymer into THF [note: the sterocomplex P(MMA) is insoluble in THF while uncomplexed P(MMA) is completely soluble] followed by drying to a constant weight.

Key evidence for the formation of stereocomplex P(MMA)–silicate nanocomposites includes the resistance to THF extraction as well as the presence of a melting transition temperature (T_m) of 201 °C. Furthermore, ^{1}H NMR analysis of the methyl triad distribution of the THF insoluble stereocomplex P(MMA)–silicate nanocomposites suggests stereocomplex formation, exhibiting enriched *it-* and *st-* content ([*mm*] = 28.3%; [*rr*] = 51.0%) while maintaining a relatively low heterotactic content ([*mr*] = 20.7%). TGA analysis of the resulting product show a narrow decomposition temperature window of 349–403 °C (Figure 9) as well as a single, high decomposition temperatures as shown by maximum rate decomposition temperatures (T_{max}) of 377 °C (Figure 10). The morphology of the stereocomplex P(MMA)–silicate nanocomposites was confirmed by TEM analysis which shows a predominantly exfoliated morphology (Figure 11).

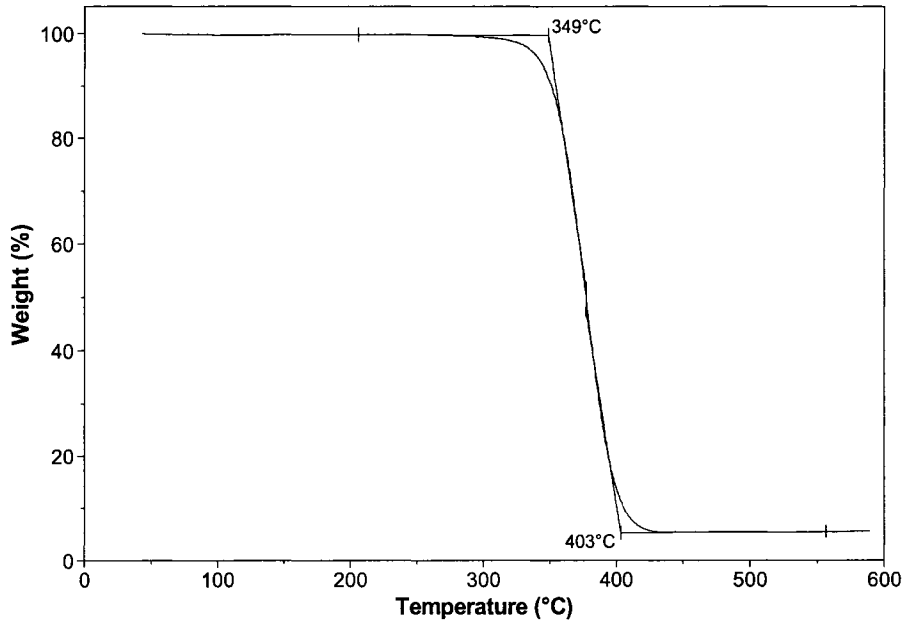

Figure 9. TGA trace of stereocomplex P(MMA)–silicate nanocomposite ($T_{initial}$ = 349 °C, T_{end} = 403 °C).

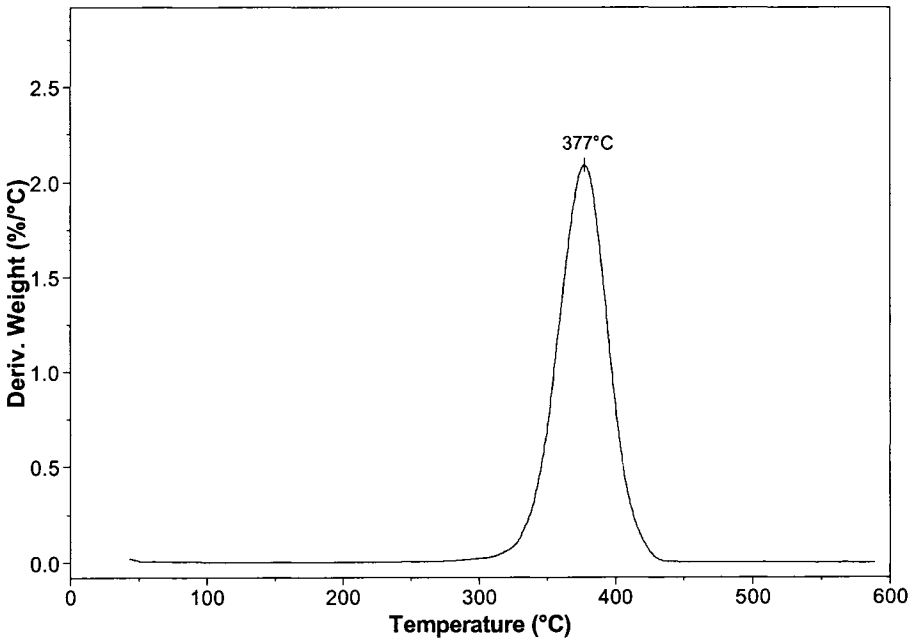

Figure 10. Derivative plot of the TGA trace of stereocomplex P(MMA)–silicate nanocomposite (T_{max} = 377 °C).

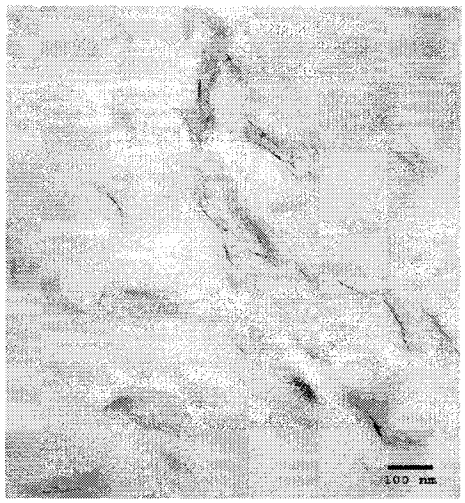

Figure 11. TEM image of the predominantly exfoliated stereocomplex P(MMA)–silicate nanocomposite.

Conclusions

In summary, we report the first synthesis and characterization of *exfoliated* P(MMA)–silicate nanocomposites consisting of stereochemically controlled polymer matrices prepared by the *in situ* polymerization of MMA using intergallery-anchored metallocenium catalysts. Specifically, polymerization of MMA catalyzed by the intergallery-anchored metallocenium cations **A**, **B**, and **C** afforded atactic ([*mr*] = 39.8%), isotactic ([*mm*] = 93.0%), and syndiotactic ([*rr*] = 72.0%) P(MMA)–silicate nanocomposites, respectively (Table 1; Scheme 3). Furthermore, the use alane-intercalated clay activators in combination with metallocene dimethys allows for *in situ* polymerized stereoregular P(MMA)–silicate nanocomposites with *intercalated* morphologies in which the combination of **D** with the metallocene dimethyl initiators Cp_2ZrMe_2 and *rac*-(EBI)$ZrMe_2$ resulted in syndiotactic ([*rr*] = 66.8%) and isotactic ([*mm*] = 60.2%) P(MMA)–silicate nanocomposites, respectively, while the combination of **E** with Cp_2ZrMe_2, $CGCTiMe_2$, and *rac*-(EBI)$ZrMe_2$ afforded syndiotactic ([*rr*] =

60.8% and 75.4%) and isotactic ([*mm*] = 86.5%) P(MMA)–silicate nanocomposites, respectively (Table 2). The access to such stereoregular P(MMA)–silicate nanocomposites allowed for further investigations into the synthesis of polymer nanocomposites consisting of matrices of higher order, namely supramolecular stereocomplex P(MMA)–silicate nanocomposites. The solution crystallization of a 2/1 ratio of *s*-/*i*-P(MMA)–silicate nanocomposites produced by intergallery-anchored metallocenium cations allowed for the first synthesis of predominantly exfoliated supramolecular stereocomplex P(MMA)–silicate nanocomposites consisting of a crystalline double-stranded helical stereocomplex polymer matrix. Access to such unique and tunable polymer matrix stereochemistries and morphologies will hopefully allow for future fundamental studies of the polymer matrix stereochemistry effect on nanocomposite properties.

Acknowledgment. This work was supported by Colorado State University. E.Y.C. gratefully acknowledges an Alfred P. Sloan Research Fellowship.

References

(1) (a) Ray, S. S.; Okamoto, M. *Prog. Polym. Sci.* **2003**, *28*, 1539-1641. (b) Vaia, R. A.; Giannelis, E. P. *MRS Bull.* **2001**, *26*, 394-401. (c) Giannelis, E. P. *Adv. Mater.* **1996**, *8*, 29-35. For recent reviews, see: (a) Krishnamoorti, R.; Vaia, R. A. Eds. *ACS Symp. Ser.* **2001**, *804*, 1–223 and references therein. (b) Pinnavaia, T. J.; Beall, G. W. Eds. *Polymer-Clay Nanocomposites*; Wiley: New York, 2000, pp 1–349 and references therein. (c) Alexandre, M.; Dubois, P. *Mater. Sci. Eng. R.* **2000**, *28*, 1–63. (d) Giannelis, E. P.; Krishnamoorti, R.; Manias. *Adv. Polym. Sci.* **1999**, *138*, 107–147.

(2) (a) Usuki, A.; Kojima, Y.; Kawasumi, M.; Okada, A.; Kurauchi, T.; Kamigaito, O. *Polym. Prepr. (Am. Chem. Soc. Div. Polym. Chem.)* **1990**, *200*, 218-219. (b) Usuki, A.; Kojima, Y.; Kawasumi, M.; Okada, A.; Fukushima, Y.; Kurauchi, T.; Kamigaito, O. *J. Mater. Res.* **1993**, *8*, 1179-1184. (c) Kojima, Y.; Usuki, A.; Kawasumi, M.; Okada, A.; Kurauchi, T.; Kamigaito, O. *J. Polym. Sci., Part A: Polym. Chem.* **1993**, *31*, 983-986.

(3) For recent examples, see (a) Su, S.; Wilkie, C. A. *J. Polym. Sci. Part A: Polym. Chem.* **2003**, *41*, 1124–1135. (b) Fan, X.; Xia, C.; Advincula, R. C. *Polym. Prep.* **2003**, *44*, 1099–1100. (c) Wang, D.; Zhu, J.; Yao, Q.; Wilkie, C. A. *Chem. Mater.* **2002**, *14*, 3837–3843. (d) Huang, X.; Brittain, W. J. *Macromolecules* **2001**, *34*, 3255–3260. (e) Zeng, C.; Lee, J. L. *Macromolecules* **2001**, *34*, 4098–4103. (f) Choi, Y. S.; Choi, M. H.; Wang, K. H.; Kim, S. O.; Kim, Y. K.; Chung, I. J. *Macromolecules* **2001**, *34*, 8978–8985. (g) Bandyopadhyay, S.; Hsieh, A. J.;

Giannelis, E. P. *ACS Symp. Ser.* **2001**, *804*, 15–25. (h) Bandyopadhyay, S.; Giannelis, E. P; Hsieh, A. J. *Polym. Mater. Sci. Eng.* **2000**, *82*, 208–209.

(4) (a) Rodriguez-Delgado, A.; Chen, E. Y.-X. *Macromolecules* **2005**, *38*, 2587–2594. (b) Rodriguez-Delgado, A.; Mariott, W. R.; Chen, E. Y.-X. *Macromolecules* **2004**, *37*, 3092–3100. (c) Bolig, A. D.; Chen, E. Y.-X. *J. Am. Chem. Soc.* **2004**, *126*, 4897–4906. (d) Jin, J.; Mariott, W. R.; Chen, E. Y.-X. *J. Polym. Sci. Part A: Polym. Chem.* **2003**, *41*, 3132–3142. (e) Chen, E. Y.-X.; M. J. Cooney. *J. Am. Chem. Soc.* **2003**, *125*, 7150–7151. (f) Karanikolopoulos, G.; Batis, C.; Pitsikalis, M.; Hadjichristidis, N. *Macromol. Chem. Phys.* **2003**, *204*, 831–840. (g) Bolig, A. D.; Chen, E. Y.-X. *J. Am. Chem. Soc.* **2002**, *124*, 5612–5613. (h) Frauenrath, H.; Keul, H.; Höcker, H. *Macromolecules* **2001**, *34*, 14–19. (i) Cameron, P. A.; Gibson, V.; Graham, A. J. *Macromolecules* **2000**, *33*, 4329–4335. (j) Nguyen, H.; Jarvis, A. P.; Lesley, M. J. G.; Kelly, W. M.; Reddy, S. S.; Taylor, N. J.; Collins, S. *Macromolecules* **2000**, *33*, 1508–1510. (k) Deng, H.; Shiono, T.; Soga, K. *Macromolecules* **1995**, *28*, 3067–3073. (l) Collins, S.; Ward, D. G.; Suddaby, K. H. *Macromolecules* **1994**, *27*, 7222–7224.

(5) Tudor, J.; Willington, O'Hare, D.; Royan, B. *Chem. Commun.* **1996**, 2031–2032.

(6) Bergman, J. S.; Chen, H.; Giannelis, E. P.; Thomas, M. G.; Coates, G. W. *Chem. Commun.* **1999**, 2179–2180.

(5) Allen, R. D.; Long, T. E.; McGrath, J. E. *Polym. Bull.* **1986**, *15*, 127–134.

(8) Biagini, P.; Lugli, G.; Abis, L.; Andreussi, P.; U.S . Pat. 5,602269, 1997.

(9) Feng, S. G.; Roof, G. R.; Chen, E. Y. X. *Organometallics* **2002**, *21*, 832-839.

(10) Samuel, E.; Rausch, M. D. *J. Am. Chem. Soc.* **1973**, *95*, 6263-6267.

(11) (a) Grossman, R. B.; Doyle, R. A.; Buchwald, S. L. *Organometallics* **1991**, *10*, 1501–1505. (b) Collins, S.; Kuntz, B. A.; Taylor, N. J.; Ward, D. G. *J. Organomet. Chem.* **1988**, *342*, 21–29.

(12) Diamond, G. M.; Jordan, R. F.; Petersen, J. L. *J. Am. Chem. Soc.* **1996**, *118*, 8024–8033.

(13) Stevens, J. C.; Timmers, F. J.; Wilson, D. R.; Schmidt, G. F.; Nickias, P. N.; Rosen, R. K.; Knight, G. W.; Lai, S. *Eur. Pat. Appl.* EP 416 815-A2, 1991.

(14) DMNST Software Manual: Version 1.37; Scintag Incorporated: Cupertino, CA, 1999.

(15) Wagner, C. D.; Naumkin, A. V.; Kraut-Vass, A.; Allison, J. W.; Powell, C. J.; Rumble, J. R. J. NIST X-ray Photoelectron Spectroscopy Database; Version 3.4; NIST: Gaithersburg, MD, 2003.

(16) (a) Bovey, F. A.; Mirau, P. A. *NMR of Polymers*; Academic Press: San Diego, 1996. (b) Ferguson, R. C.; Ovenall, D. W. *Macromolecules* **1987**, *20*, 1245–1248. (c) Ferguson, R. C.; Ovenall, D. W. *Polym. Prepr. (Am. Chem. Soc. Div. Polym. Chem.)* **1985**, *26*, 182–183. (d) Subramanian, R.; Allen, R. D.; McGrath, J. E.; Ward, T. C. *Polym. Prepr. (Am. Chem. Soc. Div. Polym. Chem.)* **1985**, *26*, 238–240.

(17) Gassman, P. G.; Callstrom, M. R. *J. Am. Chem. Soc.* **1987**, *109*, 7875–7876.

(18) Atiqullah, M.; Faiz, M.; Akhtar, M. N.; Salim, M. A.; Ahmed, S.; Khan, J. H. *Surf. Interface Anal.* **1999**, *27*, 728–734.

(19) Klosin, J.; Roof, G. R.; Chen, E. Y. X.; Abboud, K. A. *Organometallics* **2000**, *19*, 4684-4686.

(20) (a) Serizawa, T.; Hamada, K.-I.; Akashi, M. *Nature* **2004**, *429*, 52–55. (b) Serizawa, T.; Hamada, K.; Kitayama, T.; Fujimoto, N.; Hatada, K.; Akashi, M. *J. Am. Chem. Soc.* **2000**, *122*, 1891–1899. (c) Hatada, K.; Kitayama, T.; Ute, K.; Nishiura, T. *Macromol. Symp.* **1998**, *132*, 221–230. (d) Spevacek, J.; Schneider, B. *Adv. Colloid Interface Sci.* **1987**, *27*, 81–150.

CHAPTER III

MECHANISM AND SCOPE OF STEREOSPECIFIC, COORDINATIVE-ANIONIC POLYMERIZATION OF ACRYLAMIDES BY CHIRAL ZIRCONOCENIUM ESTER AND AMIDE ENOLATES

This dissertation chapter contains the manuscript of a communication [Mariott, W. R.; Chen, E. Y.-X *Macromolecules* **2004**, 37, 4741–4743] and a full paper [Mariott, W. R.; Chen, E. Y.-X *Macromolecules* **2005**, 38, 6822–6832], both published in *Macromolecules*, and describes the first highly isospecific polymerization of *N,N*-dimethylacrylamide (DMAA) by metallocene complexes. This chapter represents efforts directed at extending our current knowledge base concerning the metallocene catalyzed polymerization of methacrylates both in solution and within silicate nanogalleries to a series of previously unexplored acrylamide monomers. Specifically, the polymerization of DMAA by a chiral *ansa*-zirconocenium ester enolate affords poly(DMAA) with unprecedented isotacticities, high number-average molecular weights, low polydispersities as well as melting transition temperatures as high as 318 °C. Furthermore, mechanistic studies of the polymerization of DMAA by the chiral *ansa*-zirconcenium ester enolate reveal a living, monometallic, intramolecular coordinative-conjugate-addition propagation mechanism. Additionally, the scope of the polymerization of other acrylamides was also investigated.

Abstract

The mechanism and scope of the isospecific, coordinative-anionic polymerization of acrylamides, including *N,N*-dimethylacrylamide (DMAA), *N,N*-dimethylmethacrylamide (DMMA), and *N*-isopropylacrylamide (IPAA), using chiral *ansa*-zirconocenium ester and amide enolates, are reported. The zirconocenium ester enolate, *rac*-(EBI)Zr^{+}(THF)[$OC(O^{i}Pr)$=CMe_2][$MeB(C_6F_5)_3$]$^{-}$ [**1**; EBI = $C_2H_4(Ind)_2$], effects highly isospecific and living polymerization of DMAA via a monometallic, intramolecular coordinative-conjugate-addition mechanism, with the resting intermediate during a "catalytic" propagation cycle being the cyclic amide enolate. The results leading to these key conclusions were derived from investigations of polymerization kinetics, polymer microstructures and chain-end groups, block copolymerization behavior, as well as modeling and isolation of the active propagating species. Specifically regarding the active species modeling, isolation, and characterization, neutral chiral amide enolate *rac*-(EBI)ZrMe[$OC(NMe_2)$=CMe_2] (**2**) has been synthesized and structurally characterized and its corresponding cationic complex *rac*-(EBI)Zr^{+}(THF)[$OC(NMe_2)$=$C(Me)_2$][$MeB(C_6F_5)_3$]$^{-}$ (**3**) isolated; cation **3** is highly active for DMAA polymerization, serving as a structural model for the active propagating species. Both ester and amide enolates **1** and **3** are inactive for polymerizations of DMMA and IPAA; however, 1 equiv of IPAA or DMAA is readily added to **1** or **3**, forming the eight-membered-ring cyclic amide enolates *rac*-(EBI)Zr^{+}[$OC(NH^{i}Pr)$=$CHCH_2C(Me_2)C(O^{i}Pr)$=O][$MeB(C_6F_5)_3$]$^{-}$ (**4**) or *rac*-(EBI)Zr^{+}[$OC(NMe_2)$=$C(Me)CH_2C(Me_2)C(NMe_2)$=O][$MeB(C_6F_5)_3$]$^{-}$ **(5)**, which correspond to the structures of the first acrylamide addition products and the resting propagation intermediates.

Introduction

An important yet still challenging goal in the polymerization of many prochiral, functionalized vinyl monomers is to achieve a high degree of control over the stereochemistry of the polymerization of such monomers. One example in this context is the polymerization of *N,N*-dimethylacrylamide (DMAA); both anionic and radical polymerizations of DMAA with initiators (and additives) that can promote tacticity control yielded poly(*N,N*-dimethylacrylamide) [P(DMAA)] with only moderate isotacticities {[*mm*] = 54–81%}.[1-6] Butler and co-workers first reported the polymerization of DMAA using an anionic initiator (EtLi) in toluene, affording crystalline isotactic P(DMAA);[1] the crystalline P(DMAA) produced by *s*-BuLi was later analyzed by McGrath et al. using ^{1}H and ^{13}C NMR and was shown to exhibit an isotacticity of ~81%.[2] Xie and Hogen-Esch found that the P(DMAA) produced by Ph_3CLi or $(Ph_2CCH_2CH_2CPh_2)Li_2$ in THF at –78 °C was also isotactic-rich ([*mm*] = 54%).[3] Nakahama and co-workers used anionic initiators modified with Lewis acids such as Et_2Zn and Et_3B to effect the tacticity of the resulting P(DMAA);[4] they found that the presence of such Lewis acid additives typically reduces the P(DMAA) isotacticity and thus enhances the syndioselectivity of anionic polymerization. The trend is reversed, however, for radical polymerizations where Lewis acids such as $M(OTf)_3$ (M = Y, Sc, Yb) are shown to enhance isotacticity of the polymer, as demonstrated by the work of Okamoto and co-workers.[5] Most recently, Matyjaszewski et al. utilized this Lewis acid effect to synthesize atactic-*b*-isotactic stereoblock P(DMAA) by adding $Y(OTf)_3$ at a given time to an atom-transfer radical polymerization (ATRP) of DMAA, initially started without the Lewis acid.[6]

Recognizing the difficulty and complications in achieving high degrees of stereochemical control over the polymerization of acrylamides using anionic or radical initiators, we sought to explore the possibility of accomplishing this goal using a coordination polymerization mediated by chiral *ansa*-metallocenium complexes. A large number of investigations have been directed towards studies of the polymerization of alkyl methacrylates, especially methyl methacrylate (MMA), by group 4 metallocene and related complexes, including achiral zirconocenes,[7] chiral *ansa*-zirconocenes,[8] achiral titanocenes,[9] chiral *ansa*-titanocenes,[10] half-sandwich titanium complexes,[11] and constrained geometry titanium and zirconium complexes;[12] the polymerization of MMA by zirconocenes has also been examined computationally.[13] Despite these major advances in the polymerization of *methacrylates* using group 4 metallocene complexes, it is significant to note here that, to the best of our knowledge, there are no open publications on the polymerization of *acrylamides* using metallocene complexes and hence this became the goal of our present studies. To this end, using the well-defined, isolated chiral *ansa*-zirconocenium ester enolate complex, *rac*-(EBI)Zr^{+}(THF)[OC(O^{i}Pr)=CMe_2] [$MeB(C_6F_5)_3$]$^{-}$ [**1**; EBI = $C_2H_4(Ind)_2$][8a] we successfully synthesized P(DMAA) with unprecedented isotacticity ([*mm*] >99%)%), high M_n, low PDI (1.07), and T_m as high as 318 °C.

In our continuing studies of the polymerization of acrylamides using chiral *ansa*-zirconocenium complexes, we expanded our focus to the mechanism and scope of this polymerization and present a full account of our efforts to better understand the polymerization control, stereoregulation, comonomer selectivity, active species, and kinetics, utilizing two complementary initiating complex structures, chiral *ansa*-

zirconocenium *ester* enolate complex **1** and chiral *ansa*-zirconocenium *amide* enolate complex *rac*-(EBI)Zr^{+}(THF)[$OC(NMe_2)$=$C(Me)_2$][$MeB(C_6F_5)_3$]$^{-}$ (**3**). Key findings of this study include: (a) the living polymerization of DMAA by **1** proceeds via a monometallic, coordinative conjugate addition mechanism; (b) sequential block copolymerization of MMA and DMAA leads to the formation of the well-defined, highly isotactic block copolymer P(MMA)-*b*-P(DMAA), with a procedure starting from the MMA polymerization, but not starting from the DMAA polymerization; (c) neither complex **1** nor **3** is active for the polymerization of *N,N*-dimethylmethacrylamide (DMMA) or *N*-isopropylacrylamide (IPAA), but 1 equiv of IPAA or DMAA can be readily added to **1** or **3**, forming the corresponding single-monomer-addition products—eight-membered-ring cyclic amide enolate complexes; and (d) polymerization of DMAA by **3** proceeds in a similar manner to that by **1**, indicating that the amide enolate **3** is a suitable structural model for the active propagating species derived from the polymerization acrylamides.

Experimental Section

Materials and Methods. All syntheses and manipulations of air- and moisture-sensitive materials were carried out in flamed Schlenk-type glassware on a dual-manifold Schlenk line, a high-vacuum line (10^{-5} to 10^{-7} Torr), or in an argon-filled glovebox (<1.0 ppm oxygen and moisture). NMR-scale reactions (typically in a 0.02 mmol scale) were conducted in Teflon-valve-sealed J. Young-type NMR tubes. HPLC grade organic solvents were sparged with nitrogen during filling of the solvent reservoir and then dried by passage through activated alumina (for Et_2O, THF, and CH_2Cl_2) followed by passage through Q-5-supported copper catalyst (for toluene and hexanes) stainless steel columns.

Benzene-d_6, toluene-d_8, and THF-d_8 were dried over sodium/potassium alloy and vacuum-distilled or filtered, whereas C_6D_5Br, $CDCl_3$, CD_2Cl_2, and *o*-dichlorobenzene were dried over activated Davison 4-Å molecular sieves. NMR spectra were recorded on either a Varian Inova 300 (FT 300 MHz, ^1H; 75 MHz, ^{13}C; 282 MHz, ^{19}F) or a Varian Inova 400 spectrometer. Chemical shifts for ^1H and ^{13}C spectra were referenced to internal solvent resonances and are reported as parts per million relative to tetramethylsilane, whereas ^{19}F NMR spectra were referenced to external $CFCl_3$. Elemental analyses were performed by Desert Analytics, Tucson, AZ.

Diisopropylamine, triflic acid, *n*-butyllithium (1.6 M in hexanes), *N,N*-dimethylisobutyramide, lithium dimethylamide, and tetrachlorozirconium were purchased from Aldrich Chemical Co. and used as received, except for the amine and the amide which were degassed using three freeze-pump-thaw cycles. Trimethylaluminum (neat) was purchased from Strem Chemical Co. and methyllithium (1.6 M in diethyl ether) from Acros. 2,6-Di-*tert*-butyl-4-methylphenol (butylated hydroxytoluene, BHT-H) was purchased from Aldrich Chemical Co. and recrystallized from hexanes prior to use.

Methyl methacrylate (MMA) was purchased from Aldrich Chemical Co., whereas *N,N*-dimethylacrylamide (DMAA), *N,N*-dimethylmethacrylamide (DMMA), and *N*-isopropylacrylamide (IPAA) were purchased from TCI America. MMA, DMAA, and DMMA were first degassed and dried over CaH_2 overnight, followed by vacuum distillation; final purification of MMA involved titration with neat tri(*n*-octyl)aluminum to a yellow end point[14] followed by distillation under reduced pressure. The purified monomers were stored in brown bottles over activated Davison 4-Å molecular sieves (for DMAA and DMMA) in a –30 °C freezer inside the glovebox. IPAA was recrystallized

from a toluene/hexanes solvent mixture and stored in a –30 °C freezer inside the glovebox.

Tris(pentafluorophenyl)borane, $B(C_6F_5)_3$, was obtained as a research gift from Boulder Scientific Co. and further purified by recrystallization from hexanes at –35 °C. The $(C_6F_5)_3B•THF$ adduct was prepared by addition of THF to a toluene solution of the borane followed by removal of the volatiles and drying in vacuo. Literature procedures were employed for the preparation of the following compounds and metallocene complexes: $(EBI)H_2$ [EBI = $C_2H_4(Ind)_2$],[15] *rac*-$(EBI)Zr(NMe_2)_2$,[16] *rac*-$(EBI)ZrMe_2$,[16] *rac*-$(EBI)ZrMe^+MeM(C_6F_5)_3^-$ (M = B, Al),[17,8a] *rac*-$(EBI)Zr(OTf)_2$,[8a] *rac*-(EBI)ZrMe(OTf),[8a] *rac*-(EBI)ZrMe[OC(O^{i}Pr)=CMe_2],[8a] and *rac*-$(EBI)Zr^+(THF)[OC(O^iPr)=CMe_2]$ $[MeB(C_6F_5)_3]^-$ (**1**).[8a] The lithium amide enolate $LiOC(NMe_2)=CMe_2$ was prepared according to a modified literature procedure of Rathke and coworkers.[18]

Synthesis of *rac*-(EBI)ZrMe[OC(NMe$_2$)=CMe$_2$] (2). In an argon-filled glovebox, a 30-mL glass reactor was equipped with a magnetic stir bar, charged with 20 mL toluene, and cooled to –30 °C. To this pre-chilled reactor, with vigorous stirring, was added 0.30 g (0.58 mmol) *rac*-(EBI)ZrMe(OTf) followed by addition of 0.07 g (0.58 mmol) lithium amide enolate $LiOC(NMe_2)=CMe_2$. The resulting suspension was stirred for 1 d at ambient temperature, after which it was filtered through a pad of Celite. The solvent of the filtrate was removed in vacuo, yielding 0.27 g (96%) of the spectroscopically pure **2** as a yellow powder. Anal. Calcd. for $C_{27}H_{31}NOZr$: C, 68.02; H, 6.55; N, 2.94. Found: C, 67.75; H, 6.51; N, 2.89.

^{1}H NMR (C_6D_6, 23°C) for **2**: δ 7.42 (d, J = 9.2 Hz, 1H), 7.18–6.80 (m, 7H), 6.37 (d, J = 3.2 Hz, 1H), 6.14 (d, J = 3.2 Hz, 1H), 5.83 (d, J = 3.2 Hz, 1H), 5.62 (d, J = 3.2 Hz, 1H), 3.20–2.80 (m, 4H, CH_2CH_2), 2.22 (s, 6H, NMe_2), 1.91 (s, 3H, $=CMe_2$), 1.31 (s, 3H, $=CMe_2$), –0.53 (s, 3H, $ZrCH_3$). ^{13}C NMR (C_6D_6, 23°C): δ 156.42 [$OC(NMe_2)=$], 127.70, 126.77, 125.95, 124.97, 124.71, 124.55, 124.29, 123.24, 122.76, 121.93, 121.18, 118.94, 115.86, 114.33, 111.38, 105.10, 102.97, 95.54 (18 resonances for indenyl-ring carbons), 95.14 ($=CMe_2$), 42.48 (NMe_2), 30.68 ($ZrCH_3$), 28.39 (CH_2CH_2), 27.60 (CH_2CH_2), 19.10 ($=CMe_2$), 18.68 ($=CMe_2$).

Synthesis of *rac*-(EBI)Zr$^+$(THF)[OC(NMe$_2$)=CMe$_2$][MeB(C$_6$F$_5$)$_3$]$^-$ (3). In an argon-filled glovebox, a 30-mL glass reactor was equipped with a magnetic stir bar, charged with 100 mg (0.210 mmol) **2**, 123 mg (0.210 mmol) $(C_6F_5)_3B$•THF, and 5 mL CH_2Cl_2. The resulting dark red solution was allowed to stir for 20 min at ambient temperature before the solvent was removed in vacuo, affording a sticky orange-red residue. This residue was washed with 3 × 2 mL of hexanes and dried under vacuum for 2 h, yielding 214 mg (96%) of the analytically pure title compound as an orange-red powder. Anal. Calcd. for $C_{49}H_{39}BF_{15}NO_2Zr$: C, 55.48; H, 3.71; N, 1.32. Found: C, 55.74; H, 4.00; N, 1.38.

^{1}H NMR (CD_2Cl_2, 23°C) for **3**: δ 8.12 (d, J = 8.4 Hz, 1H), 7.95 (d, J = 8.8 Hz, 1H), 7.50–7.16 (m, 6H), 6.31 (m, 2H), 6.23 (m, 2H), 4.12 (m, 2H, CH_2CH_2), 3.85 (m, 2H, CH_2CH_2), 3.76 (s, br, 2H, α-CH_2, THF), 3.46 (s, br, 2H, α-CH_2, THF), 2.38 (s, 6H, NMe_2), 2.04 (s, br, 2H, β-CH_2, THF), 1.88 (s, br, 2H, β-CH_2, THF), 1.51 (s, 3H, $=CMe_2$), 1.40 (s, 3H, $=CMe_2$), 0.51 (s, br, 3H, BCH_3). ^{19}F NMR (CD_2Cl_2, 23°C): δ –131.50 (d, $^3J_{F\text{-}F}$ = 24.3 Hz, 6F, *o*-F), –163.51 (t, $^3J_{F\text{-}F}$ = 18.4 Hz, 3F, *p*-F), –166.13 (t, $^3J_{F\text{-}F}$ = 18.4 Hz,

6F, *m*-F). ^{13}C NMR (CD_2Cl_2, 23°C): δ 155.83 [O*C*(NMe$_2$)=], 148.83 (d, $^1J_{C\text{-}F}$ = 238.4 Hz, C_6F_5), 138.03 (d, $^1J_{C\text{-}F}$ = 249.2 Hz, C_6F_5), 136.94 (d, $^1J_{C\text{-}F}$ = 237.7 Hz, C_6F_5), 133.44, 133.30, 128.47, 128.11, 127.80, 127.54, 126.72, 126.10, 124.65, 124.36, 123.99, 123.63, 123.26, 121.62, 118.56, 117.62, 104.41, 103.85 (18 resonances for indenyl-ring carbons), 102.05 (=*C*Me$_2$), 78.62 (*α*-*C*H$_2$, THF), 42.29 (N*Me*$_2$), 31.11 (*C*H$_2$CH$_2$), 30.32 (CH$_2$*C*H$_2$), 26.63 (*β*-*C*H$_2$, THF), 19.41 (=C*Me*$_2$), 17.45 (=C*Me*$_2$), 10.11 (B*C*H$_3$).

Isolation of *rac*-(EBI)Zr$^+$[OC(NH^{i}Pr)=CHCH$_2$C(Me$_2$)C(O^{i}Pr)=O] [MeB(C$_6$F$_5$)$_3$]$^-$ (4)—the Single IPAA Addition Product of 1. In an argon-filled glovebox, a 30-mL glass reactor was charged with 49.2 mg (0.100 mmol) of *rac*-(EBI)ZrMe[OC(O^{i}Pr)=CMe$_2$], 58.4 mg (0.100 mmol) of $(C_6F_5)_3B$•THF, and 10 mL of CH_2Cl_2; this solution was allowed to stir for 10 min at ambient temperature, cleanly generating **1** in situ.[19] To this vigorously stirred solution of **1** in CH_2Cl_2 was added 11.3 mg (0.100 mmol) IPAA at ambient temperature. The color of the resulting mixture changed instantaneously from dark orange to bright yellow. The solution was stirred for 1 h, after which the volatiles were removed in vacuo to afford a sticky yellow solid. This crude product was washed with 3 × 2 mL hexanes and dried in vacuo to give 0.103 g (86%) of the pure title complex as a yellow powder. Anal. Calcd. for $C_{52}H_{43}BF_{15}NO_3Zr$: C, 55.92; H, 3.88; N, 1.25. Found: C, 56.02; H, 4.19; N, 1.20.

^{1}H NMR (CD_2Cl_2, 23°C) for **4** (generated in situ): δ 8.08 (d, *J* = 8.4 Hz, 1H), 7.81 (d, *J* = 8.4 Hz, 1H), 7.36–7.02 (m, 6H), 5.88 (d, *J* = 3.0 Hz, 1H), 5.79 (d, *J* = 3.0 Hz, 1H), 5.60 (d, *J* = 3.0 Hz, 1H), 5.46 (d, *J* = 3.0 Hz, 1H), 4.85 (d, *J* = 8.1 Hz, 1H, =C*H*), 4.65 (sept, *J* = 6.3 Hz, 1H, OC*H*Me$_2$), 4.30–3.96 (m, 2H, C*H*$_2$CH$_2$), 3.87–3.74 (m, 2H, CH$_2$C*H*$_2$), 3.68 (t, br, 4H, *α*-C*H*$_2$, free THF derived from **1**), 3.59 (sept, *J* = 6.6 Hz, 1H,

HNC*H*Me$_2$), 1.97 (d, J = 13.8 Hz, 1H, CH_2), 1.82 (t, 4H, β-CH_2, free THF), 1.75 (d, J = 13.8 Hz, 1H, CH_2), 1.37 (d, J = 6.0 Hz, 3H, NCH*Me*$_2$), 1.22 (s, 3H, C*Me*$_2$), 1.20 (d, J = 6.0 Hz, 3H, OCH*Me*$_2$), 1.19 (d, J = 6.0 Hz, 3H, OCH*Me*$_2$), 1.14 (s, 3H, C*Me*$_2$), 1.05 (d, J = 6.0 Hz, 3H NCH*Me*$_2$), 0.49 (s, br, 3H, B*Me*). ^{19}F NMR (CD_2Cl_2, 23°C): δ –131.45 (d, $^3J_{F\text{-}F}$ = 19.8 Hz, 6F, *o*-F), –163.58 (t, $^3J_{F\text{-}F}$ = 19.5 Hz, 3F, *p*-F), –166.14 (m, 6F, *m*-F). ^{13}C NMR (CD_2Cl_2, 23°C): δ 185.59 [*C*(O^{i}Pr)=O], 171.40 [O*C*(NHMe$_2$)=], 148.77 (d, $^1J_{C\text{-}F}$ = 229.0 Hz, C_6F_5), 138.00 (d, $^1J_{C\text{-}F}$ = 234.5 Hz, C_6F_5), 136.90 (d, $^1J_{C\text{-}F}$ = 238.1 Hz, C_6F_5), 133.10, 130.60, 128.62, 128.36, 127.91, 127.51, 125.43, 124.57, 122.66, 122.52, 121.82, 121.39, 120.20, 119.44, 113.61 and 99.86 (indenyl carbons), 97.38 (=*C*H), 73.76 (α-*C*H$_2$, free THF), 68.35 (O*C*HMe$_2$), 43.47 (HN*C*HMe$_2$), 42.54 (*C*H$_2$), 39.54 (*C*Me$_2$), 31.82 (C*Me*$_2$), 30.91 (β-*C*H$_2$, free THF), 27.25 (C*Me*$_2$), 26.35 (*C*H$_2$CH$_2$), 26.12 (CH$_2$*C*H$_2$), 23.79, 22.51, 21.82, 20.93 (HNCH*Me*$_2$, OCH*Me*$_2$), 10.80 (B*Me*).

Isolation of *rac*-(EBI)Zr$^+$[OC(NMe$_2$)=C(Me)CH$_2$C(Me$_2$)C(NMe$_2$)=O] [MeB(C$_6$F$_5$)$_3$]$^-$ (5)—the Single DMMA Addition Product of 3. In an argon-filled glovebox, a 30-mL glass reactor was charged with 28.5 mg (0.060 mmol) of **2**, 35.0 mg (0.060 mmol) of $(C_6F_5)_3B$•THF, and 5 mL of CH_2Cl_2; this solution was allowed to stir for 10 min at ambient temperature, cleanly generating **3** in situ (vide supra). To this vigorously stirred solution of **3** in CH_2Cl_2 was added 7.3 μL (0.060 mmol) DMMA at ambient temperature. The color of the resulting mixture changed instantaneously from dark red to light orange. The solution was stirred for 30 min, after which the volatiles were removed in vacuo to afford a sticky yellow solid. This crude product was washed with 5 × 2 mL hexanes and dried in vacuo to give 62.8 mg (95 %) of the title complex as an orange powder.

^{1}H NMR (CD_2Cl_2, 23°C) for **5**: δ 7.93 (d, J = 8.4 Hz, 1H), 7.75 (d, J = 8.4 Hz, 1H), 7.30–7.00 (m, 6H), 5.99 (d, J = 2.8 Hz, 1H), 5.71 (m, 2H), 5.56 (d, J = 2.8 Hz, 1H), 3.88–3.62 (m, 4H, CH_2CH_2), 3.23, 2.65, and 2.62 (s, 12H, NMe_2), 2.01 (d, J = 16.8 Hz, 1H, CH_2), 1.85 (d, J = 16.8 Hz, 1H, CH_2), 1.47 (s, 3H, =CMe), 1.39 (s, 3H, CMe_2), 1.38 (s, 3H, CMe_2), 0.50 (s, br, 3H, BMe). ^{19}F NMR (CD_2Cl_2, 23°C): δ –131.42 (d, $^3J_{F\text{-}F}$ = 19.2 Hz, 6F, *o*-F), –163.48 (t, $^3J_{F\text{-}F}$ = 20.3 Hz, 3F, *p*-F), –166.07 (m, 6F, *m*-F). ^{13}C NMR (CD_2Cl_2, 23°C): δ 180.56 [*C*(NMe$_2$)=O], 168.85 [O*C*(NMe$_2$)=], 148.90 (d, $^1J_{C\text{-}F}$ = 237.1 Hz, C_6F_5), 138.01 (d, $^1J_{C\text{-}F}$ = 243.0 Hz, C_6F_5), 136.97 (d, $^1J_{C\text{-}F}$ = 248.0 Hz, C_6F_5), 132.18, 130.37, 127.41, 126.80, 126.62, 126.27, 123.29, 122.88, 122.69, 122.50, 122.07, 115.83, 112.55, 103.40 (indenyl carbons), 101.56 (=*C*Me), 47.36 [C(NMe_2)=O], 41.35 (*C*H$_2$), 41.11 and 40.65 [OC(NMe_2)=], 38.14 (*C*Me$_2$), 30.36 (CMe_2), 29.27 and 28.98 (*C*H$_2$*C*H$_2$), 28.49 (CMe_2), 22.11 (=CMe), 10.80 (BMe).

X-Ray Crystallographic Analysis of 2. Single crystals suitable for X-ray diffraction studies were grown by recrystallization from hexanes at –30 °C inside a freezer of the glovebox for 3 days and then quickly covered with a layer of Paratone-N oil (Exxon, dried and degassed at 120 °C/10^{-6} Torr for 24 h) after decanting the mother liquor. A crystal was then mounted on a thin glass fiber and transferred into the cold nitrogen steam of a Bruker SMART CCD diffractometer. Crystals of **2** were twinned by 180° rotation about the *a* axis. Identification of the twin law and deconvolution of the twinned diffraction patterns were accomplished by means of the Bruker software.[20a] The structure was solved by direct methods and refined by using the Bruker SHELXTL program library.[20b] The structure was refined by full-matrix least-squares on F^2 for all reflections, with two batch scale factors included to allow refinement against the

deconvoluted data from the twinned crystal. All non-hydrogen atoms were refined with anisotropic displacement parameters, whereas hydrogen atoms were included in the structure factor calculations at idealized positions. The asymmetric unit of **2** contained two discrete molecules with similar structures. Selected crystal data and structural refinement parameters are collected in Table 1.

Table 1. Crystal Data and Structure Refinements for **2**.

	2
empirical formula	$C_{27}H_{31}NOZr$
formula weight	476.75
temperature/K	100(2) K
wavelength/Å	0.71073
crystal system	Monoclinic
space group	*P*21/*c*
a/Å	16.3387(9)
b/Å	7.5650(4)
c/Å	36.764(2)
α/deg	90
β/deg	94.2420(10)
γ/deg	90
volume/Å^3	4531.7(4)
Z	8
density (calcd)/ Mg/m^3	1.398
abs coeff/mm^{-1}	0.503
F(000)	1984
crystal size/mm^3	0.32 x 0.24 x 0.03
θ range for data collection/°	1.11 to 27.35
index ranges	$-21 \le h \le 15$, $-9 \le k \le 9$, $-47 \le l \le 47$
reflections collected	8084
independent reflections	8266
completeness to θ	27.35° 43.5 %
data /restraints/parameters	8266/1208/528
goodness-of-fit on F^2	1.104
final R indices [$I>2\sigma(I)$]	$R_1 = 0.0523$; $wR_2 = 0.0986$
R indices (all data)	$R_1 = 0.1025$; $wR_2 = 0.1052$
largest diff. Peak and hole/eÅ^{-3}	0.825 and -0.584

General Polymerization Procedures. Polymerizations were performed either in 30-mL, oven-dried glass reactors inside the glovebox, or in 25-mL oven- and flame-dried Schlenk flasks interfaced to a dual-manifold Schlenk line. In a typical procedure, for polymerizations using the in situ generated **1**, a 2.5 mL stock solution of *rac*-(EBI)ZrMe[OC(O^{i}Pr)=CMe$_2$] (24.3 μmol) in CH_2Cl_2 was mixed in a flask with a solution of $(C_6F_5)_3B$•THF (24.3 μmol) in 2.5 mL CH_2Cl_2 and stirred for 10 min to cleanly generate the cationic zirconocenium ester enolate **1**. DMAA (1.00 mL, 9.70 mmol) was quickly added via pipette (for polymerizations in the glovebox) or gastight syringe (for polymerizations on the Schlenk line), and the sealed flask was kept with vigorous stirring at the pre-equilibrated bath temperature. For polymerizations using the isolated active species **3**, 24.3 μmol **3** was dissolved in 5 mL CH_2Cl_2 in a 25 mL Schlenk flask. DMAA (1.00 mL, 9.70 mmol) was quickly added via gastight syringe, and the sealed flask was kept with vigorous stirring at the pre-equilibrated bath temperature. After the measured time interval, polymerizations were quenched by the addition of 5 mL of 5% HCl-acidified methanol. The quenched mixture was precipitated into 100 mL of diethyl ether, stirred for 30 min, and the solvent was decanted off. An additional 75 mL of diethyl ether was used to wash the polymer and then decanted. The P(DMAA) product was obtained as a sticky solid and dried in a vacuum oven at 50 °C overnight to a constant weight. The polymer was dissolved in minimum CH_2Cl_2 or MeOH, precipitated into a 10-fold excess of diethyl ether, stirred for 30 min., filtered, washed with diethyl ether, and dried in a vacuum oven at 50 °C for 48 h to a constant weight. The P(DMAA) polymers obtained are white fibrous materials.

Polymerization Kinetics. The procedures already developed for the kinetic studies of methacrylate polymerization[19] were modified for the kinetic experiments of acrylamide polymerization. The experiments were carried out in stirred Schlenk flasks at 23 °C using the same polymerization procedure as already described above, except that, at appropriate time intervals, 0.2 mL aliquots were withdrawn from the reaction mixture via syringe and quickly quenched into 1 mL vials containing 0.6 mL of undried "wet" $CDCl_3$ stabilized by 250 ppm of BHT-H. The quenched aliquots were analyzed by ^1H NMR. The ratio of $[DMAA]_0$ to $[DMAA]_t$ at a given time t, $[DMAA]_0/[DMAA]_t$, was determined by integration of the peaks for DMAA (6.3–6.1 and 5.7–5.5 ppm for the vinyl proton signals) and P(DMAA) (centered at 2.5 ppm for the methine proton signal) according to $[DMAA]_0/[DMAA]_t = (\mathbf{A}_{2.5}/\mathbf{A}_{5.6+6.2}) + 1$, where $\mathbf{A}_{2.5}$ is the total integrals for the peaks centered at 2.5 ppm (typically in the region 2.3–2.6 ppm) and $\mathbf{A}_{5.6+6.2}$ is the total integrals for the vinyl protons in the regions 5.7–5.5 and 6.3–6.1 ppm. Apparent rate constants (k_{app}) were extracted from the slopes of the best fit lines to the plots of $\ln([DMAA]_0/[DMAA]_t)$ vs time.

Polymer Characterizations. The low-molecular-weight P(DMAA) sample was analyzed by matrix-assisted laser desorption/ionization time-of-flight mass spectroscopy (MALDI–TOF MS); the experiment was performed on an Ultraflex MALDI-TOF mass spectrometer (Bruker Daltonics) operated in reflector mode using a Nd:YAG laser at 355 nm and 25 kV accelerating voltage. A thin layer of a 1% NaI solution was first deposited on the target plate, followed by 1 μl of both sample and matrix (dithranol, 10mg/mL in MeOH).

Powder X-ray diffraction (XRD) analyses were performed on powder samples with a Scintag X2 Advanced Diffraction System using Cu Kα (λ = 1.5418 Å) radiation and a Peltier detector on the diffracted beam side. In all cases measurements were performed with a step size of 0.02° with 1.0 second per step. Peak fittings were done using the Split-Pearson VII function using DMNST version 1.37 software.[21] When the annealing treatment was applied, the powdered polymer sample was clamped between two foil covered glass slides and placed in an oven at 140 °C for ~60 h.

Glass transition and melting transition temperatures (T_g and T_m) of the polymers were measured by differential scanning calorimetry (DSC) on a DSC 2920 (TA Instruments). Samples were first heated to 180 °C at 20 °C/min, equilibrated at this temperature for 4 min, and then cooled to 0 °C at 10 °C/min. After being held at this temperature for 4 min, the samples were reheated to 360 °C at 10 °C/min. All T_g and T_m values were obtained from the second scan, after removing the thermal history. Maximum rate decomposition temperatures (T_{max}) and decomposition onset temperatures (T_{onset}) were measured by thermogravimetric analysis (TGA) on a TGA 2950 (TA Instruments). All samples were heated from ambient temperature to 600 °C at a rate of 10 °C/min. Values for T_{max} were obtained from derivative (wt%/°C) vs. temperature (°C) plots, while T_{onset} values were obtained from wt% vs. temperature (°C) plots.

Gel permeation chromatography (GPC) analyses of the polymers was carried out at 40 °C and a flow rate of 1.0 mL/min, with $CHCl_3$ as the eluent, on a Waters University 1500 GPC instrument that was calibrated using 10 PMMA standards. Chromatograms were processed with Waters Empower software (2002); number-average molecular weight and polydispersity of polymers were given relative to PMMA standards.

^{1}H NMR spectra, for the analysis of PDMAA *m/r* dyads, and ^{13}C NMR spectra, for the analysis of PDMAA *mm/rr+mr* triads, were recorded in $CDCl_3$ at 50°C and in D_2O at 80°C, respectively, and analyzed according to the literature.[22] Chemical shifts for ^{1}H and ^{13}C NMR spectra in $CDCl_3$ were referenced to internal solvent resonances and are reported as parts per million relative to tetramethylsilane, whereas the Chemical shifts for ^{13}C NMR spectra in D_2O were referenced to external carbonyl carbon [*mm*] triad resonances previously measured in $CDCl_3$.

Results and Discussion

Initial DMAA polymerizations using the *in situ* generated *rac*-(EBI)ZrMe$^+$MeM$(C_6F_5)_3^-$ (EBI = $C_2H_4(Ind)_2$; M = B, Al) yielded PDMAA of low isotacticity. The control runs showed that the neutral metallocene dimethyl and the activator alane themselves, but not the borane, are active for the polymerization of DMAA (entries 1–3, Table 1). The P(DMAA) obtained, however, is atactic with a broad molecular weight distributions (MWDs) and the polymerization can be completely shut down by adding an established, effective radical inhibitor (galvinoxyl);[23] all evidence points to a radical process. It should be noted that none of these neutral alkyl metallocenes and the Lewis acid activators is active for polymerization of methacrylates.

On the basis of this finding, we subsequently used the *isolated* alkyl cations for the polymerization of DMAA (entries 4 and 5, Table 1). The cation *rac*-(EBI)ZrMe$^+$MeB$(C_6F_5)_3^-$ now produce highly isotactic P(DMAA) ([*mm*] = 93%; Figure 1), whereas *rac*-(EBI)ZrMe$^+$MeAl$(C_6F_5)_3^-$ afforded P(DMAA) with moderate isotacticity of [*mm*] = 61%, presumably due to the greater propensity for *rac*-

(EBI)ZrMe$^+$MeAl$(C_6F_5)_3^-$ to dissociate back to the neutral metal alkyl and the activator in solution than for *rac*-(EBI)ZrMe$^+$MeB$(C_6F_5)_3^-$.[24] Nevertheless, both P(DMAA)s formed exhibit high melting transition temperatures, T_m, of > 310 °C and moderate PDI of < 2.0. To inhibit any possible radical processes initiated by the neutral species derived from the dynamic ion pair reorganization processes of the alkyl cation,[25] the addition of 2 equiv of galvinoxyl to the polymerization led to enhanced isospecificity of both cations ([*mm*] = 98%; entries 6 and 7, Table 4.1), but gave high PDI of > 3.2. Although both the polymerizations with and without galvinoxyl gave quantitative polymer yields for 24 h, the polymerization activity difference is much more pronounced at a shorter reaction time. For example, the yields for 2 h polymerization reaction by *rac*-(EBI)ZrMe$^+$MeB$(C_6F_5)_3^-$ without and with galvinoxyl were 78% and 24%, respectively.

Table 1. Results of DMAA Polymerization and Properties of P(DMAA)[a]

entry	complex	yield (%)	M_n[b] (kg/mol)	PDI[b] (M_w/M_n)	T_g[c] (°C)	T_m[c] (°C)	T_{max}[d] (°C)	[*mm*]/[*mr* + *rr*][e] ([*m*/*r*])[f]
1	*rac*-(EBI)ZrMe$_2$	>99	11800	7.33	126	-	433	(52/48)
2	Al$(C_6F_5)_3$	>99	44.3	8.82	122	-	-	(51/49)
3	B$(C_6F_5)_3$	0	-	-	-	-	-	-
4	*rac*-(EBI)ZrMe$^+$ MeB$(C_6F_5)_3^-$	>99	30.2	1.51	-	310	430	93/7
5	*rac*-(EBI)ZrMe$^+$ MeAl$(C_6F_5)_3^-$	>99	106	1.97	111	313	429	61/39
6[g]	*rac*-(EBI)ZrMe$^+$ MeB$(C_6F_5)_3^-$	>99	544	3.21	-	312	427	98/2
7[g]	*rac*-(EBI)ZrMe$^+$ MeAl$(C_6F_5)_3^-$	>99	613	7.91	-	308	429	98/2
8	*rac*-(EBI)ZrMe$^+$ MeB$(C_6F_5)_3^-$	>99	270	1.90	112	306	422	82/18
9[g]	*rac*-(EBI)ZrMe$^+$ MeB$(C_6F_5)_3^-$	92	1140	7.00	-	316	431	>99
10	**1**	93	92.7	1.07	-	306	428	>99
11[g]	**1**	93	104	1.07	-	318	420	>99

[a]All polymerizations were carried out in an argon-filled glovebox (oxygen and moisture < 1.0 ppm) at ambient temperature (~25 °C) for 24 h (entries 1-9) or 2 h (entries10-11); 5 mL of toluene (entries 1-7) or CH_2Cl_2 (entries 8-11); $[DMAA]_0/[complex]_0$ = 400:1. [b]Number-average molecular weight and polydispersity index determined by GPC in $CHCl_3$ relative to PMMA standards. [c]Glass (T_g) and melting (T_m) transition temperatures determined by DSC from a second scan. [d]dwt%/dT peak max for maximum rate decomposition (T_{max}) temperatures determined by

TGA. [e] Carbonyl triads determined by ^{13}C NMR spectroscopy in D_2O at 80 °C. [f]Data in parenthesis are methylene dyads (*m/r*) determined by ^{1}H NMR spectroscopy in $CDCl_3$ at 50 °C. [g] Polymerizations ran in the presence of the free radical trap, galvinoxyl.

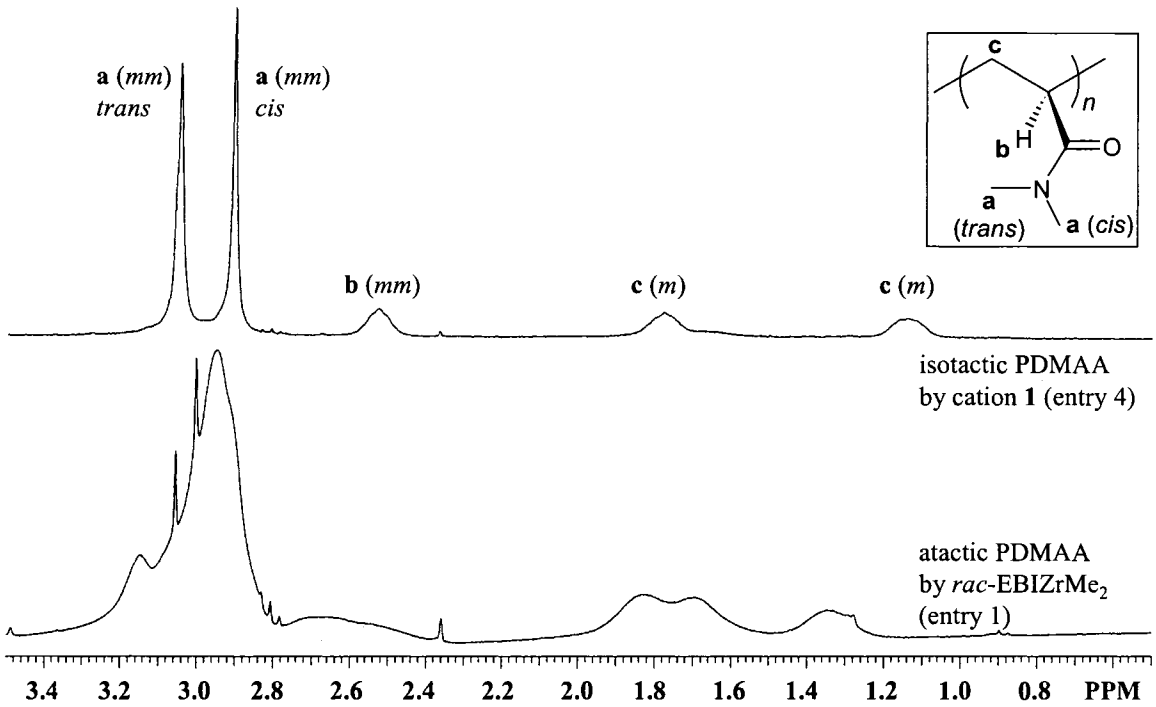

Figure 1. ^{1}H NMR spectra ($CDCl_3$, 50 °C) of isotactic P(DMAA) by *rac*-(EBI)ZrMe^{+}MeB$(C_6F_5)_3^{-}$ (top: entry 4, Table 1) and atactic P(DMAA) by neutral *rac*-(EBI)$ZrMe_2$ (bottom: entry 1, Table 1) for comparison.

The considerably increased PDI values with galvinoxyl is initially surprising, but this may be attributed to the inhomogeneity of the reaction in toluene, as a result of the enhanced P(DMAA) isotacticity ([*mm*] = 98%) and high M_n (> 5 × 10^5). In attempts to overcome the inhomogeneity, we used CH_2Cl_2 for polymerizations by *rac*-(EBI)ZrMe^{+}MeB$(C_6F_5)_3^{-}$ and *rac*-(EBI)ZrMe^{+}MeB$(C_6F_5)_3^{-}$/galvinoxyl (entries 8 and 9, Table 1). The substantially increased and uncontrolled M_n of P(DMAA) produced in CH_2Cl_2 vs. in toluene (e.g., 1.14 × 10^6 in entry 9 vs 5.44 × 10^5 in entry 6, Table 1) continued creating the inhomogeneity problem, leading to high PDI values.

A demonstrated strategy for controlling polymer M_n and PDI in the case of methacrylate polymerization is to use the cationic chiral zirconocene *ester enolate* initiator, because it simulates the active propagating species that has bypassed the slow initiation step starting from the cationic alkyl initiator.[8a,o,12d,26] Although the anticipated propagating species for DMAA polymerization is a cationic zirconocene *amide* enolate, the chiral zirconocene *ester* enolate initiator should impose a similar effect on M_n and PDI of P(DMAA). Indeed, DMAA polymerization using the isolated cationic ester enolate **1** is much more reactive than that by the alkyl cation *rac*-(EBI)ZrMe$^+$MeB$(C_6F_5)_3^-$ (2 h in entry 10 vs 24 h in entry 8, Table 1), and more importantly, the polymerization is now much more controlled, as indicated by M_n of 9.27 $\times$ 10^4 and low PDI of 1.07 (right column, Figure 2). The formation of a virtually stereodefect-free isotactic P(DMAA) by ^{13}C NMR ([*mm*] > 99%; Figure 3), even in the absence of the radical inhibitor, is another remarkable feature of this polymerization. The same polymerization, but in the presence of 2 equiv of galvinoxyl, gave nearly identical polymerization results (entry 11 vs 10, Table 1), except for a noticeably higher T_m of 318 °C, presumably due to a higher M_n of 1.04 $\times$ 10^5. These results demonstrate the DMAA polymerization initiated by the cationic ester enolate **1** is free of radical processes, well controlled, and highly isospecific.

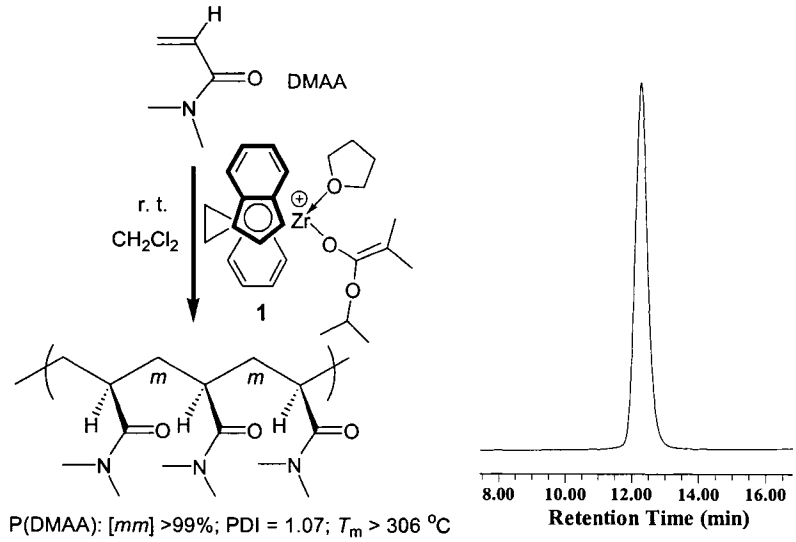

Figure 2. Polymerization of DMAA by **1**, producing P(DMAA) (left) with PDI = 1.07 (right: GPC trace).

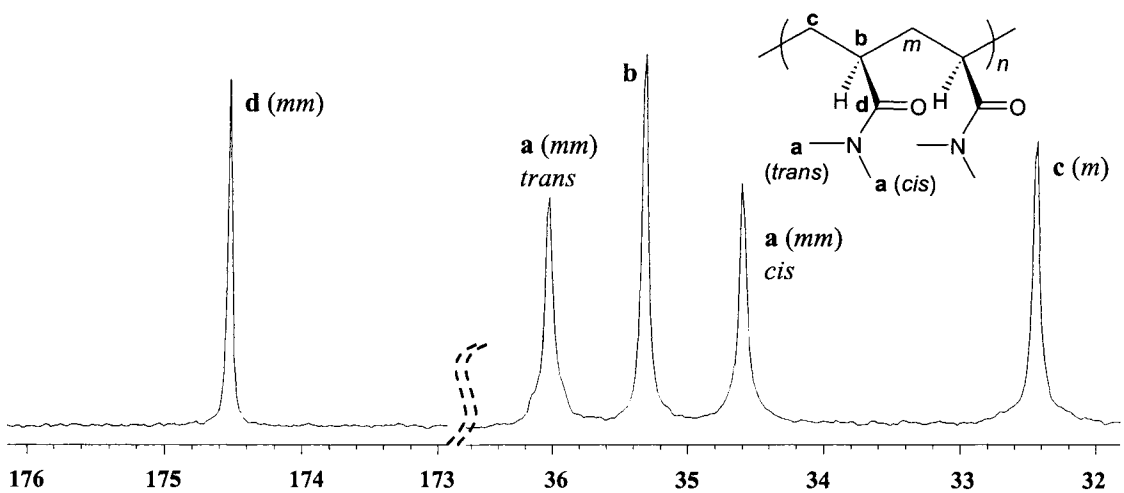

Figure 3. ^{13}C NMR spectrum (D_2O, 80 °C) of highly isotactic P(DMAA) by cation **1** ([mm] > 99%, entry 10, Table 1).

All isotactic PDMAAs obtained from this study are insoluble in toluene, diethyl ether, THF, or DMF, but soluble in methanol, water, and chloroform. They exhibit high T_m (> 306 °C) and single, high decomposition temperatures as shown by maximum rate

decomposition temperatures (T_{max}) of 420–430 °C with narrow decomposition temperature windows (Table 1).

Unlike the amorphous or moderately isotactic PDMAAs, which exhibit defined glass transition (T_g) endothermic peaks on DSC traces (entries 1, 2, 5, and 8, Table 1), the PDMAAs with isotacticity [*mm*] > 90% do not show noticeable T_g's (or are too broad to define) because of their high crystallinity (Figure 4). The crystallization temperature (T_c) of isotactic PDMMA is typically in the range of 260–270 °C under our DSC conditions (see Experimental section for details). The isotactic PDMAAs are crystalline when isolated (quenched) directly from a polymerization reaction. As shown by the X-ray diffraction (XRD) plots in Figure 5, no annealing treatment is necessary for isotactic PDMAA to develop substantial crystallinity (plot **b**, Figure 5), although annealing can further increase the crystallinity as the two characteristic scattering peaks (*d* spacing: 0.78 and 0.50 nm) increase their intensity and sharpness after being annealed at 140 °C for 60 h (plot **c**, Figure 5). The XRD of atactic PDMAA produced by *rac*-(EBI)$ZrMe_2$ is included in the plot for comparison (plot **a**, Figure 5).

These results nicely demonstrate the first stereospecific coordination polymerization of DMAA which was effected by the chiral *ansa*-zirconocenium ester enolate **1**, producing P(DMAA) with unprecedented isotacticities ([*mm*]) of >99%, high M_n of ~10^5 g/mol, narrow MWDs (M_w/M_n) of 1.07, T_m of >306 °C, and T_{max} of >420 °C (Figure 2). However, mechanistic details about the DMAA polymerization by chiral *ansa*-zirconocenium enolates and the scope of this polymerization for other acrylamides were unknown and, thus, became the next challenge undertaken.

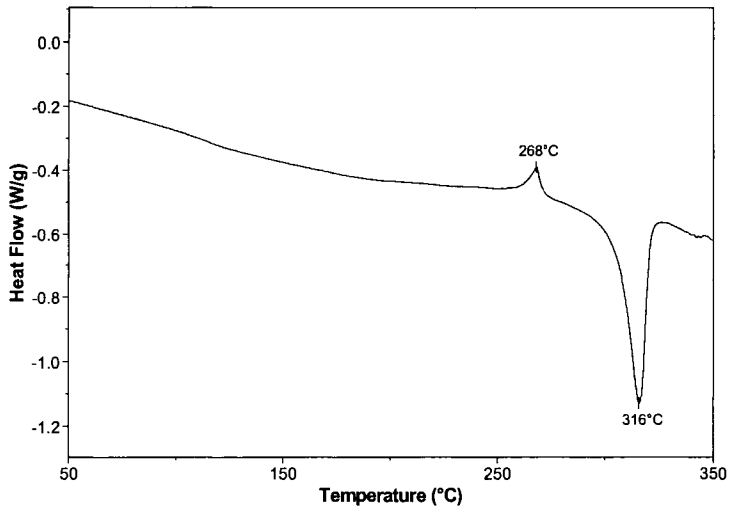

Figure 4. DSC trace of highly isotactic PDMAA by *rac*-(EBI)ZrMe^{+}MeB$(C_6F_5)_3^{-}$ /galvinoxyl (T_c = 268 °C, T_m = 316 °C; entry 9, Table 1).

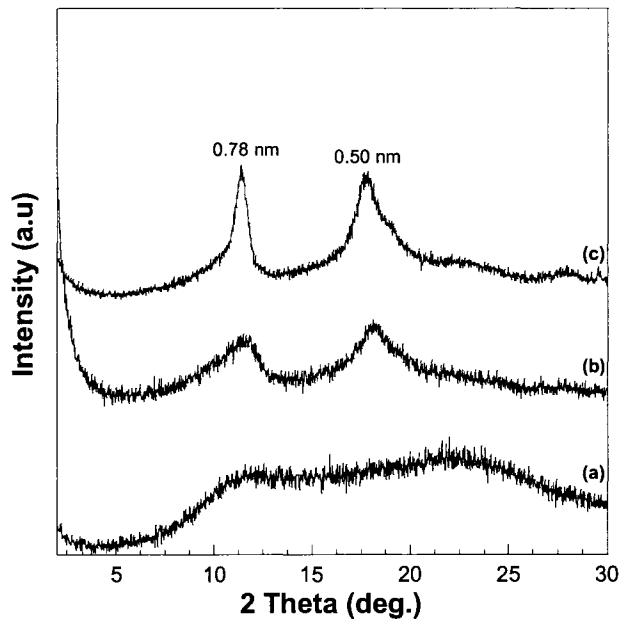

Figure 5. Overlay of XRD plots for PDMAA: (**a**) atactic (entry 1, Table 1); (**b**) isotactic (entry 6, Table 1); (**c**) same as (**b**) but annealed at 140 °C for 60 h.

Kinetics of DMAA Polymerization by 1. The chiral *ansa*-zirconocenium ester enolate **1** can be either isolated[8a] or cleanly generated in situ by mixing of the neutral

methyl zirconocene ester enolate precursor, *rac*-(EBI)ZrMe[OC(O^{i}Pr)=CMe$_2$], with $(C_6F_5)_3B$•THF in CH_2Cl_2 at room temperature.[19] The cation **1** is stable in a solution of CH_2Cl_2 at room temperature; subsequently, the in situ generated **1** in CH_2Cl_2 was used for the DMAA polymerization and kinetic studies. Typical results of DMAA polymerization by **1** in CH_2Cl_2 at 23 °C are summarized in Table 2.

As shown in Table 2, the polymerization of DMAA by **1** with $[DMAA]_0/[\mathbf{1}]_0$ ratios = 400 to 1500 is rapid and efficient with initiator efficiencies (I^*) ranging from moderate 70% to high 93%, and produces P(DMAA) with low PDI values ranging from 1.04 to 1.24. All P(DMAA) produced are highly isotactic ([*mm*] > 99%).

Several lines of evidence, including the aforementioned polymerization characteristics, the production of the well-defined diblock copolymer P(MMA)-*b*-P(DMAA) with a small PDI value of 1.07 (vide infra), and the observed linear increase of the polymer M_n with $[DMAA]_0/[\mathbf{1}]_0$ ratios and with monomer conversion, which is coupled with the small, nearly constant PDI values (Figure 6), clearly demonstrate living characteristics of this polymerization.

Results of the polymerization kinetic studies using complex **1** at 23 °C in CH_2Cl_2 with a broad range of $[DMAA]_0/[\mathbf{1}]_0$ ratios from 400 to 1500 clearly show that propagation is first order in [DMAA] for all the $[DMAA]_0/[\mathbf{1}]_0$ ratios investigated in this study (Figure 7). A double logarithm plot (Figure 8) of the apparent rate constants (k_{app}), obtained from the slopes of the best-fit lines to the plots of $\ln([DMAA]_0/[DMAA]_t)$ vs time, as a function of ln[**1**] was fit to a straight line ($R^2 = 0.998$) of slope = 1.1(1). The

Table 2. Selected DMAA Polymerization Results by Chiral *ansa*-Zirconocenium Ester Enolate Complex **1** in CH_2Cl_2 at 23 °C [a]

entry	[**1**] (mmol/L)	$[DMAA]_0/[\mathbf{1}]_0$	time (min)	conv. (%)	$10^4 M_n$ [b] (g/mol)	PDI [b] (M_w/M_n)	I^* [c] (%)
1	4.85	400	1	16	0.75	1.06	0.85
2			2	28	1.47	1.05	0.75
3			3	37	2.05	1.05	0.71
4			8	69	3.61	1.06	0.76
5			12	80	4.07	1.08	0.78
6			15	88	4.21	1.09	0.83
7			25	96	4.53	1.10	0.84
8	3.23	600	1	10	0.61	1.09	0.93
9			2	18	1.27	1.06	0.86
10			3	25	1.87	1.05	0.79
11			8	52	4.03	1.05	0.76
12			12	65	4.87	1.06	0.79
13			15	72	5.32	1.07	0.80
14			20	80	5.30	1.11	0.89
15			25	88	5.88	1.10	0.89
16			45	98	6.42	1.12	0.90
17	1.94	1000	2	9	1.13	1.08	0.80
18			3	13	1.78	1.07	0.73
19			5	28	2.98	1.06	0.91
20			14	46	6.25	1.07	0.74
21			20	56	7.25	1.11	0.77
22			30	78	10.30	1.09	0.75
23			40	84	10.24	1.13	0.81
24			60	95	13.03	1.11	0.72
25	1.62	1200	5	21	3.52	1.05	0.70
26			14	46	7.90	1.06	0.70
27			20	55	8.87	1.10	0.74
28			40	81	11.41	1.20	0.84
29			60	90	13.31	1.21	0.80
30			70	91	13.35	1.23	0.81
31			90	92	13.77	1.22	0.80
32	1.29	1500	2	8	1.26	1.06	0.90
33			5	17	3.12	1.05	0.80
34			8	23	4.79	1.04	0.70
35			14	37	7.29	1.05	0.74
36			20	45	8.83	1.07	0.76
37			30	58	10.46	1.11	0.83
38			40	68	11.61	1.16	0.87
39			50	75	13.48	1.17	0.82
40			100	90	15.85	1.24	0.84

[a] All polymerizations were carried out in flame-dried Schlenk flasks on a Schlenk line using an external temperature-control bath set at 23 °C. [b] M_n and PDI determined by GPC relative to PMMA standards in $CHCl_3$. [c] Initiator efficiency (I^*) = M_n(calcd)/M_n(exptl), where M_n(calcd) = MW(DMAA) × $[DMAA]_0/[\mathbf{1}]_0$ × conversion.

kinetic order with respect to [**1**], given by the slope of 1.1(1), reveals that propagation is also first order in [Zr], indicating a *monometallic*, intramolecular coordinative-conjugate-addition propagation mechanism.

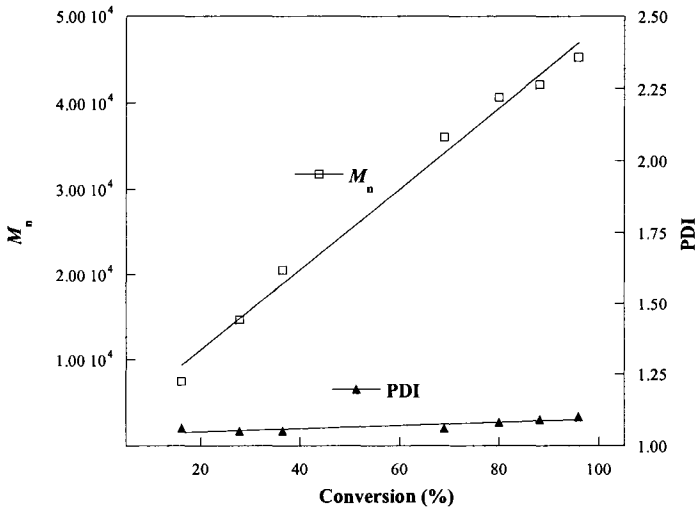

Figure 6. Plot of M_n and PDI of PDMAA by **1** {$[DMAA]_0/[1]_0$ = 400; 23 °C} vs monomer conversion.

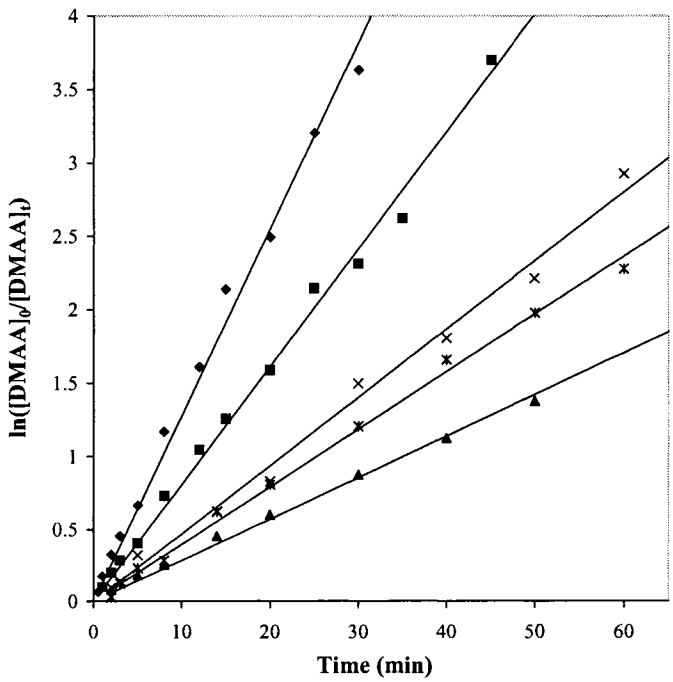

Figure 7. Semilogarithmic plots of $\ln\{[DMAA]_0/[DMAA]_t\}$ vs time for the polymerization of DMAA by **1** in CH_2Cl_2 at 23 °C. Conditions: $[DMAA]_0$ = 1.94 M, $[1]_0$ = 4.85 mM (♦), 3.23 mM (■); 1.94 mM (×), 1.62 mM (∗), and 1.29 mM (▲).

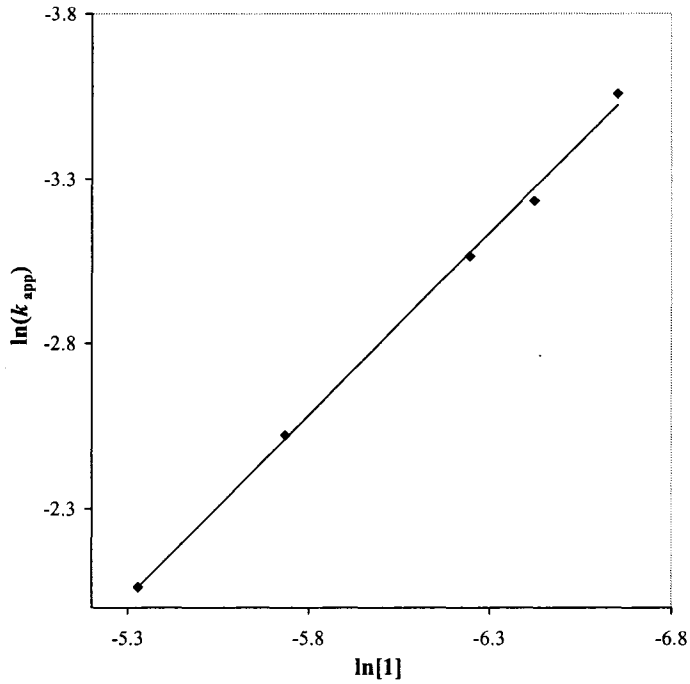

Figure 8. Plot of $\ln(k_{app})$ versus ln[**1**] for the DMAA polymerization by **1** in CH_2Cl_2 at 23 °C.

Polymer Chain-End Groups. To identify the initiation and termination chain-end groups and further confirm the living nature of this polymerization, the low-molecular-weight P(DMAA) produced by **1** in a $[DMAA]_0/[\mathbf{1}]_0$ ratio of 20:1 was characterized by MALDI-TOF mass spectrometry (Figure 9). The plot of *m/z* values in the MALDI-TOF mass spectrum vs the number of DMAA repeat units (*n*) yielded a straight line with a slope of 99.07 and an intercept of 152.86 (Figure 10); the slope corresponds to the mass of the DMAA monomer, whereas the intercept is the sum of the masses of Na^+ (from the added NaI) and the chain-end groups which correspond to a formula of $C_7H_{14}O_2$. This analysis clearly shows that the polymer has a structural formula of ^{i}PrOC(=O)C(Me_2)–(DMAA)$_n$–H, where the initiation chain end [^{i}PrOC(=O)C(Me_2)–] is derived from the initiating isopropyl isobutyrate group in complex **1** and the termination chain end (H) from the HCl-acidified methanol during the work-up procedure.

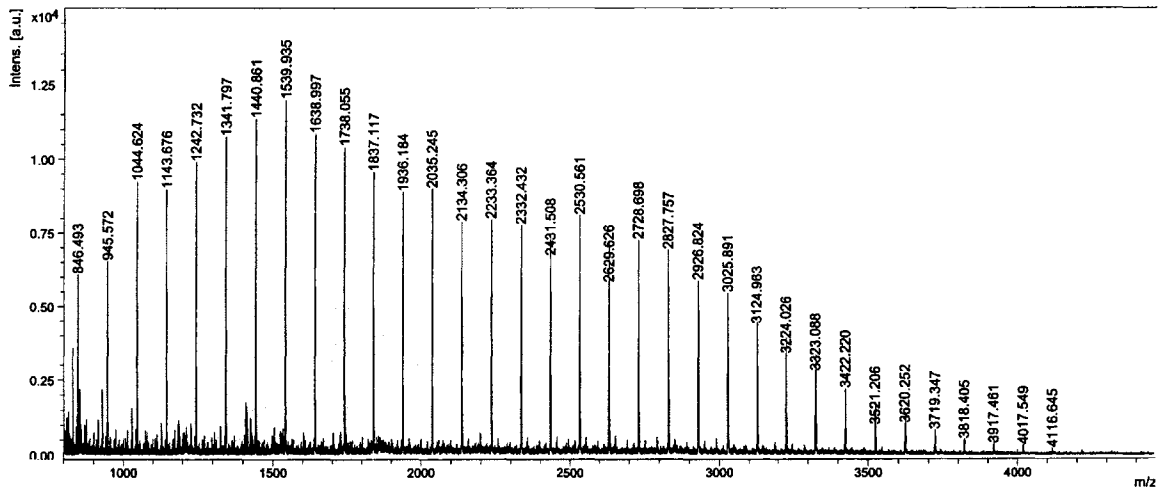

Figure 9. MALDI-TOF mass spectrum of the low-molecular-weight P(DMAA) produced by 1 in CH_2Cl_2 at 23 °C with $[DMAA]_0/[\mathbf{1}]_0$ = 20:1; the sample analyzed was as quenched and unpurified.

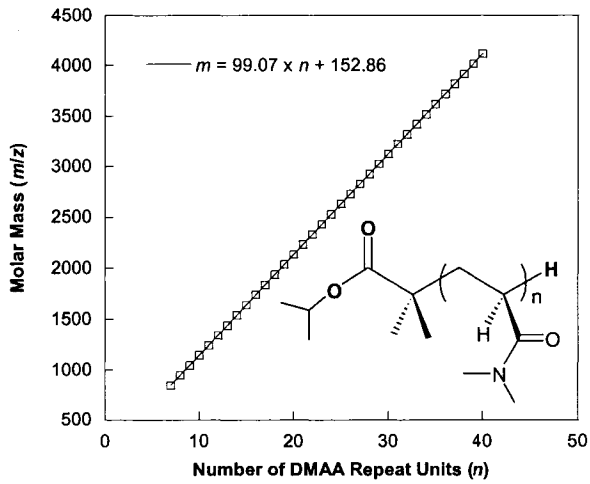

Figure 10. Plot of *m/z* values from Figure 4.9 vs the number of DMAA repeat units (*n*).

Block Copolymerization of MMA and DMAA. Sequential block copolymerization of MMA and DMAA by **1** in CH_2Cl_2 at 23 °C with $[MMA]_0/[DMAA]_0/[\mathbf{1}]_0$ = 400/400/1, starting from polymerization of MMA followed by polymerization of DMAA, afforded the well-defined diblock copolymer P(MMA)-*b*-

P(DMAA) (Figure 11). The block copolymer has an M_n of 1.33 × 10^5 g/mol and a PDI value of 1.07.

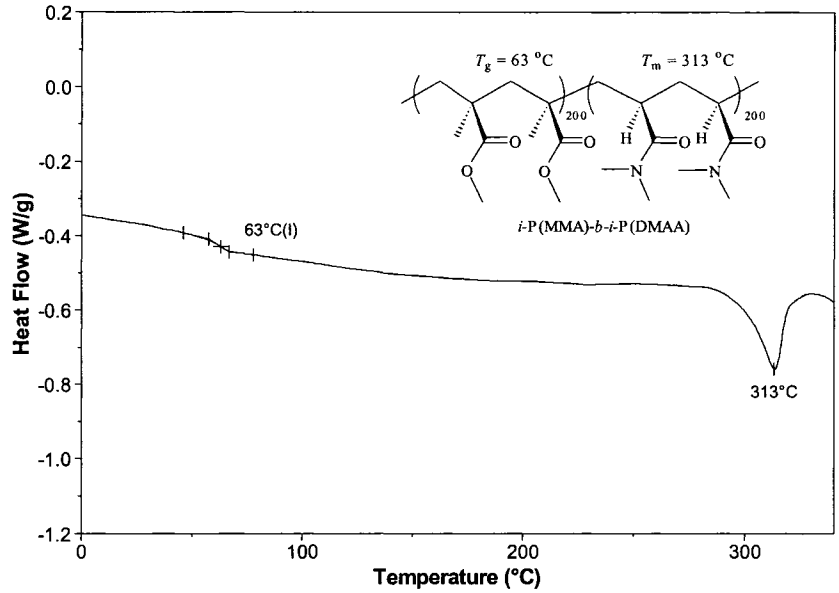

Figure 11. DSC trace of diblock copolymer P(MMA)-*b*-P(DMAA) produced by **1** in CH_2Cl_2 at 23 °C.

The molar composition of the two monomer units in the block copolymer obtained from the ^{1}H NMR analysis is the same as the monomer molar feed ratio (i.e., 1:1). Both blocks are highly isotactic, with isotacticity of [*mm*] = 93% for the P(MMA) block and of [*mm*] > 99% for the P(DMAA) block. As can be seen in Figure 11, this block copolymer exhibits a T_g characteristic of the isotactic P(MMA) component segment (T_g = 63 °C) and a T_m characteristic of the isotactic P(DMAA) component segment (T_m = 313 °C). Owing to the high crystallinity of the highly isotactic P(DMAA) block, there is no apparent T_g, but a distinct T_m, for this component segment, similar to what has been observed for the highly isotactic homopolymer P(DMAA).

Polymerization Mechanism. In sharp contrast to the facile formation of the previously mentioned diblock copolymer P(MMA)-*b*-P(DMAA), the sequential block

copolymerization starting from polymerization of DMAA followed by polymerization of MMA, or the statistical copolymerization using a 1:1 DMAA:MMA monomer pool, afforded only homopolymer P(DMAA)! The results of the DMAA homopolymerization by **1** showed living characteristics (vide supra); to further confirm the living nature of the active propagating species derived from the DMAA polymerization, a re-initiation experiment was carried out (**1** to **A** to **B** to **C**, Scheme 1). Note that structures **A**, **B**, and **C** were modeled by isolated complexes (vide infra), and that the DMAA propagation cycle (**B** ↔ **C**) is the same as that proposed for the MMA polymerization,[19] on the basis of the kinetic results. Thus, after the first portion of DMAA was completely consumed by **1**, a 45-min delay was implemented before addition of a second portion of DMAA. This polymerization sequence yielded highly isotactic P(DMAA)-*b*-P(DMAA) in quantitative yield with an M_n greater than double that of the individual block and a low PDI of 1.07, further confirming the living nature of the active propagating species **B**. On the basis of these results, the inability of the living propagating species derived from the DMAA polymerization by **1** to further polymerize MMA can be attributed to either of the following two scenarios: (a) MMA is unable to enter the preoccupied coordination site of the cationic Zr center due to stronger binding of the amide oxygen of the penultimate DMAA unit to Zr than the ester oxygen of MMA to Zr (i.e., step (iii), **C** → **D**, is not feasible), and subsequently MMA cannot be activated for the polymerization to proceed; or (b) MMA is able to displace the coordinated penultimate amide group and thus enter the coordination site of the cationic Zr center, but the polymeric amide enolate ligand derived from DMAA polymerization is not active enough to undergo nucleophilic addition to the activated MMA (i.e., step (iv), **D** → **E**, is not feasible).

Scheme 1

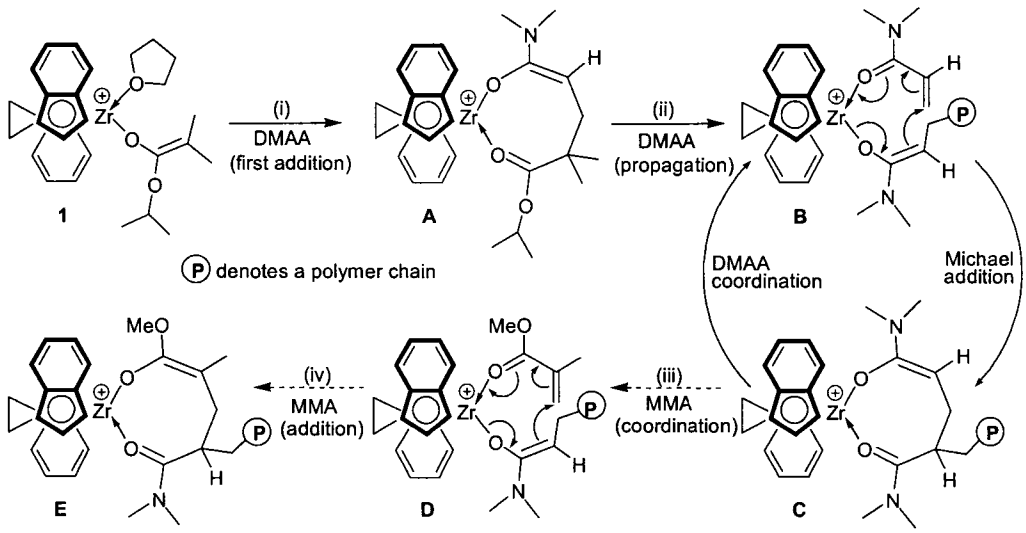

To test these hypotheses, it became necessary to independently synthesize the chiral *ansa*-zirconocene amide enolate *rac*-(EBI)ZrMe[OC(NMe$_2$)=CMe$_2$] (**2**) and the corresponding cationic complex *rac*-(EBI)Zr$^+$(THF)[OC(NMe$_2$)=CMe$_2$][MeB(C$_6$F$_5$)$_3$]$^-$ (**3**). Intuitively, the amide enolate moiety in structure **D** should be more nucleophilic than the ester enolate moiety in **1** and, thus, step (iv) is unlikely the reason for the inability of the living propagating species **B** to further polymerize MMA; however, ruling out this possibility requires an independent study of the MMA polymerization behavior using the isolated cationic amide enolate **3**. Furthermore, complex **3** models the structure of the proposed active propagating species **B** (Scheme 1). Therefore, polymerization studies using complex **3** will offer unique opportunities for a better understanding of the polymerization of acrylamides and copolymerization of acrylamides with MMA by metallocene complexes.

Scheme 2 outlines the reaction sequences leading to **2** and **3** through the *ansa*-zirconocene methyl triflate intermediate *rac*-(EBI)ZrMe(OTf),[8a] which was synthesized

utilizing the comproportionation reaction between *rac*-(EBI)$ZrMe_2$ and *rac*-(EBI)$Zr(OTf)_2$, the latter of which was prepared from the reaction *rac*-(EBI)$Zr(NMe_2)_2$ with excess triflic acid (TfOH). The subsequent reaction of *rac*-(EBI)ZrMe(OTf) with lithium amide enolate $LiOC(NMe_2)=CMe_2$ in toluene proceeds cleanly to produce the chiral zirconocene amide enolate **2** in 96% isolated yield. The ^1H NMR spectrum shows C_1-symmetry for **2** in solution, featuring four nonequivalent protons for the C_5-rings of the bis(indenyl) ligand (Figure 12, bottom), whereas the X-ray crystal structure of **2** reveals a unique s-*trans* conformation as to the Zr–Me and C=C bonds about the nearly linear Zr–O–C vector (Scheme 2). We have previously shown that metallocene *ester* enolates adopt a s-*cis* conformation;[8a,12a] the observed s-*trans* conformation in the solid state structure of the *amide* enolate **2** is presumably a result of placing the bulky NMe_2 group into the coordination sphere voids of the *rac*-structure by minimizing the steric interactions of the NMe_2 group with the indenyl phenyl ring. Adopting such an s-*trans* conformation for the zirconocenium amide enolate impacts its polymerization behavior (vide infra).

Scheme 2

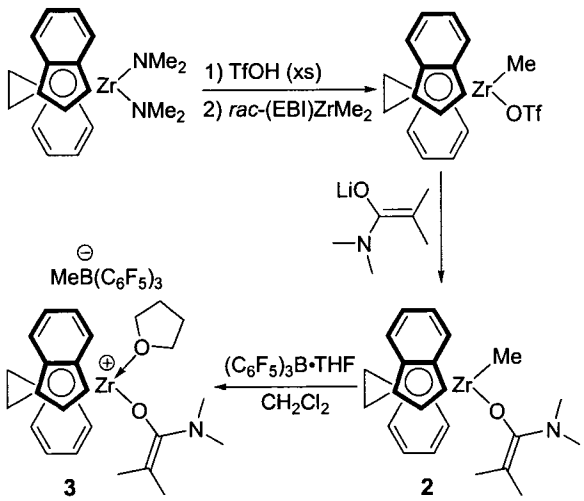

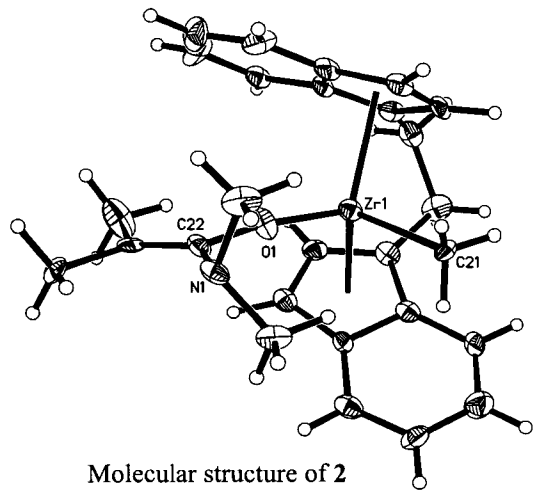

Molecular structure of **2**

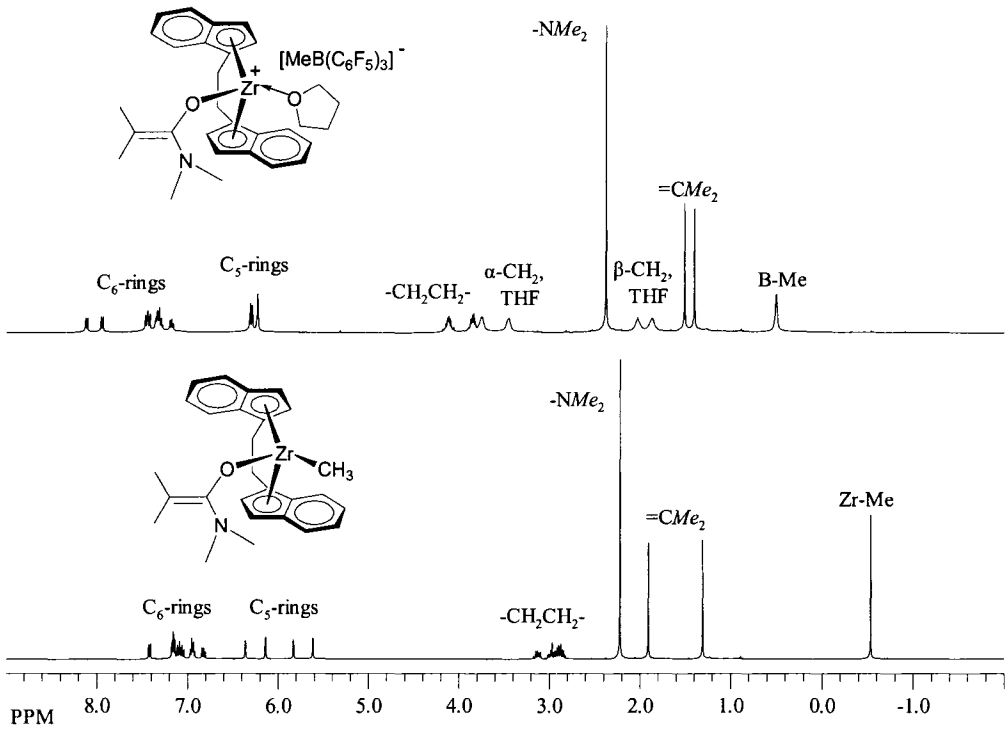

Figure 12. ^{1}H NMR spectra (23 °C) of **2** (C_6D_6, bottom) and **3** (CD_2Cl_2, top).

Erker and co-workers showed that the reaction of zirconocene *ketone* enolates with $B(C_6F_5)_3$ forms direct adducts via borane addition to the nucleophilic enolate carbon center.[27] However, the NMR-scale reaction of the methyl zirconocene *N,N*-dimethylisobutyramide enolate **2** with $(C_6F_5)_3B$•THF in CD_2Cl_2 at ambient temperature cleanly produces the methide-abstraction product—the cationic zirconocenium amide enolate **3** (Figure 12, top). This conclusion is established chiefly by the observation of the disappearance of the Zr*Me* signal (–0.53 ppm) in **2** and appearance of a characteristic, broad singlet at 0.51 ppm for the B*Me* in **3**; this chemical shift for the methyl group in the $[MeB(C_6F_5)_3]^-$ anion in CD_2Cl_2 is identical to that reported in the literature for the free $[MeB(C_6F_5)_3]^-$ anion.[28] The noncoordinating nature of the $[MeB(C_6F_5)_3]^-$ anion in **3** is also established by the ^{19}F NMR spectrum in which a small chemical shift difference of < 3 ppm [$\Delta(m,p\text{-F})$ = 2.6 ppm in **3**] between the *para*- and *meta*-fluorines is diagnostic of the

noncoordinating $[MeB(C_6F_5)_3]^-$ anion.[28,29] The preparative scale reaction in CH_2Cl_2 at ambient temperature gave the analytically pure cationic zirconocenium amide enolate **3** in 96% isolated yield. The selectivity of the methide abstraction over the possible borane addition in the reaction of **2** with the borane seems to be sterically directed; the reaction of the analogous but less bulky methyl zirconocene *N,N*-dimethylpropanamide enolate with $(C_6F_5)_3B$•THF under identical conditions yielded a messy product mixture, presumably due to a scenario where both reaction modes (i.e., methide abstraction by the borane and borane addition to the C=C bond) are operative in this reaction.

Subsequently, we carried out polymerizations of DMAA and MMA using the isolated cation **3** in CH_2Cl_2 at 23 °C, key results of which are summarized in Table 3. The polymerization of DMAA by **3** ($[DMAA]_0/[\mathbf{3}]_0 = 400/1$) proceeded in a similar manner to that of **1** and achieved a high monomer conversion of 96% in 30 min, producing highly isotactic P(DMAA) with a low PDI value and essentially a quantitative initiator efficiency (entry 1, Table 4.3). It is interesting to note, however, a subtle difference in the DMAA polymerization behavior between **1** and **3**: unlike the *ester* enolate **1**, which does not exhibit any induction (initiation) period (see Table 2 or Figure 7), the *amide* enolate **3** shows a *ca.* 5-min induction period, after which the kinetic profile is similar to that of **1**. This observed difference between **1** and **3** can be directly related to the difference in their preferred conformations—the s-*cis* conformation (as to the Zr←monomer and C=C bonds about the Zr–O–C vector) for the ester enolate vs the s-*trans* conformation for the amide enolate (vide supra), assuming that the cations (where the Zr←monomer bond displaces the Zr–Me bond in the neutral species) adopt the same more stable conformation as the corresponding neutral precursors. In this context, a conversion from

the preferred s-*trans* amide enolate conformation to the s-*cis* amide enolate conformation shown in **B** (Scheme 1) is required before the intramolecular Michael addition can take place, accounting for the observed induction period of the amide enolate **3**. After this induction period, the needed s-*cis* amide enolate conformation ready for the facile C–C formation step is preserved throughout the polymerization reaction because the Michael addition is faster than the rate-limiting monomer coordination step in the proposed "catalytic" propagation cycle (Scheme 1).

Table 3. DMAA and MMA Polymerization Results by Chiral *ansa*-Zirconocenium Amide Enolate Complex **3**[a]

entry	monomer	[**3**] (mmol/L)	[monomer]$_o$/[**3**]$_o$	time (min)	conv. (%)	$10^4 M_n$[b] (g/mol)	PDI[b] (M_w/M_n)	I^*[c] (%)
1	DMAA	4.85	400	30	96	3.58	1.12	1.06
2	MMA	4.85	400	120	~0	-	-	-

[a]See Table 2 footnotes for explanations of parameters listed in the table.

As anticipated, the MMA polymerization using **3** in CH_2Cl_2 afforded no polymeric products over a 2 h period; however, monitoring the equimolar reaction of **3** and MMA via ^{1}H NMR (CD_2Cl_2, 23 °C) clearly shows the disappearance of the MMA vinyl signals and the appearance of a new set of resonances consistent with the formation of the single-MMA-addition product,[19] *rac*-(EBI)Zr$^+$[OC(OMe)=C(Me)CH$_2$C(Me$_2$)C(NMe$_2$)=O] [MeB(C$_6$F$_5$)$_3$]$^-$ (i.e., structure **E**, Scheme 1). These results indicate that the observed copolymerization behavior can be attributed to the inability of MMA to displace the coordinated, more basic amide oxygen of the cyclic amide enolate intermediate **C** (i.e. step (iii) is not feasible); this is further supported by the competitive binding experiment which shows the ion pair *rac*-(EBI)ZrMe$^+$MeB(C$_6$F$_5$)$_3^-$ prefers to bind *N*-isopropylacrylamide over methyl isobutyrate in a 1:1:1 mixture.

Scope of Polymerization of Acrylamides. Polymerizations of *N,N*-dimethylmethacrylamide (DMMA) and *N*-isopropylacrylamide (IPAA) using both ester

and amide enolates **1** and **3** were attempted, but neither complex yielded polymer products. The lack of polymerizability of DMMA has also been previously noted in anionic polymerizations by organolithium initiators, which was attributed to insufficient stabilization of the amide enolate intermediates as a result of nonbonding interactions between the α-methyl group or the vinyl proton and the *N*-methyl group;[3] such nonbonding interactions are believed to cause twisting of the carbonyl-vinyl C–C single bond, leading to a twisted monomer conformation for a less effective overlap of the vinyl carbonyl π bonds (i.e., conjugation between two π bonds) than usually found in the planar conformation.[30] The problems associated with the polymerization of IPAA by common anionic initiators seem more straightforward because of the presence of the acidic amide NH hydrogen in IPAA. Nevertheless, the observed same non-polymerizability of DMMA or IPAA in coordination polymerization using chiral *ansa*-zirconocenium enolates could be due to the very same or a completely different reason. To seek for this answer, we set out to investigate stoichiometric reactions of **1** with IPAA and **3** with DMMA, as well as subsequent reactions of their products with an excess of monomer.

We initially reasoned that the lack of activity of the IPAA polymerization by **1** was likely due to the presence of the acidic amide NH hydrogen in IPAA. However, monitoring the reaction of **1** with 1 equiv of IPAA by ^{1}H and ^{19}F NMR in CD_2Cl_2 shows facile addition of IPAA to **1**, with no evidence for catalyst decomposition, but all evidence pointing to a *clean* formation of the single IPAA addition product, *rac*-(EBI)Zr^{+}[OC(NH^{i}Pr)=CHCH$_2$C(Me$_2$)C(O^{i}Pr)=O][MeB(C$_6$F$_5$)$_3$]$^{-}$ (**4**), Figure 13.

The single IPAA addition product **4** is stable in CD_2Cl_2 at ambient temperature, and no decomposition was detected over a period of 8 h at this temperature. Subsequently, a preparative scale reaction afforded **4** in 86% isolated yield, Scheme 3. (Note that in the preparative scale reaction, the displaced THF can be removed during drying the product in vacuo.) In the presence of excess IPAA, no further IPAA additions took place after the first IPAA addition to **1**, even with an extended reaction time (24 h). Attempts to polymerize IPAA by mixing **1** with 400 equiv of IPAA in 1,2-dichlorobenzene at temperatures from 23 to 80 °C, or in bulk at 100 °C, afforded no polymer products. Likewise, polymerizations of IPAA by **3** under varied conditions also afforded no polymer products.

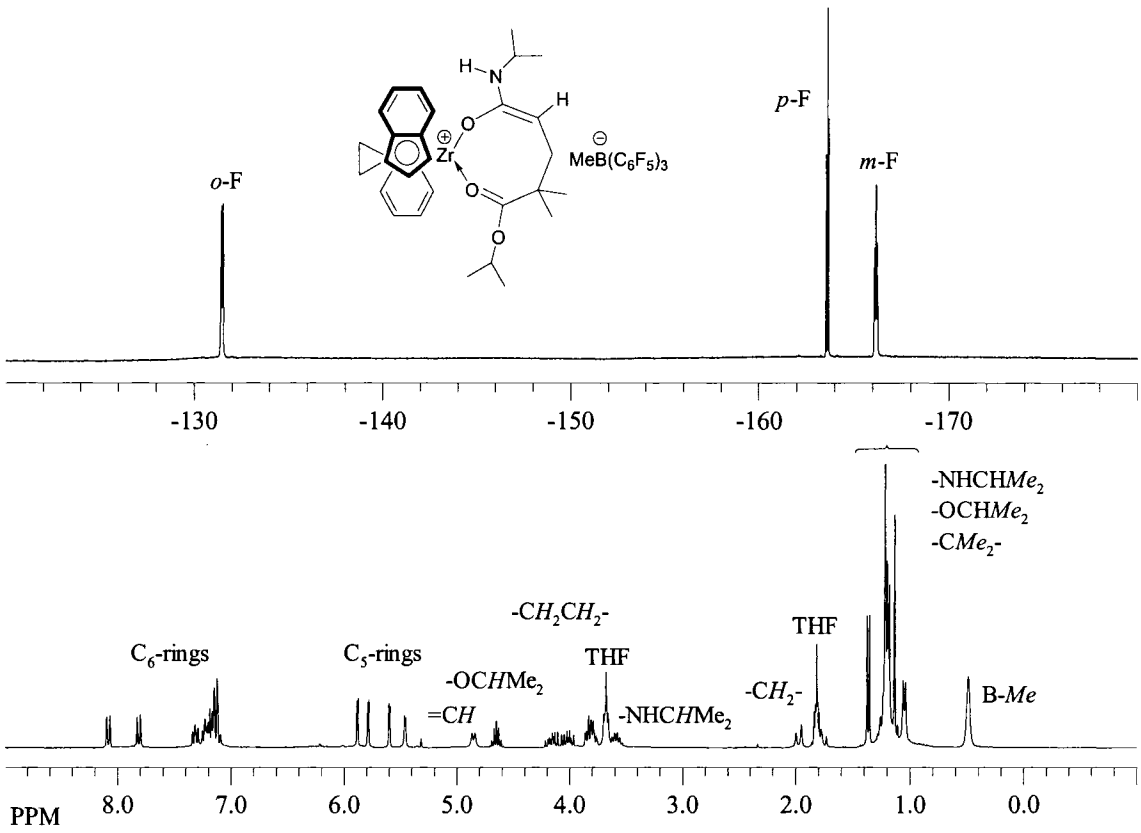

Figure 13. ^1H (bottom) and ^{19}F NMR spectra of **4** generated in situ by mixing of **1** and IPAA in CD_2Cl_2 at 23 °C (note the internal NMR solvent reference peak at 5.32 ppm).

Scheme 3

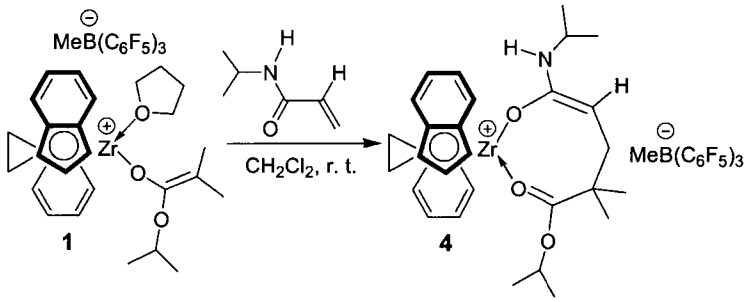

The proposed structure for **4** was based on the spectroscopic and analytical characterizations (see Figure 13 and Experimental section), while attempts to obtain its crystal structure were unsuccessful. Nevertheless, both ^{1}H and ^{13}C NMR spectra of **4** feature characteristic signals for a zirconocenium amide enolate structure and additionally an isopropyl ester group [–C(O^{i}Pr)=O]. Specifically, the ^{1}H NMR signal for –OC*H*Me$_2$ (3.73 ppm) attached to the enolate ligand in **1**[8a] is substantially down-field shifted to 4.65 ppm (sept) for –OC*H*Me$_2$ now attached to the ester group in **4**; the ^{13}C NMR chemical shift difference confirms these assignments: 154.07 ppm for the enolate *C*(O) carbon [(O*C*(O^{i}Pr)=] in **1**[8a] vs 185.59 ppm for the ester *C*(O) carbon [*C*(O^{i}Pr)=O] in **4**. In agreement with these spectroscopic changes for the reaction of **1** + IPAA → **4**, the added IPAA becomes an isopropyl amide enolate ligand [i.e., –OC(NH^{i}Pr)=CHCH$_2$–] attached to Zr in **4**, which can be readily characterized by ^{1}H NMR [4.85 (=C*H*), 3.59 (HNC*H*Me$_2$), 1.97 and 1.75 (C*H*$_2$), 1.37 and 1.05 (HNCH*Me*$_2$)] and by ^{13}C NMR {171.40 [O*C*(NH^{i}Pr)=], 97.38 (=*C*H), 43.47 (HN*C*HMe$_2$), 42.54 (*C*H$_2$)}.

The single IPAA addition product **4** does not effect further IPAA additions, but it rapidly polymerizes DMAA to highly isotactic P(DMAA), much like the cationic

complexes **1** and **3**. Thus, the inability of **1**, **3**, or **4** to polymerize IPAA is likely due to sterics of IPAA vs DMAA, not because of the reactivity of the cyclic amide enolate **4**. The significance of isolating the cyclic zirconocenium amide enolate species **4** is that it corresponds to the structure of the eight-membered-ring propagating intermediates (i.e., structures **A** and **C**, Scheme 1) involved in the acrylamide polymerization, thereby providing further direct evidence supporting the proposed monometallic, coordination polymerization of acrylamides by zirconocenium enolates proposed in Scheme 1.

The reaction **3** with DMMA was also investigated in the same manner as the reaction of **1** with IPAA. Significantly, the single DMMA addition product (**5**) was isolated in quantitative yield (Scheme 4; see Experimental for spectroscopic data). Upon addition of another equivalent DMMA, no further addition took place and the added second equivalent DMAA remains as free monomer in solution. The reaction of **3** with IPAA follows a similar pattern. These results indicate that initiations via conjugate addition occur readily; however, propagation steps involving further monomer additions are problematic, primarily due to steric reasons that keep the incoming monomer from entering the coordination site at the metal via ring opening of the chelate amide enolate intermediate.

Scheme 4

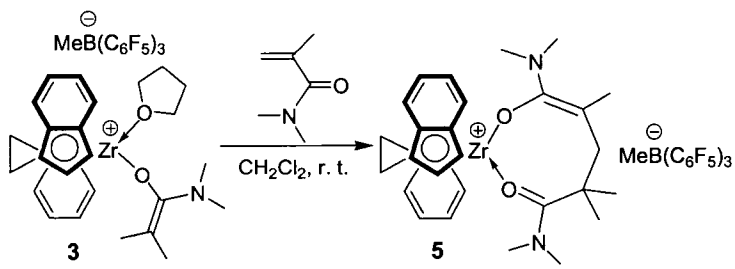

3 **5**

Conclusions

We have investigated the mechanism and scope of the metallocene-mediated isospecific coordinative-anionic polymerization of acrylamides, using the chiral zirconocenium ester and amide enolates **1** and **3**. The ester enolate complex **1** effects the highly isospecific[31] and living polymerization of DMAA, producing P(DMAA) with remarkably high [*mm*], T_m, and T_{max} values. Kinetic studies of the DMAA polymerization by **1** have shown that propagation is first order in both concentrations of the monomer and the active species. These results, coupled with those from the studies of the isolation and characterization of several model complexes, demonstrate that this DMAA polymerization proceeds via a monometallic, coordinative-conjugate-addition mechanism through cyclic amide enolate intermediates (i.e., structure **C**, Scheme 1). The results imply that the resting state during a "catalytic" propagation cycle is the cyclic amide enolate **C** and associative displacement of the coordinated amide group by incoming acrylamide monomer to regenerate the active species **B** is the rate-determining step.

Success in the production of the well-defined isotactic diblock copolymers of methacrylates and acrylamides hinges on the comonomer addition sequence. Thus, sequential block copolymerization starting from polymerization of MMA by **1**, followed by polymerization of DMAA, produces isotactic diblock copolymer P(MMA)-*b*-P(DMAA). However, owing to the inability of MMA to enter the coordination site of Zr that is preoccupied by the amide group of the penultimate DMAA unit, only homopolymer P(DMAA) is produced when the monomer addition sequence is reversed.

To confirm the proposed active propagating structure for the polymerization of acrylamides, we have synthesized model zirconocene amide enolate complexes: neutral

chiral amide enolate **2** and the corresponding cationic species **3**. Much like the ester enolate species **1**, except for the initiation behavior, the isolated amide enolate species **3** effects facile DMAA polymerization leading to highly isotactic and high-molecular-weight P(DMAA) with high initiator efficiency, thereby serving as a suitable structural model for the living active propagating species (i.e., structure **B**, Scheme 1).

Unlike DMAA, sterically hindered acrylamides such as DMMA and IPAA are not polymerized by either chiral zirconocenium ester enolate **1** or amide enolate **3**, primarily due to steric reasons incurred in the propagation step. However, initiation occurs readily, supported by the observation of the facile additions of 1 equiv of IPAA to **1** and 1 equiv of DMMA to **3**, generating the isolable eight-membered-ring cyclic amide enolates **4** and **5**, respectively; these cyclic amide enolates correspond to the structures of the first acrylamide addition product of **1** (i.e., structure **A**, Scheme 1) and the resting propagation intermediate (i.e., structure **C**, Scheme 1).

Acknowledgment. This work was supported by the National Science Foundation and Colorado State University. The Bruker X-ray diffractometer was purchased with a grant from the NIH Shared Instrumentation Grant Program. We thank Prof. Oren P. Anderson (CSU), Ms. Susie M. Miller (CSU), and Dr. Charles Campana (Bruker AXS) for determination of the crystal structure, as well as Boulder Scientific Co. for the gift of $B(C_6F_5)_3$. E.Y.C. acknowledges an Alfred P. Sloan Research Fellowship.

References and Notes

(1) Butler, K.; Thomas, P. R.; Tyler, G. J. *J. Polym. Sci.* **1960**, *48*, 357–366.

(2) (a) Huang, S. S.; McGrath, J. E. *Polym. Prepr. (Am. Chem. Soc. Div. Polym. Chem.)* **1983**, *24*, 138–140. (b) Gia, H.; McGrath, J. E. *Polym. Bull.* **1980**, *2*, 837–840.

(3) Xie, X.; Hogen-Esch, T. E. *Macromolecules* **1996**, *29*, 1746–1752.

(4) (a) Kobayashi, M.; Ishizone, T.; Nakahama, S. *Macromolecules* **2000**, *33*, 4411–4416. (b) Kobayashi, M.; Okuyama, S.; Ishizone, T.; Nakahama, S. *Macromolecules* **1999**, *32*, 6466–6477.

(5) (a) Okamoto, Y.; Habaue, S.; Isobe, Y. in *Advances in Controlled/Living Radical Polymerization*; Matyjaszewski, K. Ed.; *ACS Symp. Ser.* **2003**, *854*, 59–71. (b) Isobe, Y.; Fujioka, D.; Habaue, S.; Okamoto, Y. *J. Am. Chem. Soc.* **2001**, *123*, 7180–7181.

(6) Lutz, J.-F.; Neugebauer, D.; Matyjaszewski, K. *J. Am. Chem. Soc.* **2003**, *125*, 6986–6993.

(7) (a) Stojcevic, G.; Kim, H.; Taylor, N. J.; Marder, T. B.; Collins, S. *Angew. Chem. Int. Ed.* **2004**, *43*, 5523–5526. (b) Lian, B.; Toupet, L.; Carpentier, J.-F. *Chem. Eur. J.* **2004**, *10*, 4301–4307. (c) Ferenz, M.; Bandermann, F.; Sustmann, R.; Sicking, W. *Macromol. Chem. Phys.* **2004**, *205*, 1196–1205. (d) Karanikolopoulos, G.; Batis, C.; Pitsikalis, M.; Hadjichristidis, N. *J. Polym. Sci. Part A: Polym. Chem.* **2004**, *42*, 3761–3774. (e) Wang, J.; Odian, G.; Haubenstock, H. *Polym. Prepr. (Am. Chem. Soc. Div. Polym. Chem.)* **2003**, *44*, 673–674; Wang, J.; Haubenstock, H.;

Odian, G. *Polym. Prepr. (Am. Chem. Soc. Div. Polym. Chem.)* **2003**, *44*, 675–676. (f) Bandermann, F.; Ferenz, M.; Sustmann, R.; Sicking, W. *Macromol. Symp.* **2001**, *174*, 247–253. (g) Karanikolopoulos, G.; Batis, C.; Pitsikalis, M.; Hadjichristidis, N. *Macromolecules* **2001**, *34*, 4697–4705. (h) Bandermann, F.; Ferenz, M.; Sustmann, R.; Sicking, W. *Macromol. Symp.* **2000**, *161*, 127–134. (i) Shiono, T.; Saito, T.; Saegusa, N.; Hagihara, H.; Ikeda, T.; Deng, H.; Soga, K. *Macromol. Chem. Phys.* **1998**, *199*, 1573–1579. (j) Li, Y.; Ward, D. G.; Reddy, S. S.; Collins, S. *Macromolecules* **1997**, *30*, 1875–1883. (k) Deng, H.; Shiono, T.; Soga, K. *Macromol. Chem. Phys.* **1995**, *196*, 1971–1980. (l) Collins, S.; Ward, S. G. *J. Am. Chem. Soc.* **1992**, *114*, 5460–5462. (m) Farnham, W. B.; Hertler, W. U.S. Pat. 4,728,706, 1988.

(8) (a) Bolig, A. D.; Chen, E. Y.-X. *J. Am. Chem. Soc.* **2004**, *126*, 4897–4906. (b) Strauch, J. W.; Fauré, J.-L.; Bredeau, S.; Wang, C.; Kehr, G.; Fröhlich, R.; Luftmann, H.; Erker, G. *J. Am. Chem. Soc.* **2004**, *126*, 2089–2104. (c) Chen, E. Y.-X.; Cooney, M. J. *J. Am. Chem. Soc.* **2003**, *125*, 7150–7151. (d) Karanikolopoulos, G.; Batis, C.; Pitsikalis, M.; Hadjichristidis, N. *Macromol. Chem. Phys.* **2003**, *204*, 831–840. (e) Batis, C.; Karanikolopoulos, G.; Pitsikalis, M.; Hadjichristidis, N. *Macromolecules* **2003**, *36*, 9763–9774. (f) See ref 8(e). (g) Bolig, A. D.; Chen, E. Y.-X. *J. Am. Chem. Soc.* **2002**, *124*, 5612–5613. (h) Frauenrath, H.; Keul, H.; Höcker, H. *Macromolecules* **2001**, *34*, 14–19. (i) Bolig, A. D.; Chen, E. Y.-X. *J. Am. Chem. Soc.* **2001**, *123*, 7943–7944. (j) Cameron, P. A.; Gibson, V.; Graham, A. J. *Macromolecules* **2000**, *33*, 4329–4335. (k) Stuhldreier, T.; Keul, H.; Höcker, H.

Macromol. Rapid Commun. **2000**, *21*, 1093–1098. (l) Chen, Y.-X.; Metz, M. V.; Li, L.; Stern, C. L.; Marks, T. J. *J. Am. Chem. Soc.* **1998**, *120*, 6287–6305. (m) Deng, H.; Shiono, T.; Soga, K. *Macromolecules* **1995**, *28*, 3067–3073. (n) Soga, K.; Deng, H.; Yano, T.; Shiono, T. *Macromolecules* **1994**, *27*, 7938–7940. (o) Collins, S.; Ward, D. G.; Suddaby, K. H. *Macromolecules* **1994**, *27*, 7222–7224.

(9) (a) Saegusa, N.; Shiono, T.; Ikeda, T.; Mikami, K. JP 10330391, 1998. (b) Farnham, W. B.; Hertler, W. U.S. Pat. 4,728,706, 1988.

(10) (a) Jin, J.; Mariott, W. R.; Chen, E. Y.-X. *J. Polym. Chem. Part A: Polym. Chem.* **2003**, *41*, 3132–3142. (b) Jin, J.; Chen, E. Y.-X. *Organometallics* **2002**, *21*, 13–15.

(11) (a) Chen, E. Y.-X. *J. Polym. Sci. Part A: Polym. Chem.* **2004**, *42*, 3395–3403. (b) Jensen, T. R.; Yoon, S. C.; Dash, A. K.; Luo, L.; Marks, T. J. *J. Am. Chem. Soc.* **2003**, *125*, 14482–14494.

(12) (a) Rodriguez-Delgado, A.; Mariott, W. R.; Chen, E. Y.-X. *Macromolecules* **2004**, *37*, 3092–3100. (b) Jin, J.; Chen, E. Y.-X. *Macromol. Chem. Phys.* **2002**, *203*, 2329–2333. (c) Jin, J.; Wilson, D. R.; Chen, E. Y.-X. *Chem. Comm.* **2002**, 708–709. (d) Nguyen, H.; Jarvis, A. P.; Lesley, M. J. G.; Kelly, W. M.; Reddy, S. S.; Taylor, N. J.; Collins, S. *Macromolecules* **2000**, *33*, 1508–1510.

(13) (a) Hölscher, M.; Keul, H.; Höcker, H. *Macromolecules* **2002**, *35*, 8194–8202. (b) Hölscher, M.; Keul, H.; Höcker, H. *Chem. Eur. J.* **2001**, *7*, 5419–5426. (c) Sustmann, R.; Sicking, W.; Bandermann, F.; Ferenz, M. *Macromolecules* **1999**, *32*, 4204–4213.

(14) Allen, R. D.; Long, T. E.; McGrath, J. E. *Polym. Bull.* **1986**, *15*, 127–134.

(15) (a) Grossman, R. B.; Doyle, R. A.; Buchwald, S. L. *Organometallics* **1991**, *10*, 1501–1505. (b) Collins, S.; Kuntz, B. A.; Taylor, N. J.; Ward, D. G. *J. Organomet. Chem.* **1988**, *342*, 21–29.

(16) Diamond, G. M.; Jordan, R. F.; Petersen, J. L. *J. Am. Chem. Soc.* **1996**, *118*, 8024–8033.

(17) Chen, E. Y.-X.; Kruper, W. J.; Roof, G.; Wilson, D. R. *J. Am. Chem. Soc.* **2001**, *123*, 745–746.

(18) Woodbury, R. P.; Rathke, M. W. *J. Org. Chem.* **1977**, *42*, 1688–1690.

(19) Rodriguez-Delgado, A.; Chen, E. Y.-X. *Macromolecules* **2005**, *38*, 2587–2594.

(20) (a) SMART, SAINT, and cell_now, Bruker Analytical X-ray Solutions: Madison, WI, 2001. (b) *SHELXTL*, Version 6.12; Bruker Analytical X-ray Solutions: Madison, WI, 2001.

(21) DMNST Software Manual: Version 1.37; Scintag Incorporated: Cupertino, CA, 1999.

(22) (a) Lutz, J.-F.; Neugebauer, D.; Matyjaszewski, K. *J. Am. Chem. Soc.* **2003**, *125*, 6986–6993. (b) Kobayashi, M.; Okuyama, S.; Ishizone, T.; Nakahama, S. *Macromolecules* **1999**, *32*, 6466–6477. (c) Xie, X.; Hogen-Esch, T. E. *Macromolecules* **1996**, *29*, 1746–1752. (d) Bulai, A.; Jimeno, M. L.; de Queiroz, A.-A. A.; Gallardo, A.; Roman, J. S. *Macromolecules* **1996**, *29*, 3240–3246. (e) Huang, S. S.; McGrath, J. E. *Polym. Prepr. (Am. Chem. Soc. Div. Polym. Chem.)* **1983**, *24*, 138–140. (f) Gia, H.; McGrath, J. E. *Polym. Bull.* **1980**, *2*, 837–840.

(23) Tian G.; Boone, H. W.; Novak, B. M. *Macromolecules* **2001**, *34*, 7658–7663.

(24) Liu, Z.; Somsook, E.; Landis, C. R. *J. Am. Chem. Soc.* **2001**, *123*, 2915–2916.

(25) Deck, P. A.; Marks, T. J. *J. Am. Chem. Soc.* **1995**, *117*, 6128–6129.

(26) (a) Bandermann, F.; Ferenz, M.; Sustmann, R.; Sicking, W. *Macromol. Symp.* **2001**, *174*, 247–253. (b) Li, Y.; Ward, D. G.; Reddy, S. S.; Collins, S. *Macromolecules* **1997**, *30*, 1875–1883.

(27) Spaether, W.; Klaß, K.; Erker, G.; Zippel, F.; Fröhlich, R. *Chem. Eur. J.* **1998**, *4*, 1411–1417.

(28) Klosin, J.; Roof, G. R.; Chen, E. Y. X.; Abboud, K. A. *Organometallics* **2000**, *19*, 4684-4686.

(29) Horton, A. D.; de With, J.; van der Linder, A. J.; van de Weg, H. *Organometallics* **1996**, *15*, 2672–2674.

(30) Kodaira, T.; Tanahashi, H.; Hara, K. *Polym. J.* **1990**, *26*, 649–659.

(31) The P(DMAA)s produced from the chiral *ansa*-zirconocenium ester and amide enolates employed in this study exhibit no measurable [*mr*] + [*rr*] triad sequences from ^{13}C NMR spectra and are essentially stereodefect free within this detection limit ([*mm*] > 99%, Chart 1). For this reason, we could not directly determine, on the basis of spectroscopic data available, if this polymerization is enantiomorphic-site or chain-end controlled. In addition, the [*mr*] and [*rr*] sequences in the carbonyl carbon region of lower tactic P(DMAA) samples produced by other initiators are not well-resolved. However, we have previously determined that, using the P(MMA)s by the chiral enolate **1**, which show a small amount of stereodefects suitable for such an analysis, the polymerization is enantiomorphic-site controlled.[19] Because methacrylate and acrylamide polymerizations by these chiral *ansa*-

zirconocenium enolates proceed via essentially the same mechanisms (monometallic, intramolecular coordinative-conjugation addition), and because the P(DMAA) produced by an achiral analog, $Cp_2Zr^+(THF)[OC(OEt)=CMe_2][MeB(C_6F_5)_3]^-$, is virtually atactic ([*m*]/[*r*] = 58/42]), we conclude that the polymerization of DMAA by chiral *ansa*-zirconocenium enolates is most likely enantiomorphic-site controlled.

CHAPTER IV

CHAIN TERMINATION AND TRANSFER REACTIONS IN THE ACRYLATE POLYMERIZATION BY A MONOMETALLIC CHIRAL ZIRCONOCSNIUM CATALYST SYSTEM

This dissertation chapter contains the manuscript of a full paper published in *Macromolecules* [Mariott, W. R.; Rodriguez-Delgado, A.; Chen, E. Y.-X *Macromolecules* **2006**, *39*, 1318–1327] and represents efforts directed at extending the scope of the solution polymerization of functionalized alkenes by chiral *ansa*-zirconocenes to alkyl acrylates. Specifically, the polymerization of *n*-butyl acrylate (*n*-BA) by a chiral *ansa*-zirconocenium ester enolate proceeds in an uncontrolled fashion to only moderate monomer conversions due to chain termination and transfer reactions occurring on the polymerization time-scale. Combined polymerization, chain structure, and model reaction studies demonstrate the presence of significant chain termination and transfer processes and have yielded a mechanism responsible for these processes.

Dr. A.R.D. performed some initial *n*-butyl acrylate polymerization runs, but the bulk of the mechanistic studies of this work were carried out by W.R.M.

Abstract

Unlike the living polymerization of methacrylates and acrylamides by the monometallic propagating, chiral *ansa*-zirconocenium ester enolate *rac*-(EBI)Zr^{+}(THF)[OC(O^{i}Pr)=CMe_2][$MeB(C_6F_5)_3$]$^{-}$ [**1**; EBI = $C_2H_4(Ind)_2$], the polymerization of acrylates such as *n*-butyl acrylate (*n*-BA) by **1** proceeds in an uncontrolled fashion to only moderate monomer conversions, producing poly(*n*-BA) with three types of chain structures—one major linear and two minor cyclic *β*-ketoester-terminated poly(*n*-BA) chains. The combined polymerization, chain structure, and model reaction studies have shown the presence of substantial chain termination processes in this system that prevent it from achieving high monomer conversions and producing only the living linear chain structure. The proposed overall three-step mechanism, involving isomerization of the cyclic reactive intermediate, back-biting cyclization to eliminate an alcohol, and chain termination by the alcohol, explains the catalyst deactivation pathways as well as the resulting polymer chain structures. Chain transfer reactions involving acidic α-protons are insignificant as compared to back-biting cyclizations involving the activated antepenultimate ester group of the growing polymer chain, which is the chief catalyst deactivation pathway for the current monometallic catalyst system.

Introduction

Since the initial discovery of metallocene-based systems for the polymerization of alkyl methacrylates,[1] particularly methyl methacrylate (MMA), with a patent disclosure by Farnham and Hertler[1c] in 1988 as well as two independent journal publications by Yasuda et al.[1b] and Collins and Ward[1a] in 1992, the field has attracted increasing attention

due to the demonstrated remarkable versatility of these systems in terms of catalyst structures and polymerization characteristics. The polymerization of alkyl methacrylates mediated by group 4 metallocene and related complexes, including achiral zirconocenes,[2] chiral *ansa*-zirconocenes,[3] achiral titanocenes, [1a,4] chiral *ansa*-titanocenes,[5] half-sandwich titanium complexes,[6] and constrained geometry titanium and zirconium complexes,[7] has been extensively and computationally[8] studied. When used in suitable initiating complex forms (e.g., metallocene ester enolates), these systems are living, allowing for control over polymer number-average molecular weights (M_n) and molecular weight distributions (MWD = M_w/M_n)[2b,g,k] as well as the synthesis of well-defined block copolymers.[2h,3a,f,7a] A high degree of control over polymer tacticity[3,7] and the production of stereoblock P(MMA)[3d,g] are also possible using appropriate chiral metallocene complexes.

While the polymerization of alkyl methacrylates by group 4 metallocene and related complexes has been extensively investigated and considerable success achieved,[1-8] reports on the polymerization of alkyl acrylates—that contain an active α-proton as opposed to a methyl group in methacrylates—by these systems are scarce and only limited success has been met. Soga and Deng[9] employed a three-component system consisting of *rac*-(EBI)$ZrMe_2$/$[Ph_3C][B(C_6F_5)_4]$/$MeAl(BHT)_2$ [EBI = $C_2H_4(Ind)_2$; BHT = 2,6-di-*tert*-butyl-4-methyl phenoxy] for the polymerization of the sterically hindered *tert*-butyl acrylate (*t*-BA), affording P(*t*-BA) with moderate to broad MWDs (M_w/M_n = 1.23 – 2.20) in low to moderate polymer yields (6 – 60 %) with extended reaction times (17 – 24 h). Collins and co-workers[2k] investigated the polymerization of the unhindered *n*-butyl acrylate (*n*-BA) by a two-component bimetallic system consisting of the well-defined catalyst $[Cp_2Zr^+Me(THF)][BPh_4]^-$ and initiator $Cp_2ZrMe[OC(O^tBu)=CMe_2]$; a monomer

conversion of 55% and a polymer MWD of M_w/M_n = 2.02 were observed for the polymerization at 0 °C in a [*n*-BA]/[initiator] ratio of ~ 100, with higher conversions and lower polymer MWDs being achieved only at lower polymerization temperatures. This process is not living, and analysis of the low-molecular-weight P(*n*-BA) by matrix-assisted laser desorption/ionization time-of-flight mass spectroscopy (MALDI–TOF MS) led to two proposed modes of chain termination processes, the predominate of which involves the back-biting cyclization of the growing polymer chain. Most recently, a third report on the polymerization of acrylates (*t*-BA and *n*-BA) by Hadjichristidis et al. appeared,[10] which employed Soga's three-component systems, including $Cp_2ZrMe_2/B(C_6F_5)_3/ZnEt_2$, *rac*-(EBI)$ZrMe_2/B(C_6F_5)_3/ZnEt_2$, and *rac*-(EBI)$ZrMe_2/[HNMe_2Ph][B(C_6F_5)_4]/ZnEt_2$; the polymer yields obtained from these polymerizations of *n*-BA and *t*-BA for 24 h did not exceed 30 and 32%, respectively, in any case, regardless of the catalyst system or polymerization conditions employed. The results from the above three reports clearly indicate the presence of considerable chain termination processes in the polymerization of α-proton-containing acrylates by group 4 metallocene complexes; this observation is in sharp contrast to the isoelectronic, neutral organolanthanide complexes such as $(C_5Me_5)_2SmMe(THF)$ which mediate the living polymerization of alkyl acrylates.[11] However, the polymerization of acrylates using a well-defined single-component, chiral *monometallic* propagating zirconocenium ester enolate system, which has been shown to behave similarly to lanthanocenes, serving as both catalyst and initiator for the polymerization of methacrylates,[3a,b] has not been experimentally investigated[12] and is the focus of this current contribution.

We have recently elucidated mechanisms for the polymerizations of alkyl methacrylates[3a,b] and acrylamides[13] mediated by the well-defined, single-component chiral *ansa*-zirconocenium ester enolate complex, *rac*-(EBI)Zr^{+}(THF)[OC(O^{i}Pr)=CMe_2][$MeB(C_6F_5)_3$]$^{-}$ (**1**). Our combined studies of synthesis, polymerization, kinetics, as well as polymer microstructures and chain structures have shown that the polymerization of methacrylates and acrylamides by **1** proceeds in a living fashion through a monometallic, enantiomorphic site-control mechanism, affording the corresponding highly isotactic polymers. The objective of the current study was to investigate the polymerization of acrylates using this well-defined chiral, monometallic propagating zirconocenium ester enolate system. To this end, we have studied the polymerization of *n*-BA by **1** in detail, obtained unambiguous evidence for chain termination reactions occurring in this polymerization that prevent high monomer conversions, as well as elucidated the mechanism of these reactions that are responsible for the overall catalyst deactivation.

Experimental Section

Materials and Methods. All syntheses and manipulations of air- and moisture-sensitive materials were carried out in flamed Schlenk-type glassware on a dual-manifold Schlenk line, a high-vacuum line, or in an argon-filled glovebox. NMR-scale reactions were conducted in Teflon-valve-sealed J. Young-type NMR tubes. HPLC grade organic solvents were sparged with nitrogen during filling of the solvent reservoir and then dried by passage through activated alumina (for THF, and CH_2Cl_2) followed by passage through Q-5-supported copper catalyst (for toluene and hexanes) stainless steel columns.

Benzene-d_6 and toluene-d_8 were dried over sodium/potassium alloy and filtered before use, whereas $CDCl_3$ and CD_2Cl_2 were dried over activated Davison 4 Å molecular sieves. NMR spectra were recorded on either a Varian Inova 300 (FT 300 MHz, ^1H; 75 MHz, ^{13}C; 282 MHz, ^{19}F) or a Varian Inova 400 spectrometer. Chemical shifts for ^1H and ^{13}C spectra were referenced to internal solvent resonances and are reported as parts per million relative to tetramethylsilane, whereas ^{19}F NMR spectra were referenced to external $CFCl_3$.

n-Butyllithium (1.6 M in hexanes), diethyl malonate (DEM), diisopropylamine, 2,6-di-*tert*-butyl-4-methylphenol (butylated hydroxytoluene, BHT-H), ethyl acetoacetate (EAA), lithium dimethylamide, methyl isobutyrate (MIB), and zirconium tetrachloride were purchased from Aldrich Chemical Co., trimethylaluminum (neat) from Strem Chemical Co., methyllithium (1.6 M in diethyl ether) from Acros, and dimethyl malonate (DMM), dimethyl succinate (DMS), di-*tert*-butyl malonate (DBM), and trimethylsilyl trifluoromethanesulfonate (TMSOTf) from Alfa Aesar. These reagents were used as received, except for the following reagents that were further treated or purified: the amine was degassed using three freeze-pump-thaw cycles; BHT-H was recrystallized from hexanes; all esters including DBM, DEM, DMM, DMS, EAA, and MIB were purified by first degassing and drying over CaH_2 overnight, followed by vacuum distillation and stored over activated Davison 4 Å molecular sieves inside the glovebox.

Methyl methacrylate (MMA) was purchased from Aldrich Chemical Co. and purified by first degassing and drying over CaH_2 overnight, followed by vacuum distillation; final purification of MMA involved titration with neat tri(*n*-octyl)aluminum to a yellow end point[14] followed by a second vacuum distillation. *n*-Butyl acrylate (*n*-BA)

was purchased from Acros and purified by first degassing and drying over CaH_2 overnight followed by distillation under reduced pressure. The purified monomers were stored in brown glass bottles over activated Davison 4 Å molecular sieves (for *n*-BA) in a –30 °C freezer inside the glovebox.

Tris(pentafluorophenyl)borane, $B(C_6F_5)_3$, was obtained as a research gift from Boulder Scientific Co. and further purified by recrystallization from hexanes at –30 °C. The $(C_6F_5)_3B$•THF adduct was prepared by addition of THF to a toluene solution of the borane followed by removal of the volatiles and drying in vacuo. Literature procedures were employed for the preparation of the following compounds and metallocene complexes: $(EBI)H_2$ [EBI = $C_2H_4(Ind)_2$],[15] *rac*-$(EBI)Zr(NMe_2)_2$,[16] *rac*-$(EBI)ZrMe_2$,[15] *rac*-$(EBI)Zr^+(THF)[OC(O^iPr)=CMe_2][MeB(C_6F_5)_3]^-$ (**1**).[3a,b]

Modified Synthesis of *rac*-(EBI)ZrMe[OC(O^{i}Pr)=CMe$_2$]. In an argon-filled glovebox, a 50-mL Schlenk flask was equipped with a magnetic stir bar, charged with 0.567 g (1.50 mmol) *rac*-$(EBI)ZrMe_2$ and 30 mL toluene, capped with a septum, removed from the glovebox, and interfaced to a Schlenk line. The flask was cooled to 0 °C in an ice bath under positive nitrogen pressure before the addition of 1.6 mL (1.6 mmol, 1.0 M in hexanes) TMSOTf via gastight syringe to the above vigorously stirred solution. The reaction mixture was stirred at 0 °C for 1 h before being allowed to warm to ambient temperature and stir for an additional 21 h. An aliquot of the reaction mixture revealed approximately 13% unreacted *rac*-$(EBI)ZrMe_2$ remaining, and therefore an additional 0.22 mL (0.22 mmol, 1.0 M in hexanes) TMSOTf was added to the reaction mixture via gastight syringe. The reaction mixture was allowed to stir for an additional 4 h in a warm water bath. The volatiles were removed in vacuo and the resulting residue dried before

being taken into the glovebox, where the product was extracted into 40 mL of toluene and filtered through a pad of celite. The filtrate was transferred to a 60 mL reactor and cooled to –30 °C in the freezer of the glovebox before the addition of 0.205 g [1.50 mmol, 1 equiv based on *rac*-(EBI)$ZrMe_2$] $Me_2C{=}C(O^iPr)OLi$ to the vigorously stirred solution. The reaction mixture was allowed to gradually warm to ambient temperature and stir for 24 h before being filtered through a pad of celite. The volatiles of the filtrate were removed in vacuo and the resulting yellow powder dried, affording 0.665 g [90%, based on *rac*-(EBI)$ZrMe_2$] of the spectroscopically pure title complex. The spectroscopic data are the same as those reported in literature.[3b]

Isolation of the Initiation (Single *n*-BA Addition) Product of 1: *rac*-(EBI)$Zr^+[OC(O^nBu){=}CHCH_2C(Me_2)C(O^iPr){=}O][MeB(C_6F_5)]^-$ (2). In an argon-filled glovebox, a 30 mL glass reactor was charged with 29.5 mg (0.060 mmol) of *rac*-(EBI)$ZrMe[OC(O^iPr){=}CMe_2]$, 35.0 mg (0.060 mmol) of $(C_6F_5)_3B{\bullet}THF$, and 10 mL CH_2Cl_2; this solution was allowed to stir for 10 min at ambient temperature, cleanly generating **1**.[3a] To this *in situ* generated and vigorously stirred CH_2Cl_2 solution of **1** was added 8.6 μL (0.060 mmol) *n*-BA at ambient temperature. The color of the resulting mixture changed instantaneously from dark orange to light orange. The solution was allowed to stir for 30 min at ambient temperature before the volatiles were removed in vacuo, yielding a sticky light orange solid. The crude product was washed with 5 × 2 mL hexanes and dried in vacuo to give 62.0 mg (91%) of the title complex as an orange powder. The spectroscopic data of the isolated product are the same as those obtained by the *in situ* generation method listed as follows, except for the absence of signals for THF,

which was removed upon drying of the isolated product. Anal. Calcd. for $C_{53}H_{44}BF_{15}O_4Zr$: C, 56.24; H, 3.92. Found: C, 56.16; H, 3.82.

^{1}H NMR (CD_2Cl_2, 23°C) for *rac*-(EBI)Zr$^+$[OC(O^{n}Bu)=CHCH$_2$C(Me$_2$)C(O^{i}Pr)=O] [MeB(C_6F_5)]$^-$ (generated *in situ*): δ 8.16 (d, J = 8.7 Hz, 1H), 7.85 (d, J = 8.7 Hz, 1H), 7.38–7.09 (m, 6H), 5.94 (d, J = 3.0 Hz, 1H), 5.83 (d, J = 3.0 Hz, 1H), 5.61 (d, J = 3.0 Hz, 1H), 5.44 (d, J = 3.0 Hz, 1H), 4.61 (sept, J = 6.3 Hz, 1H, OC*H*Me$_2$), 4.31–4.03 (m, 2H, C*H*$_2$CH$_2$), 3.92–3.78 (m, 2H, CH$_2$C*H*$_2$), 3.74 (s, br, 4H, α-CH$_2$, free THF derived from **1**), 2.15 (d, J = 15.0 Hz, 1H, C*H*$_2$), 1.88–1.82 (m, 1H, C*H*$_2$; 4H, *β*-C*H*$_2$, free THF), 1.69–1.56 (m, 2H, OCH$_2$C*H*$_2$CH$_2$CH$_3$), 1.43–1.31 (m, 2H, OCH$_2$CH$_2$C*H*$_2$CH$_3$), 1.38 (d, J = 6.3 Hz, 3H, OCH*Me*$_2$), 1.25 (s, 3H, C*Me*$_2$), 1.20 (d, J = 6.3 Hz, 3H, OCH*Me*$_2$), 1.18 (s, 3H, C*Me*$_2$), 0.94 (t, J = 7.5 Hz, 3H, OCH$_2$CH$_2$CH$_2$C*H*$_3$), 0.49 (s, br, 3H, B*Me*). The proton signals for OC*H*$_2$CH$_2$CH$_2$CH$_3$ and =C*H* could not be assigned with confidence due to overlap with other peaks. ^{19}F NMR (CD_2Cl_2, 23°C): δ –131.50 (d, $^3J_{F\text{-}F}$ = 20.0 Hz, 6F, *o*-F), –163.64 (t, $^3J_{F\text{-}F}$ = 20.3 Hz, 3F, *p*-F), –166.20 (m, 6F, *m*-F).

Generation of *rac*-(EBI)Zr$^+$(O^{t}Bu)(THF)[MeB(C_6F_5)]$^-$ (3). An authentic sample (**3**) of cationic zirconocene *tert*-butoxide complexes[17] was prepared using modified literature procedures.[17a] In an argon-filled glovebox, a 25 mL Schlenk flask was loaded with *rac*-(EBI)ZrMe$_2$ (200 mg, 0.530 mmol) and 15 mL toluene; the flask was sealed with a septum, removed from the glovebox, and suspended in a 23 °C water bath. A 5 mL toluene solution of ^{t}BuOH (70.7 mg, 0.954 mmol) was added to the above stirred solution via gastight syringe. The reaction was stirred at 23 °C for 1.3 h before the volatiles were removed in vacuo. The resulting light yellow powder was dried in vacuo affording 140 mg (73%) of *rac*-(EBI)ZrMe(O^{t}Bu). Next, the isolated *rac*-(EBI)ZrMe(O^{t}Bu) (7.3 mg,

0.02 mmol) was mixed with an equimolar amount of $(C_6F_5)_3B$•THF (11.7 mg, 0.02 mmol) in 0.7 mL CD_2Cl_2 to cleanly generate the corresponding cationic species (**3**) as a bright yellow homogeneous solution.

^{1}H NMR (CD_2Cl_2, 23°C) for *rac*-(EBI)ZrMe(O^{t}Bu): δ 7.74 (dd, 1H), 7.44 (dd, 1H), 7.33 (dt, 1H), 7.23 (dt, 1H), 7.12–6.96 (m, 4H), 6.36 (d, J = 3.3 Hz, 1H), 6.30 (d, J = 3.3 Hz, 1H), 6.02 (d, J = 3.3 Hz, 1H), 5.82 (d, J = 3.3 Hz, 1H), 3.63–3.51 (m, 1H, C*H*$_2$CH$_2$), 3.49–3.25 (m, 3H, CH$_2$C*H*$_2$), 0.82 (s, 9H, C*Me*$_3$), –1.13 (s, 3H, Zr*Me*). ^{1}H NMR (CD_2Cl_2, 23°C) for **3**: δ 8.04–7.99 (m, 1H), 7.88–7.83 (m, 1H), 7.51–7.22 (m, 6H), 6.58 (dd, 1H), 6.41 (d, J = 3.6 Hz, 1H), 6.29–6.23 (m, 2H), 4.00–3.76 (m, 4H, C*H*$_2$C*H*$_2$), 3.74–3.66 (m, 2H, α-C*H*$_2$, THF), 3.49–3.42 (m, 2H, α-C*H*$_2$, THF), 2.11–1.82 (m, 4H, *β*-C*H*$_2$, THF), 1.01 (s, 9H, C*Me*$_3$), 0.49 (s, br, 3H, B*Me*). ^{19}F NMR (CD_2Cl_2, 23°C): δ –131.51 (d, $^3J_{F\text{-}F}$ = 21.2 Hz, 6F, *o*-F), –163.61 (t, $^3J_{F\text{-}F}$ = 20.3 Hz, 3F, *p*-F), –166.21 (m, 6F, *m*-F).

Generation of *rac*-(EBI)Zr$^+$[OC(Me)=CHC(=O)(OEt)][MeB(C$_6$F$_5$)$_3$]$^-$ (4). In an argon-filled glovebox, to a solution of complex **2** (7.4 mg, 6.5 μmol) in 0.6 mL CD_2Cl_2 was added ethyl acetoacetate (0.8 μL, 6.5 μmol) via micropipette, and the resulting mixture was briefly mixed before being transferred to a J. Young-type NMR tube for ^{1}H and ^{19}F NMR analyses. The NMR spectra clearly showed the complete disappearance of both starting materials and are consistent with the formation of the protonolysis product, complex **4**, and the corresponding coproduct ^{n}BuOC(=O)CH$_2$CH$_2$C(Me$_2$)C(=O)O^{i}Pr.

^{1}H NMR (CD_2Cl_2, 23°C) for **4**: δ 7.50–7.05 (m, 8H), 6.87 (m, 1H), 6.65 (m, 1H), 6.25 (m, 1H), 6.03 (m, 1H), 5.38 (s, 1H, =C*H*), 4.21–3.89 (m, 4H, C*H*$_2$C*H*$_2$), 1.98 (s, 3H, OC*Me*), 0.46 (s, br, 3H, B*Me*). (The O*Et* protons could not be assigned with confidence due to overlap with both ethylene bridging and the coproduct ^{n}BuO peaks.) ^{19}F NMR

(CD_2Cl_2, 23°C): δ –131.56 (d, $^3J_{F\text{-}F}$ = 19.2 Hz, 6F, *o*-F), –163.76 (t, $^3J_{F\text{-}F}$ = 20.3 Hz, 3F, *p*-F), –166.33 (m, 6F, *m*-F).

Chain Transfer Model Reactions of 1 with Methyl Isobutyrate and Dimethyl Malonate. In an argon-filled glovebox, to a CD_2Cl_2 solution of **1** (0.02 mmol) was added 2.3 μL of MIB (0.020 mmol) at ambient temperature. The solution was quickly transferred to a Teflon-valve-sealed J. Young-type NMR tube and the ^1H and ^{19}F NMR were monitored over a 5-h period. The reaction mixture gave NMR spectra consistent with the formation of the protonolysis product *rac*-(EBI)Zr^+(L)][OC(OMe)=CMe_2][$MeB(C_6F_5)_3$]$^-$ [**5**, L = isopropyl isobutyrate (PIB), MIB, or THF] as well as the presence of the unreacted starting material in a 1:2 ratio; there was no noticeable change in this ratio after 5 h.

^1H NMR (CD_2Cl_2, 23°C) for **5**: δ 8.00 (d, *J* = 8.7 Hz, 1H), 7.96–7.92 (m, 1H, overlapping with **1**), 7.50–7.14 (m, 6H, overlapping with **1**), 6.69 (d, *J* = 3.3 Hz, 1H), 6.26 (m, 2H), 6.08 (d, *J* = 3.3 Hz, 1H), 4.15–3.80 (m, 4H, CH_2CH_2, overlapping with **1**), 3.67 (s, 3H, O*Me*), 1.45 (s, 3H, =CMe_2), 1.35 (s, 3H, =CMe_2), 0.49 (s, br, 3H, B*Me*). ^{19}F NMR (CD_2Cl_2, 23°C): δ –131.51 (d, $^3J_{F\text{-}F}$ = 20.0 Hz, 6F, *o*-F), –163.55 (t, $^3J_{F\text{-}F}$ = 20.3 Hz, 3F, *p*-F), –166.16 (m, 6F, *m*-F).

A similar procedure was followed for the reaction of **1** and DMM, which resulted in a rapid consumption of all starting materials and the appearance of a new set of resonances consistent with the formation of the corresponding protonolysis product, *rac*-(EBI)Zr^+[OC(OMe)=CHC(OMe)=O] [$MeB(C_6F_5)_3$]$^-$ (**6**), and the readily identifiable free isopropyl isobutyrate coproduct. ^1H NMR (CD_2Cl_2, 23°C) for **6**: δ 7.80 (d, *J* = 8.7 Hz, 2H), 7.70–7.15 (m, 6H), 6.62 (d, *J* = 3.3 Hz, 2H), 6.26 (d, *J* = 3.3 Hz, 2H), 4.05–3.29 (m,

4H, CH_2CH_2), 3.43 (s, 6H, O*Me*), 0.49 (s, br, 3H, B*Me*). (The =C*H* proton could not be assigned with confidence due to overlap with other peaks.) ^{19}F NMR (CD_2Cl_2, 23°C): δ –131.53 (d, $^3J_{F\text{-}F}$ = 18.9 Hz, 6F, *o*-F), –163.59 (t, $^3J_{F\text{-}F}$ = 20.3 Hz, 3F, *p*-F), –166.19 (m, 6F, *m*-F).

General Polymerization Procedures. Polymerizations were performed either in 30-mL glass reactors inside the glovebox, or in 25-mL Schlenk flasks interfaced to a dual-manifold Schlenk line. In a typical procedure, for polymerizations of *n*-BA using the *in situ* generated **1**, 10.3 mg (20.9 μmol) *rac*-(EBI)ZrMe[OC(O^{i}Pr)=CMe$_2$] and 12.2 mg (20.9 μmol) $(C_6F_5)_3B$•THF were dissolved in 5 mL CH_2Cl_2 in a 25 mL Schlenk flask and allowed to stir 10 min at ambient temperature to cleanly generate the cationic zirconocenium ester enolate **1** before being suspended in a pre-equilibrated bath at the desired temperature. *n*-BA (0.3 mL, 2.09 mmol) was quickly added via gastight syringe, and the sealed flask was kept with vigorous stirring at the bath temperature. After the desired time interval, the polymerization was quenched by the addition of 5 mL 5% HCl-acidified methanol followed by removal of the volatiles in vacuo and drying in a vacuum oven at 50 °C overnight to a constant weight. Polymer conversions were monitored, either throughout the course of the polymerization or immediately before quenching, by removing 0.2 mL aliquots of the reaction mixture via syringe and quickly quenching into 4 mL vials containing 0.6 mL of undried "wet" $CDCl_3$ stabilized by 250 ppm of BHT-H. The quenched aliquots were analyzed by ^1H NMR to obtain conversion data. For NMR scale polymerization runs, *rac*-(EBI)ZrMe[OC(O^{i}Pr)=CMe$_2$] (0.02 mmol) and $(C_6F_5)_3B$•THF (0.02 mmol) were dissolved in 0.7 mL CD_2Cl_2 or toluene-d_8 and allowed

to mix for 10 min at ambient temperature before the addition of a predetermined ratio of monomer. These polymerizations were monitored by ^{1}H NMR to obtain conversion data.

For the sequential copolymerization of MMA and *n*-BA, 11.5 mg (23.4 μmol) *rac*-(EBI)ZrMe[OC(O^{i}Pr)=CMe$_2$] and 13.7 mg (23.4 μmol) $(C_6F_5)_3B$•THF were dissolved in 5 mL CH_2Cl_2 in a 30 mL glass reactor and allowed to stir 10 min at ambient temperature, generating **1** *in situ*. MMA (0.5 mL, 4.67 mmol) was quickly added to the vigorously stirred solution of **1** in CH_2Cl_2 at ambient temperature via pipette and the polymerization mixture was allowed to stir for 15 min before the addition of *n*-BA (0.34 mL, 2.34 mmol). The reactor was kept with vigorous stirring at ambient temperature for 30 min before the copolymerization was quenched by the addition of 5 mL 5% HCl-acidified methanol. The quenched mixture was precipitated into 100 mL methanol and stirred for 30 min before the polymer was filtered off, washed with methanol, and dried in a vacuum oven at 50 °C overnight to a constant weight.

For the chain transfer polymerization of MMA by **1** using enolizable esters as chain transfer reagents (CTRs), *rac*-(EBI)ZrMe[OC(O^{i}Pr)=CMe$_2$] (18.7 μmol) and $(C_6F_5)_3B$•THF (18.7 μmol) were dissolved in 5 mL CH_2Cl_2 and allowed to stir 10 min at ambient temperature to generate **1**. A solution of a predetermined ratio of a CTR in MMA (9.35 mmol) was added to the catalyst solution via pipette and the polymerization was allowed to stir for 30 min at ambient temperature before being quenched by the addition of 5 mL 5% HCl-acidified methanol. The quenched mixture was precipitated into 100 mL MeOH and allowed to stir for 30 min before the polymer was filtered off, washed with MeOH, and dried in a vacuum oven at 50 °C overnight to a constant weight.

Polymer Characterizations. The low-molecular-weight P(*n*-BA) sample was analyzed by matrix-assisted laser desorption/ionization time-of-flight mass spectroscopy (MALDI–TOF MS); the experiment was performed on an Ultraflex MALDI-TOF mass spectrometer (Bruker Daltonics) operated in reflector mode using a Nd:YAG laser at 355 nm and 25 kV accelerating voltage. A thin layer of a 1% NaI solution was first deposited on the target plate, followed by 1 μL of both sample and matrix (dithranol, 10 mg/mL in THF). Gel permeation chromatography (GPC) analyses of the polymers were carried out at 40 °C and a flow rate of 1.0 mL/min, with $CHCl_3$ as the eluent, on a Waters University 1500 GPC instrument equipped with four 5 μm PL gel columns (Polymer Laboratories) and calibrated using 10 PMMA standards. Chromatograms were processed with Waters Empower software (2002); number-average molecular weight and polydispersity of polymers are given relative to PMMA standards. NMR spectra of the resulting polymers were recorded in $CDCl_3$ and analyzed according to literature procedures.[18]

Results and Discussion

Polymerization of *n*-Butyl Acrylate by 1. The literature route to the chiral *ansa*-zirconocene precatalyst *rac*-(EBI)ZrMe[OC(O^{i}Pr)=CMe$_2$][3b] was considerably revised to allow for a semi-one-pot approach starting from the zirconocene dimethyl precursor. As can be seen in Scheme 1, the revised synthesis involves the reaction of *rac*-(EBI)ZrMe$_2$ with 1.2 equiv of TMSOTf in toluene followed by removal of the volatiles and drying (to remove any remaining excess TMSOTf) to give *rac*-(EBI)ZrMe(OTf), which was subsequently treated with 1 equiv of Me$_2$C=C(O^{i}Pr)OLi, affording the pure *rac*-(EBI)ZrMe[OC(O^{i}Pr)=CMe$_2$] in 90% isolated yield (based on *rac*-(EBI)ZrMe$_2$). This yield is substantially higher than the overall yield of 54% obtained from the previously

reported three-step process[3b] involving transformations from *rac*-(EBI)$ZrMe_2$ to *rac*-(EBI)$Zr(OTf)_2$ to *rac*-(EBI)ZrMe(OTf) to *rac*-(EBI)ZrMe[$OC(O^iPr)=CMe_2$]. The chiral cationic *ansa*-zirconocene ester enolate complex **1** can be either isolated[3b] or cleanly generated *in situ* by mixing *rac*-(EBI)ZrMe[$OC(O^iPr)=CMe_2$] with $(C_6F_5)_3B$•THF in CH_2Cl_2 at room temperature.[3a] The cation **1** is stable in a solution of CH_2Cl_2 at room temperature; subsequently, the *in situ* generated **1** in CH_2Cl_2 was used for all polymerization and model reaction studies.

Scheme 1

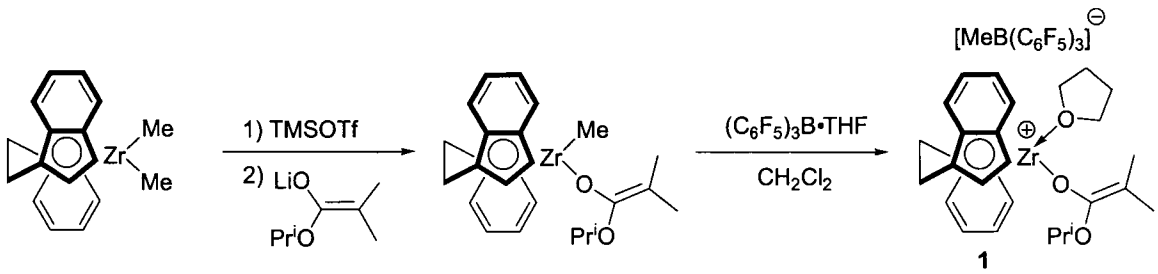

1

We have previously demonstrated that the methacrylate polymerization by complex **1**, which models the isospecific active propagating species for the methacrylate polymerization, proceeds in a living fashion via a monometallic propagation, enantiomorphic site-control mechanism, enabling the efficient synthesis of highly isotactic homopolymers having narrow MWDs with typical M_w/M_n values of 1.03–1.05 and high initiator efficiencies as well as stereodiblock copolymers with well-defined structures.[3a,b] In sharp contrast, the polymerization of *n*-BA by this well-defined complex is not controlled. Polymerizations of *n*-BA carried out in Teflon-valve-sealed J. Young-type NMR tubes in toluene-d_8 at high catalyst loadings ($[n\text{-BA}]_0/[\mathbf{1}]_0$ = 10–20) proceeded to high conversions (100–92%) within 10 min; as the $([n\text{-BA}]_0/[\mathbf{1}]_0$ ratio increases to 100, the conversions dropped drastically to 40%, even after extended reaction times, with

maximum conversions being reached typically within the first 10 min. Preparative-scale polymerizations of *n*-BA in CH_2Cl_2 at 23 °C {$[n\text{-BA}]_0/[\mathbf{1}]_0$ = 25, 50, 100} in the stirred reactors also gave low monomer conversions between 44–57% (runs 1–3, Table 1). Kinetic profiling of the polymerization of *n*-BA at $[n\text{-BA}]_0/[\mathbf{1}]_0$ = 100 by ^{1}H NMR analysis of reaction mixture aliquots revealed a maximum conversion of only 47% reached within the first 10 min, with no further conversion after extended polymerization times (run 3). Lowering of the reaction temperature to 0 and –22 °C only slightly increases the maximum conversions to 52% and 63%, respectively (runs 4 and 5). The isolated P(*n*-BA) samples have relatively broad MWDs with M_w/M_n values ranging from 1.26 to 1.51. Additionally, the measured M_n values are considerably higher than the expected M_n values, giving low initiator efficiencies of ≤ 65%. These results clearly show that the polymerization of *n*-BA by **1** proceeds only to moderate conversions with low to moderate initiator efficiencies in even a low monomer/initiator ratio of {$[n\text{-BA}]_0/[\mathbf{1}]_0 \leq$ 100}, indicative of the presence of chain termination reactions that prevent high monomer conversions.

Table 1. *n*-BA Polymerization Results by Chiral Zirconocenium Ester Enolate Complex 1[a]

entry	$[n\text{-BA}]_0/[\mathbf{1}]_0$	time (min)	temp (°C)	conv (%)	$10^3 M_n$[b] (g/mol)	PDI[b] (M_w/M_n)	I^*[c] (%)
1	25	10	23	57	4.5	1.27	41
2	50	10	23	44	6.7	1.41	42
3	100	10	23	47	9.2	1.38	65
4	100	10	0	52	14.0	1.51	48
5	100	30	–22	63	12.8	1.26	63

[a] Carried out in CH_2Cl_2 using an external temperature-control bath at the indicated temperatures. [b]Number average molecular weight (M_n) and polydispersity index (PDI) determined by GPC relative to PMMA standards in $CDCl_3$. [c] Initiator efficiency (I^*) = M_n(calcd)/M_n(exptl), where M_n(calcd) = MW(*n*-BA) × $[n\text{-BA}]_0/[\mathbf{1}]_0$ × conversion%.

Polymer Chain Structures of P(*n*-BA) Produced by 1. Analysis of a low-molecular-weight P(*n*-BA) sample by MALDI–TOF mass spectrometry provided

unambiguous evidence for the presence of chain termination/transfer reactions in the polymerization of *n*-BA by **1**. As can be seen in Figure 1, the mass spectrum of the P(*n*-BA) sample consists of one major (**A**) and two minor (**B** and **C**) series of mass ions, with the spacing of the mass ions within each series being that of the mass of the P(*n*-BA) repeat unit (*m/z* = 128). A plot of *m/z* values for series **A** in the MALDI-TOF mass spectrum vs the number of *n*-BA repeat units (n) afforded a straight line with a slope of 128.03 and an intercept of 153.34 (Figure 2); the slope corresponds to the mass of the *n*-BA monomer, whereas the intercept is the sum of the masses of Na^+ (from the added NaI) and the chain-end groups which corresponds to a formula of $C_7H_{14}O_2$. This analysis clearly shows that the polymer for series **A** has a structural formula of ^{i}PrOC(=O)C(Me$_2$)–(*n*-BA)$_n$–H, where the initiation chain end [^{i}PrOC(=O)C(Me$_2$)–] is derived from the initiating isopropyl isobutyrate group in complex **1** and the termination chain end (H) from either the acidic work-up after the polymerization or a chain termination process during the polymerization (vide infra). Hence, the peaks in series **A** correspond to the linear (living if terminated during the work-up) polymer chains produced by complex **1**.

The remaining two minor series of peaks (**B** and **C**) in the MALDI–TOF mass spectrum maintain a respective spacing of mass ions that corresponds to the repeat unit of P(*n*-BA) (*m/z* = 128); however, they do not exhibit a linear chain structure similar to **A**. A closer examination of these minor series of mass ions revealed a relationship to the linear polymer chain structure mass ions (series **A**) through the loss of one and two ^{n}BuOH molecules for series **B** and **C**, respectively, resulting in the formation of two corresponding cyclic structures at different stages of the polymerization (vide infra).

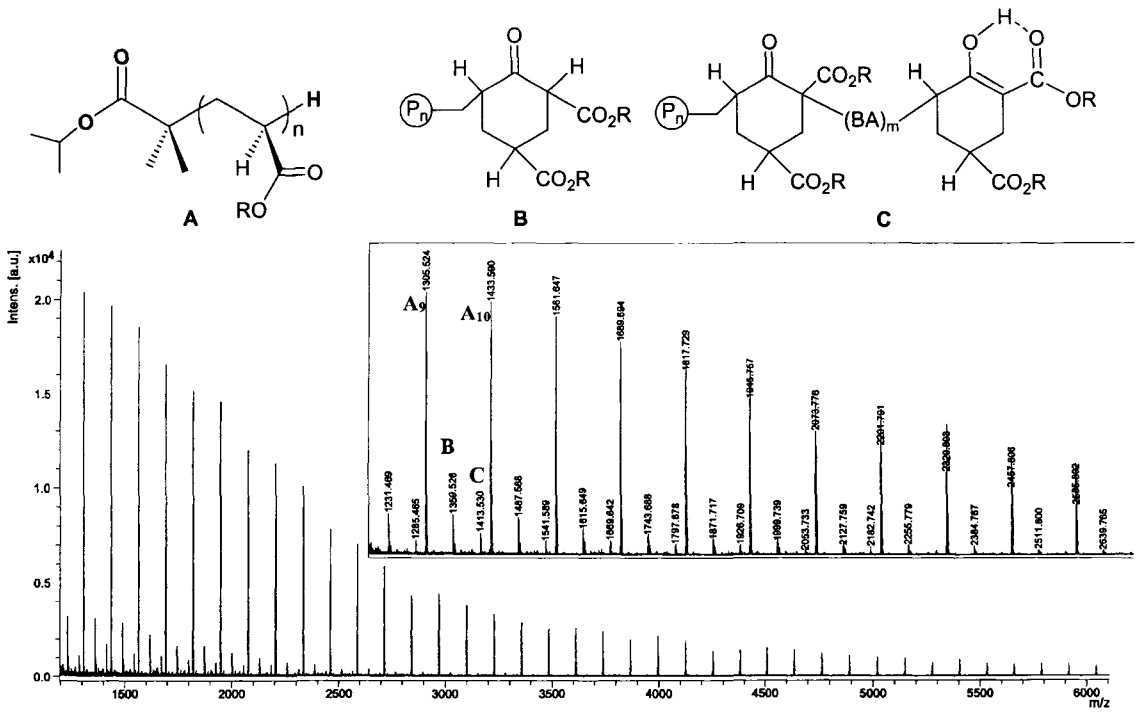

Figure 1. MALDI-TOF mass spectrum of the low-molecular-weight P(*n*-BA) produced by **1** in CH_2Cl_2 at 23 °C (R = ^{n}Bu); the sample was analyzed as quenched and unpurified.

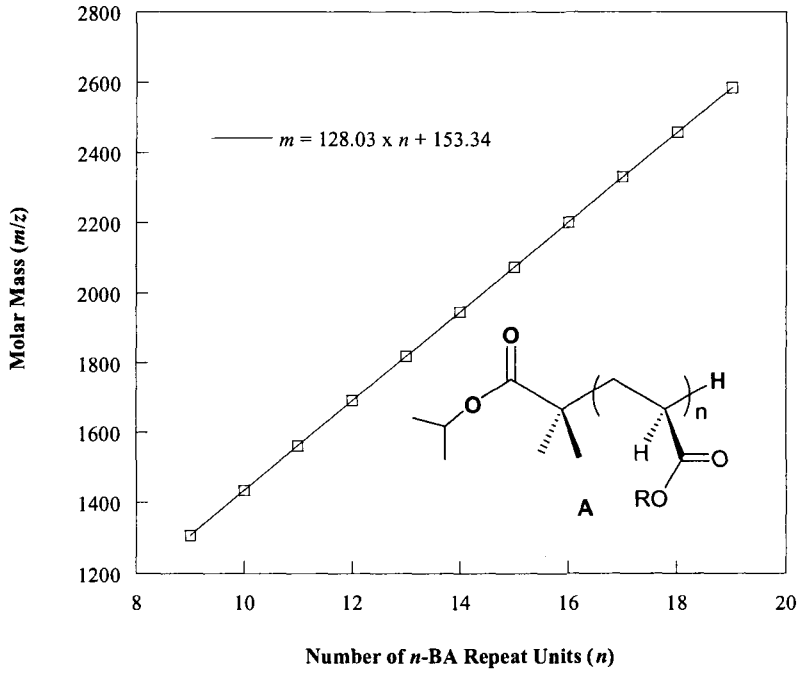

Figure 2. Plot of *m/z* values of series **A** from Figure **1** vs the number of *n*-BA repeat units (n).

Chain Termination Reactions in the Acrylate Polymerization by 1. To examine whether the *n*-BA monomer would decompose catalyst **1** or not, we carried out the stoichiometric reaction of *n*-BA and **1**, which clearly shows the rapid, complete disappearance of the *n*-BA vinyl signals and the appearance of a new set of resonances corresponding to the formation of the single *n*-BA addition (chain initiation) product, *rac*-(EBI)Zr^{+}[OC(O^{n}Bu)=$CHCH_2C(Me_2)C(O^{i}Pr)$=O][$MeB(C_6F_5)$]$^{-}$ (**2**; Scheme 2); analogous single MMA, *N*-isopropyl acrylamide, and *N*,*N*-dimethyl methacrylamide addition products have been previously isolated and characterized.[3a,13a] Next, we examined the catalytic competency of species **2** via its isolation and subsequent use for the polymerization of 500 equiv of MMA, which led to quantitative formation of highly isotactic P(MMA) having a narrow MWD (PDI = 1.03), with polymerization characteristics being similar to those obtained directly by **1**. These results clearly indicate a facile initiation process for the polymerization of *n*-BA by **1** via conjugate addition to generate the highly active propagating species **2** and suggest that chain termination reactions must occur during the propagating steps with the growing P(*n*-BA) chain bound to the metal center.

Scheme 2

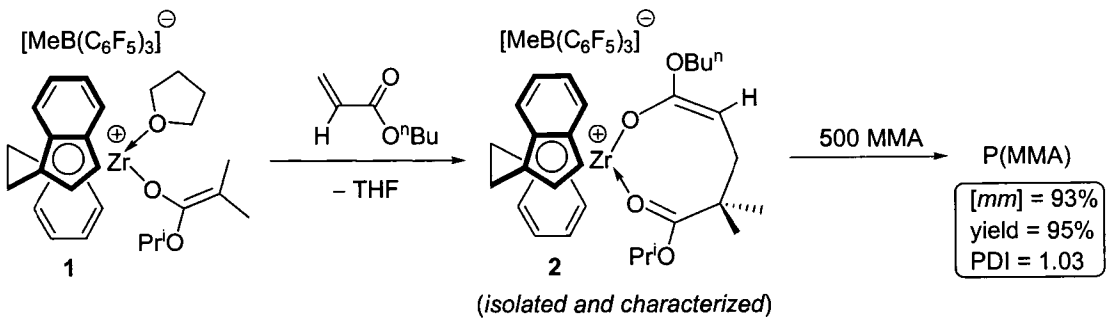

As evidenced by the MALDI–TOF mass spectrum, the polymerization of *n*-BA by **1** produces P(*n*-BA) exhibiting three types of chain structures, for which mechanism of

formation is proposed in Scheme 3. Linear chain structure **A** can be produced by the same mechanism previously established for the polymerization of MMA, which proceeds through the cyclic ester enolate intermediate **D** (resting state)[3a]; this is a living process, giving the well-defined living linear chain structure. However, this linear chain structure can also be produced from a chain-termination step involving the reaction between resting intermediate **D** and ^{n}BuOH generated by the back-biting cyclization (vide infra). Cyclic structures **B** and **C** are derived from six-membered-ring zirconocenium *β*-ketoester enolate **E**, which is produced from intramolecular back-biting cyclizations involving the activated antepenultimate ester group of the growing polymer chain. Specifically, cyclic intermediate **E** and its coproduct ROH (R = ^{n}Bu in this example, Scheme 3) are formed by a single back-biting cyclization via ten-membered-ring cyclic ester enolate intermediate **D'**; this process requires ring-expansion isomerization of eight-membered-ring intermediate **D** to ten-membered ring homolog **D'**, allowing for more thermodynamically favorable formation of a six-membered-ring transition state for nucleophilic attack of the enolate carbon onto the antepenultimate ester carbonyl carbon. An intermolecular polymer termination involving intermediate **D** and a dead polymer chain is unlikely because this pathway would utilize the unactivated ester group of another polymer chain. Hydrolysis of **E** during the acidic work-up procedure yields cyclic *β*-ketoester-terminated poly(*n*-BA) **B**, whereas the ROH formed from the back-biting cyclization deactivates the active propagating species **D** to give also linear chain **A** and the inactive zirconocenium alkoxide species. Further addition of m equiv of monomer to less reactive **E** (vs. **D**) followed by a second back-biting cyclization gives

the observed doubly cyclic β-ketoester-terminated poly(*n*-BA) **C** (after acidic work-up) and also results in further catalyst deactivation.

Scheme 3

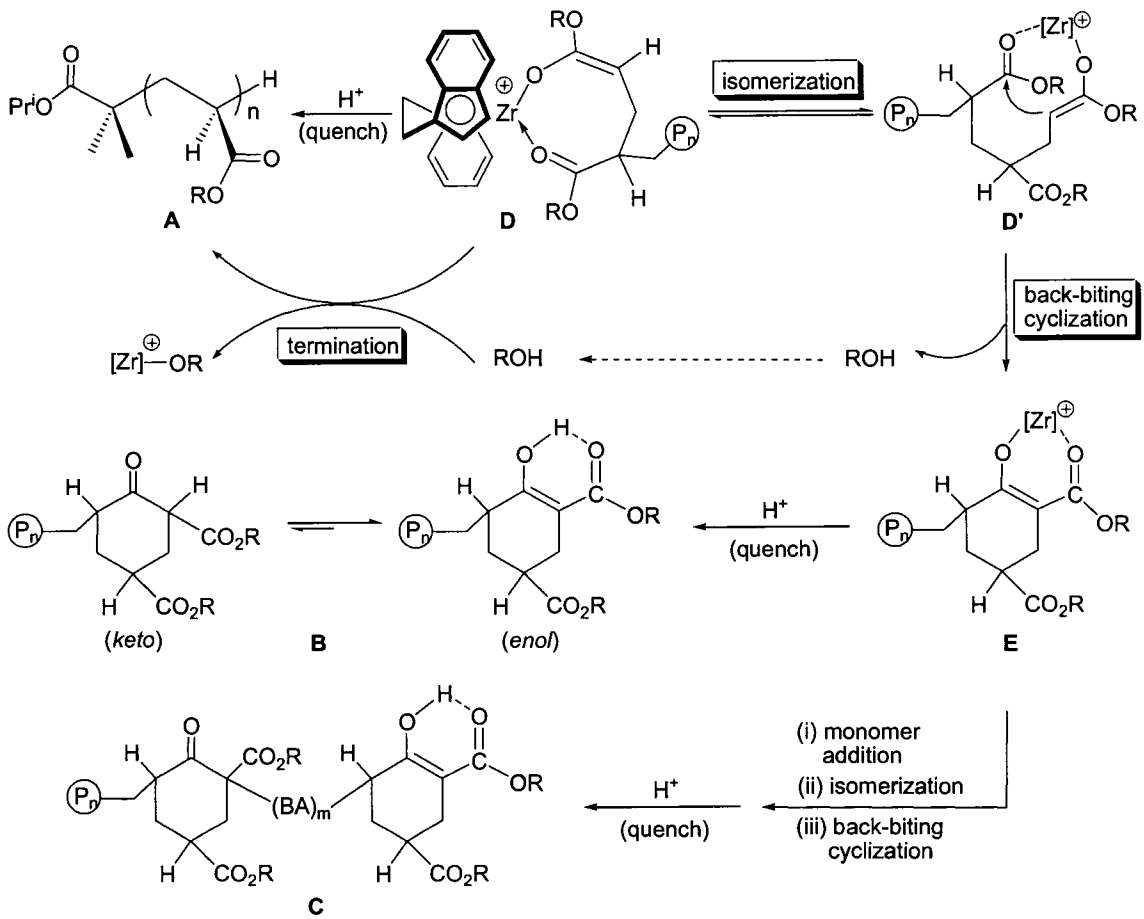

Back-biting cyclization leading to a cyclic β-ketoester-terminated polyacrylate chain end (i.e., type **B** structure) is ubiquitous in the anionic polymerization of acrylates;[19] such a back-biting cyclization typically does not occur in the metallocene-mediated polymerization of methacrylates, presumably due to sterics at the α-C of the enolate moiety and the absence of the readily enolizable acidic α-proton (cf. structure **D'**). Increasing the steric protection of the carbonyl carbon of alkyl acrylates apparently does not play a measurable role in suppressing the back-biting cyclization in the current system because the polymerization of *tert*-butyl acrylate behaves similarly to that of the

n-butyl acrylate polymerization. The acrylate-derived cyclic β-ketoester structure exists predominately in its enol form, and the proton of such an enol form in cyclic structures **B** or **C** produced in the current system can be readily identified in the ^{1}H NMR spectrum of the P(*n*-BA) produced with two small peaks at 12.21 and 12.46 ppm.[20,21] Reinitiation of a cyclic β-ketoester-terminated polyacrylate chain end (**B**-type structure) and subsequent formation of multiple cyclic β-ketoester-terminated polyacrylate chain ends (**C**-type structure) have been previously observed in the anionic polymerization of *n*-BA by a three-component system consisting of ethyl α-lithioisobutyrate/tetralkylammonium halide/trialkylaluminum.[22] What needs to be further confirmed in this overall mechanism, however, are the products of the back-biting cyclization and the reaction involving resting intermediate **D** and ROH.

The back-biting cyclization via intermediate **D'** could produce two possible product pairs, regardless how it occurs: (a) a cationic zirconocenium alkoxide complex and cyclic β-ketoester (**B**) pair, or (b) a cationic zirconocenium cyclic β-ketoester enolate (**E**) and ROH pair. On the basis of pK_a values of the β-ketoester (~14) vs ROH (~30),[23] the **E**/ROH pair is expected to be the thermodynamic products. To determine the products of the reaction between resting intermediate **D** and ROH, an authentic sample of cationic zirconocenium tert-butoxide complex **3** was prepared and a model reaction carried out (Scheme 4). Thus, treatment of the single *n*-BA addition product **2** (which models intermediate **D**) with ^{t}BuOH readily generates the cationic zirconocenium *tert*-butoxide complex **3**; the control experiment showed complex **3** to be inactive toward polymerization of *n*-BA over 24 h. Furthermore, to test whether zirconocenium cyclic β-ketoester enolate **E** can undergo further *n*-BA addition, or not, complex **2** was treated

with ethyl acetoacetate (EAA) to generate in situ cyclic β-ketoester enolate **4** (as a model for structure **E**). Upon addition of 10 equiv of *n*-BA, **4** consumed only ~18% of the monomer within the initial 10 min and without further monomer consumption over 24 h; this experiment implies that **E** is still active for *n*-BA addition, but it is much less active than **D**, satisfactorily accounting for the formation of a much smaller amount of doubly cyclic β-ketoester-terminated poly(*n*-BA), structure **C** (vs. **B**).

Scheme 4

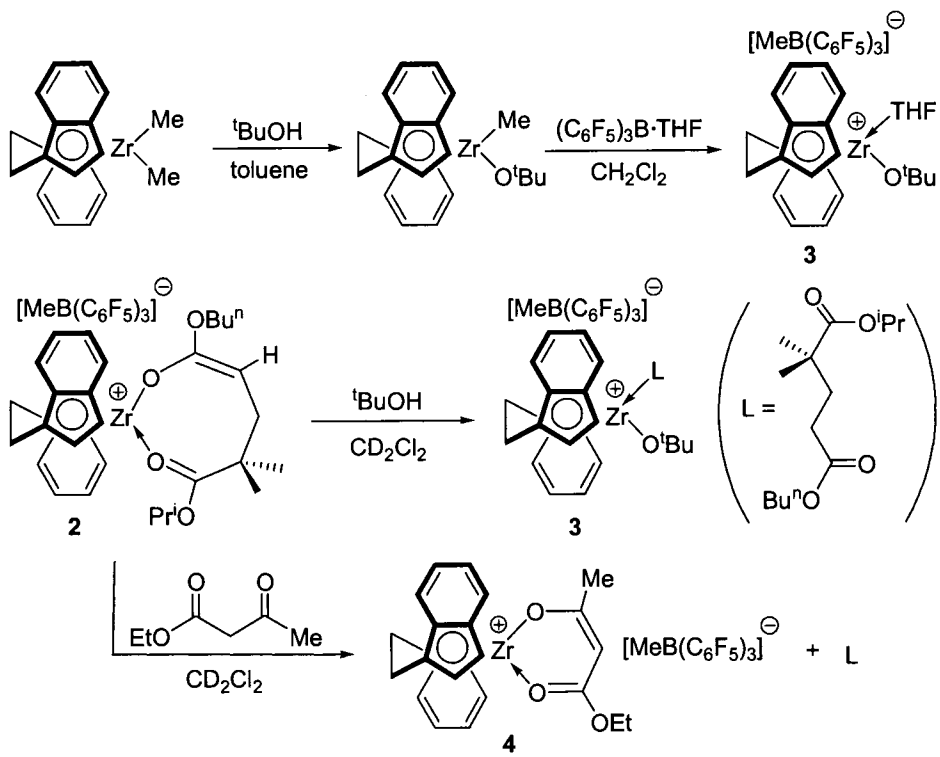

Lastly, the termination mechanism proposed in Scheme 3 shows that linear chain **A** can be produced by either the post-polymerization acidic methanol quench of living intermediate **D** or in-polymerization termination of intermediate **D** by ^{n}BuOH generated from the back-biting cyclization, the latter process of which was demonstrated by the above model reaction. To show that the former process also contributes to the formation of **A**, the behavior of the block copolymerization starting out with *n*-BA and finishing

with MMA was investigated. The hypothesis is that if the former process is operative, then there must be a fraction of the living propagating species (prior to work-up) that is preserved and competent for initiation of MMA polymerization to yield a diblock copolymer at least at low $[n\text{-BA}]_0/[\mathbf{1}]_0$ ratios. Thus, after a polymerization of 20 equiv of *n*-BA by **1** in CH_2Cl_2 at 23 °C for 10 min, 200 equiv of MMA was added and allowed to react for 1 h, yielding a polymer product that contains ~10 mol% of the MMA units in 10% isolated polymer yield based on the total monomer feed. The content of the MMA units in the polymer product increased to ~39 mol% when the sequential copolymerization was carried out at 0 °C. Owing to substantial chain termination reactions during the polymerization of *n*-BA, the resulting polymer products have low molecular weights with multimodal GPC molecular weight distributions and are presumably mixtures of homopolymer P(*n*-BA) and block copolymer P(*n*-BA)-b-P(MMA). Furthermore, the unreacted n-BA in the first step substantially affects the polymerization of MMA in the second step. For example, in statistical copolymerizations of MMA and *n*-BA by **1**, only 1 mol% of *n*-BA in the feed significantly deactivates the catalyst, and 10 mol% of *n*-BA shuts down the polymerization! This phenomenon can be attributed to the facile termination via back-biting cyclization whenever the unhindered enolate is formed (i.e., when a *n*-BA molecule is enchained).[21] Although these complications prevented us from estimating the percentage of chains that are still living prior to work-up, it is evident that at least a fraction of such living polymer chains contributes to the formation of structure **A** as a result of the work-up quench. Overall, the results from the above analysis, model reaction, and polymerization studies are consistent

with the overall chain termination mechanism shown in Scheme 3 for the acrylate polymerization by the current monometallic system.

Chain Transfer Reactions in the Acrylate Polymerization by 1. An investigation into reactions of the well-defined zirconocenium ester enolate complexes, including **1** and its single *n*-BA addition product **2**, with various types of enolizable esters, *β*-diesters, and *β*-ketoesters will not only provide direct evidence for possible chain transfer reactions, but also shed light on whether certain types of enolizable esters could potentially serve as chain transfer reagents (CTRs) for the development of an efficient chain transfer polymerization of (meth)acrylates mediated by group 4 metallocene complexes. An important feature of the current monometallic propagating system is that the zirconocenium complex employed is bifunctional; it can be called either catalyst or initiator because a single complex serves as both initiator (containing the nucleophilic initiating group) and catalyst (activating the enchaining monomer via coordination). Thus, it is a catalyst when emphasizing the fundamental catalytic event of monomer enchainment, but it is not a "true" catalyst when the catalytic production of polymer chains is concerned. In efforts to transform zirconocene complexes into "true" catalysts, Carpentier and co-workers[24] investigated the feasibility of using enolizable ketones and thiols as CTRs—an approach that had been employed by Nodono et al.[25] to effect the chain transfer polymerization of MMA with organolanthanide complexes such as $(C_5Me_5)_2SmMe(THF)$—for MMA polymerization mediated by the $Cp_2ZrMe_2/B(C_6F_5)_3$ system. Thus, stoichiometric reactions of the cationic ester enolate complex $[Cp_2Zr^+(THF)(O(^tBuO)C{=}CMe_2)]$ $[MeB(C_6F_5)_3]^-$ with these organic acids resulted in the formation of the undesired, inactive Zr-aldol product when enolizable ketones were used,

and the corresponding thiolates such as $[Cp_2Zr^+(S^tBu)(THF)][MeB(C_6F_5)_3]^-$ when thiols were employed. Although the resulting tert-butyl thiolate complex is still active for reinitiation of MMA polymerization, its poor initiation efficiency largely limited the effectiveness of ^{t}BuSH as a CTR in the MMA polymerization by the $Cp_2ZrMe_2/B(C_6F_5)_3$ system; hence, other types of organic acids are called for in order to achieve effective chain transfer polymerization.

Scheme 5

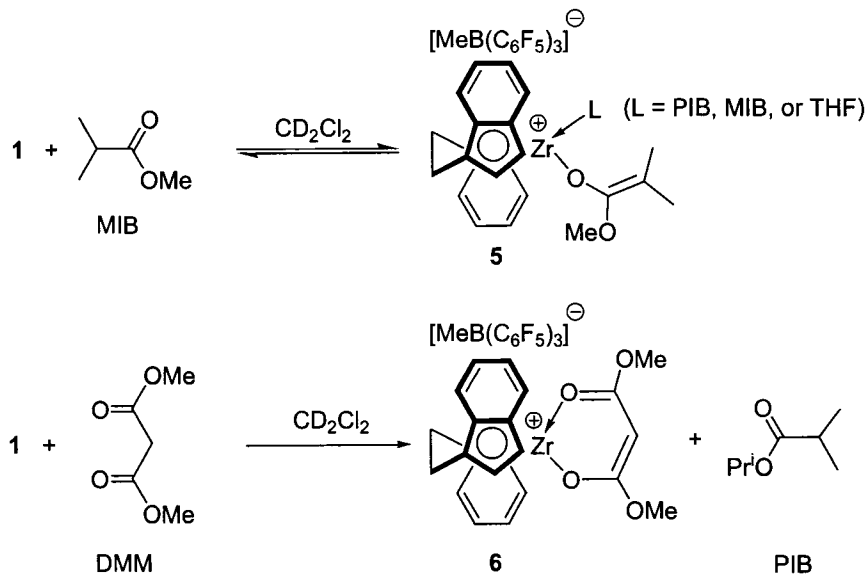

The equimolar reaction of **1** and methyl isobutyrate (MIB) in CD_2Cl_2 at ambient temperature resulted in the formation of an equilibrium mixture consisting of both the protonolysis product, rac-(EBI)Zr^+(L)[OC(OMe)=CMe_2][$MeB(C_6F_5)_3$]$^-$ (**5**, L = PIB, MIB, or THF, Scheme 5), and the starting materials in an approximate ratio of 1:2, with no noticeable change in this ratio after 5 h. On the other hand, monitoring the equimolar reaction of **1** with dimethyl malonate (DMM) in CD_2Cl_2 by ^{1}H NMR clearly shows the rapid disappearance of the peaks due to the starting materials and the appearance of a new set of resonances consistent with the formation of the corresponding protonolysis

product, rac-(EBI)Zr^{+}[OC(OMe)=CHC(OMe)=O][$MeB(C_6F_5)_3$]$^{-}$ (**6**), and the readily identifiable free isopropyl isobutyrate (PIB) co-product. The ^{1}H NMR spectrum of **6** exhibits an average C_2 symmetry in solution, suggesting a delocalized "acac"-type structure.

The above model reaction results also imply that enolizable esters such as MIB and DMM would not be suitable as effective chain transfer reagents for the polymerization of (meth)acrylates due to either inefficient chain transfer in the case of MIB or sluggish reinitiation in the case of DMM; to effect catalytic production of polymer chains, added CTRs must cleave or exchange the Zr–enolate bond (i.e., growing polymer chain) in a facile fashion on the polymerization time scale as well as efficiently reinitiate the polymerization. Indeed, the MMA polymerization by **1** in the presence of 1, 5, 10, 20, and 50 equiv (vs **1**) of MIB did not effect chain transfer polymerization. Within the MIB series, only small variations in activity with nearly constant [*mm*] (93%) and PDI (1.03) values as well as no change in M_n up to 20 equiv of MIB were observed. For the series of β-diesters (dimethyl-, diethyl-, and di-tert-butyl malonates), 10 equiv of CTR loadings resulted in diminished activity or complete shutting down of the polymerization, while at lower CTR loadings initiator efficiencies were much lower than expected for a chain transfer polymerization system.

Chain transfer reactions involving activation of protons in the α-position to the ester group of the polymer chain, the process indicated to be involved in the polymerization of *n*-BA by the bimetallic propagating system,[2k] were also considered in the current monometallic propagating system. Scheme 6 shows two possible pathways for proton transfer involving the resting intermediate **D**: intramolecular proton shift to the enolate

oxygen (i.e., formal cleavage of the Zr–enolate bond by the acidic α-proton) to give structure **F** and intermolecular proton transfer from a dead polymer chain to the enolate oxygen to give similar structure **G**, along with a release of a newly formed dead chain. In the intramolecular route, it is also possible other acidic α-protons further down the polymer chain can transfer the protons in the similar fashion, whereas in the intermolecular pathway, proton transfer involving two **D** molecules is less likely considering the sterics and charge repulsion between these two molecules. As compared to a tertiary α-C of the terminal ester enolate in structure **D**, the resulting structures **F** and **G** bear a quaternary α-C in the terminal (**F**) or internal (**G**) ester enolate moiety.

Scheme 6

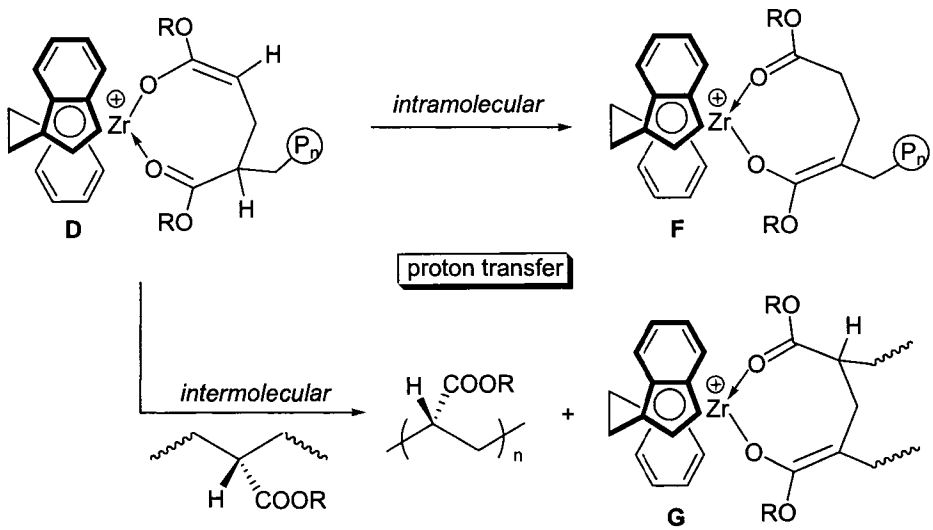

Structures **F** and **G** derived from proton transfer, if indeed formed on the polymerization time scale, could potentially exhibit different reactivity toward further chain growth from that of **D**. However, the reactivity of structure **F** should be comparable with that of **D** because structurally **F** is equivalent to **1** and thus **D**. Furthermore, structure **F** closely resembles that of the MMA propagating cyclic ester enolate structure **H** (Scheme 7) that is modeled by the isolated single-MMA-addition product,[3a] which has

been shown to exhibit similar activity toward polymerization of *n*-BA to that obtained by complex **2** that models structure **D**. Specifically, after a complete consumption of 200 equiv of MMA by **1**, 100 equiv of *n*-BA was added to yield block copolymer product P(MMA)-b-P(*n*-BA) that contains 15 mol% of the n-BA units based on ^{1}H NMR; this composition corresponds to a 45% *n*-BA conversion, the value of which is consistent with that observed for the independent homopolymerization of 100 equiv of *n*-BA by **1** at 23 °C (i.e., 47%; run 3, Table 1). Extraction of the bulk polymer product with methanol at ambient temperature for extended times ($\geq$ 12 h) resulted in a quantitative recovery of the insoluble polymer that has the same molar ratio of the MMA and *n*-BA units in the copolymer within experimental errors, confirming that it is the true copolymer product. (Note that low to medium molecular weight homopolymer P(*n*-BA) produced in this system is completely soluble in methanol.) The measured M_n and PDI of the copolymer product are 50K and 1.18, respectively, giving an overall initiator efficiency of ~52% (based on 100% MMA and 45% *n*-BA conversions); this proportions to a ~80% efficiency for the MMA polymerization[3a] and a ~65% for the n-BA polymerization, again consistent with the independent homopolymerization of *n*-BA. There is a bimodal distribution of the obtained copolymer, however, as indicated by two sharp peaks (PDI = 1.04 for each peak) within a relatively broad overall peak (PDI = 1.18) on the GPC trace; the formation of this ill-defined block copolymer structure is anticipated due to the presence of the chain termination/transfer processes for the *n*-BA polymerization as described above. In short, the possible intramolecular proton transfer process, if indeed occurring in this monometallic system, should apparently neither deactivate the catalyst nor affect the apparent rate of further chain growth.

Scheme 7

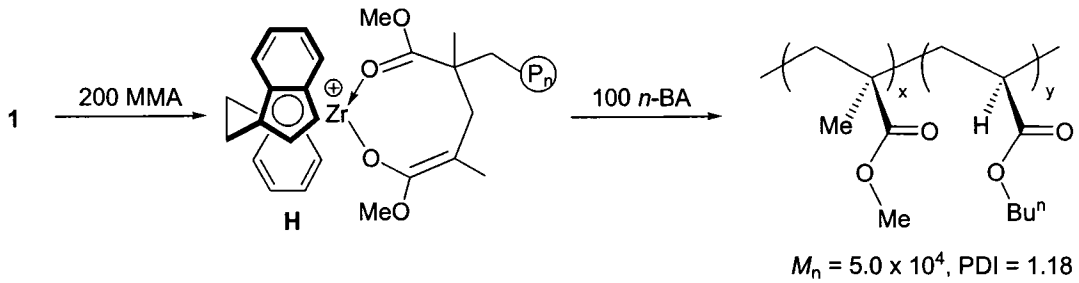

M_n = 5.0 x 10^4, PDI = 1.18

To directly assess the reactivity of the internally located ester enolate of structure **G** derived from the proposed intermolecular proton transfer (Scheme 6) remains a challenge because its reactivity is complicated by possible main chain mobility and entanglement issues. However, the model reaction between **1** and dimethyl succinate (DMS), a γ-diester, shows none to marginal reaction over a 14 h period; this is further backed by the results from the chain-transfer-type polymerization of MMA by **1** in the presence of various amounts of DMS. As can be seen from Table 2, addition of up to 50 equiv (vs **1**) of DMS neither deactivated the catalyst nor effected chain transfer polymerization, with only small variations in isolated polymer yield, M_n, PDI, and I^*. On the basis of these findings, it is evident that the possible intermolecular proton transfer in the current system appears to be too slow on the polymerization time scale (note that polymerization of *n*-BA is even faster than MMA) to affect chain transfer to polymer. If such chain transfer is facile relative to chain growth, polymer chain branching would occur. To provide additional support to the conclusion that proton transfer is insignificant in the current monometallic system, a model reaction directly relevant to the *n*-BA polymerization, outlined in Scheme 8, showed that there is no reaction between complex **2** (as a model for propagating intermediate **D**) and MIB (as a model for dead chain) for

up to 4 hrs in a CD_2Cl_2 solution at ambient temperature (i.e., under polymerization conditions).

Table 2. MMA Polymerization Results by 1 in the Presence of DMS (as Dead Chain Model) [a]

run no.	MMA/DMS/1 (molar ratio)	time (min)	temp (°C)	yield (%)	$10^3 M_n$ (g/mol)	PDI (M_w/M_n)	I^* (%)
1	500/1/1	30	23	92	56.8	1.03	81
2	500/5/1	30	23	88	55.6	1.03	80
3	500/10/1	30	23	88	57.5	1.03	77
4	500/20/1	30	23	87	56.4	1.04	77
5	500/50/1	30	23	86	58.3	1.11	74

[a] See Table 1 footnotes for explanations of the abbreviations listed in this table.

Scheme 8

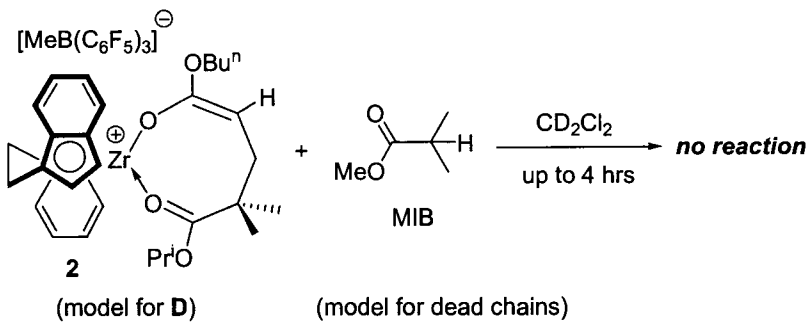

Conclusions

The well-defined monometallic propagating, chiral ansa-zirconocenium ester enolate complex **1** effects living polymerization of methacrylates and acrylamides; in sharp contrast, the polymerization of acrylates such as *n*-BA mediated by **1** proceeds in an uncontrolled fashion to only moderate conversions, producing P(*n*-BA) with one major linear structure **A** as well as two minor cyclic *β*-ketoester-terminated P(*n*-BA) structures **B** and **C**. Our investigations into polymerization characteristics, polymer chain structures, and model reactions have yielded unambiguous evidence for the presence of

termination processes in this polymerization system that prevent it from achieving high monomer conversions and producing all living chains. The proposed overall three-step mechanism adequately explains these catalyst deactivation pathways and the resulting polymer chain structures. Some of the key features about this mechanism are summarized as follows.

First, isomerization of the eight-membered-ring zirconocenium ester enolate propagating species **D** (resting state) to its ten-membered-ring homolog **D'** followed by intramolecular back-biting cyclization involving the antepenultimate ester group of the growing polymer chain generates the much less active six-membered-ring zirconocenium β-ketoester enolate species **E** [which leads to cyclic β-ketoester-terminated **B** after acidic work-up] and ^{n}BuOH. Second, the in situ eliminated ^{n}BuOH deactivates propagating species **D** to yield the inactive zirconocenium alkoxide species and linear chain **A**. Third, further addition of monomer to **E** followed by a second back-biting cyclization gives doubly cyclic β-ketoester-terminated **C** (after the acidic work-up), accompanied by additional catalyst deactivation and chain termination as shown above. Overall, the lack of steric protection at the unhindered α-C of the ester enolate moiety in the propagating species facilitates the back-biting cyclization, whereas the active (readily enolizable) α-proton provides access for elimination of ^{n}BuOH that subsequently terminates the chain.

Model reactions and polymerization studies show that possible chain transfer reactions involving acidic α-protons are insignificant as compared with back-biting cyclizations in the current monometallic catalyst system. With the catalyst deactivation pathways being identified and the mechanism of which understood, it is envisioned that strategies, such as prevention of isomerization of the active cyclic ester enolate resting

state by virtue of ligand design, can be developed to overcome these side reactions and thus render a living/controlled polymerization of acrylates mediated by group 4 metallocene catalysts.

Acknowledgements. Funding for this work was provided by the National Science Foundation and Colorado State University. We thank Boulder Scientific Co. for the gift of $B(C_6F_5)_3$ and the reviewers for their valuable comments and suggested additional experiments. A. P. Sloan Foundation (Research Fellowship to E.Y.C.) and ARCS/Hach Foundation (Graduate Fellowship to W.R.M.) are gratefully acknowledged.

References and Notes

(1) (a) Collins, S.; Ward, S. G. *J. Am. Chem. Soc.* **1992**, *114*, 5460–5462. (b) Yasuda, H.; Yamamoto, H.; Yokota, K.; Miyake, S; Nakamura, A. *J. Am. Chem. Soc.* **1992**, *114*, 4908–4909. (c) Farnham, W. B.; Hertler, W. U. S. Pat. 4,728,706, 1988.

(2) (a) Kostakis, K.; Mourmouris, S.; Kotakis, K.; Nikogeorgos, N.; Pitsikalis, M.; Hadjichristidis, N. *J. Polym. Sci. Part A: Polym. Chem.* **2005**, *43*, 3305–3314. (b) Stojcevic, G.; Kim, H.; Taylor, N. J.; Marder, T. B.; Collins, S. *Angew. Chem. Int. Ed.* **2004**, *43*, 5523–5526. (c) Lian, B.; Toupet, L.; Carpentier, J.-F. *Chem. Eur. J.* **2004**, *10*, 4301–4307. (d) Ferenz, M.; Bandermann, F.; Sustmann, R.; Sicking, W. *Macromol. Chem. Phys.* **2004**, *205*, 1196–1205. (e) Karanikolopoulos, G.; Batis, C.; Pitsikalis, M.; Hadjichristidis, N. *J. Polym. Sci. Part A: Polym. Chem.* **2004**, *42*, 3761–3774. (f) Wang, J.; Odian, G.; Haubenstock, H. *Polym. Prepr.* **2003**, *44*, 673–674; Wang, J.; Haubenstock, H.; Odian, G. *Polym. Prepr.* **2003**, *44*, 675–676. (g) Bandermann, F.; Ferenz, M.; Sustmann, R.; Sicking, W. *Macromol. Symp.* **2001**, *174*, 247–253. (h) Karanikolopoulos, G.; Batis, C.; Pitsikalis, M.; Hadjichristidis, N. *Macromolecules* **2001**, *34*, 4697–4705. (i) Bandermann, F.; Ferenz, M.; Sustmann, R.; Sicking, W. *Macromol. Symp.* **2000**, *161*, 127–134. (j) Shiono, T.; Saito, T.; Saegusa, N.; Hagihara, H.; Ikeda, T.; Deng, H.; Soga, K. *Macromol. Chem. Phys.* **1998**, *199*, 1573–1579. (k) Li, Y.; Ward, D. G.; Reddy, S. S.; Collins, S. *Macromolecules* **1997**, *30*, 1875–1883. (l) Deng, H.; Shiono, T.; Soga, K. *Macromol. Chem. Phys.* **1995**, *196*, 1971–1980.

(3) (a) Rodriguez-Delgado, A.; Chen, E. Y.-X. *Macromolecules* **2005**, *38*, 2587–2594. (b) Bolig, A. D.; Chen, E. Y.-X. *J. Am. Chem. Soc.* **2004**, *126*, 4897–4906. (c) Strauch, J. W.; Fauré, J.-L.; Bredeau, S.; Wang, C.; Kehr, G.; Fröhlich, R.; Luftmann, H.; Erker, G. *J. Am. Chem. Soc.* **2004**, *126*, 2089–2104. (d) Chen, E. Y.-X.; Cooney, M. J. *J. Am. Chem. Soc.* **2003**, *125*, 7150–7151. (e) Karanikolopoulos, G.; Batis, C.; Pitsikalis, M.; Hadjichristidis, N. *Macromol. Chem. Phys.* **2003**, *204*, 831–840. (f) Batis, C.; Karanikolopoulos, G.; Pitsikalis, M.; Hadjichristidis, N. *Macromolecules* **2003**, *36*, 9763–9774. (g) Bolig, A. D.; Chen, E. Y.-X. *J. Am. Chem. Soc.* **2002**, *124*, 5612–5613. (h) Frauenrath, H.; Keul, H.; Höcker, H. *Macromolecules* **2001**, *34*, 14–19. (i) Bolig, A. D.; Chen, E. Y.-X. *J. Am. Chem. Soc.* **2001**, *123*, 7943–7944. (j) Cameron, P. A.; Gibson, V.; Graham, A. J. *Macromolecules* **2000**, *33*, 4329–4335. (k) Stuhldreier, T.; Keul, H.; Höcker, H. *Macromol. Rapid Commun.* **2000**, *21*, 1093–1098. (l) Chen, Y.-X.; Metz, M. V.; Li, L.; Stern, C. L.; Marks, T. J. *J. Am. Chem. Soc.* **1998**, *120*, 6287–6305. (m) Deng, H.; Shiono, T.; Soga, K. *Macromolecules* **1995**, *28*, 3067–3073. (n) Soga, K.; Deng, H.; Yano, T.; Shiono, T. *Macromolecules* **1994**, *27*, 7938–7940. (o) Collins, S.; Ward, D. G.; Suddaby, K. H. *Macromolecules* **1994**, *27*, 7222–7224.

(4) Saegusa, N.; Shiono, T.; Ikeda, T.; Mikami, K. JP 10330391, 1998.

(5) (a) Jin, J.; Mariott, W. R.; Chen, E. Y.-X. *J. Polym. Chem. Part A: Polym. Chem.* **2003**, *41*, 3132–3142. (b) Jin, J.; Chen, E. Y.-X. *Organometallics* **2002**, *21*, 13–15.

(6) (a) Chen, E. Y.-X. *J. Polym. Sci. Part A: Polym. Chem.* **2004**, *42*, 3395–3403. (b) Jensen, T. R.; Yoon, S. C.; Dash, A. K.; Luo, L.; Marks, T. J. *J. Am. Chem. Soc.* **2003**, *125*, 14482–14494.

(7) (a) Rodriguez-Delgado, A.; Mariott, W. R.; Chen, E. Y.-X. *Macromolecules* **2004**, *37*, 3092–3100. (b) Jin, J.; Chen, E. Y.-X. *Macromol. Chem. Phys.* **2002**, *203*, 2329–2333. (c) Jin, J.; Wilson, D. R.; Chen, E. Y.-X. *Chem. Comm.* **2002**, 708–709. (d) Nguyen, H.; Jarvis, A. P.; Lesley, M. J. G.; Kelly, W. M.; Reddy, S. S.; Taylor, N. J.; Collins, S. *Macromolecules* **2000**, *33*, 1508–1510.

(8) (a) Hölscher, M.; Keul, H.; Höcker, H. *Macromolecules* **2002**, *35*, 8194–8202. (b) Hölscher, M.; Keul, H.; Höcker, H. *Chem. Eur. J.* **2001**, *7*, 5419–5426. (c) Sustmann, R.; Sicking, W.; Bandermann, F.; Ferenz, M. *Macromolecules* **1999**, *32*, 4204–4213.

(9) Deng, H.; Soga, K. *Macromolecules* **1996**, *29*, 1847–1848.

(10) Kostakis, K.; Mourmouris, S.; Pitsikalis, M.; Hadjichristidis, N. *J. Polym. Sci. Part A: Polym. Chem.* **2005**, *43*, 3337–3348.

(11) Ihara, E.; Morimoto, M.; Yasuda, H. *Macromolecules* **1995**, *28*, 7886–7892.

(12) The Ziegler group at the University of Calgary informed us of their on-going computational study of the polymerization of acrylates by monometallic cationic zirconocenes; we thank Dr. Simone Tomasi for helpful discussions.

(13) (a) Mariott, W. R.; Chen, E. Y.-X. *Macromolecules* **2005**, *38*, 6822–6832. (b) Mariott, W. R.; Chen, E. Y.-X. *Macromolecules* **2004**, *37*, 4741–4743.

(14) Allen, R. D.; Long, T. E.; McGrath, J. E. *Polym. Bull.* **1986**, *15*, 127–134.

(15) (a) Grossman, R. B.; Doyle, R. A.; Buchwald, S. L. *Organometallics* **1991**, *10*, 1501–1505. (b) Collins, S.; Kuntz, B. A.; Taylor, N. J.; Ward, D. G. *J. Organomet. Chem.* **1988**, *342*, 21–29.

(16) Diamond, G. M.; Jordan, R. F.; Petersen, J. L. *J. Am. Chem. Soc.* **1996**, *118*, 8024–8033.

(17) (a) Stoebenau, E. J.; III, Jordan, R. F. *J. Am. Chem. Soc.* **2003**, *125*, 3222–3223. (b) Hong, Y.; Kuntz, B. A.; Collins, S. *Organometallics* **1993**, *12*, 964–969.

(18) (a) Kawamura, T.; Toshima, N.; Matsuzaki. *Macromol. Chem. Phys.* **1995**, *196*, 3415–3424. (b) Bovey, F. A.; Mirau, P. A. *NMR of Polymers*; Academic Press: San Diego, 1996. (c) Ferguson, R. C.; Ovenall, D. W. *Macromolecules* **1987**, *20*, 1245–1248. (d) Ferguson, R. C.; Ovenall, D. W. *Polym. Prepr.* **1985**, *26*, 182–183. (e) Subramanian, R.; Allen, R. D.; McGrath, J. E.; Ward, T. C. *Polym. Prepr.* **1985**, *26*, 238–240.

(19) For a recent review, see: Baskaran, D. *Prog. Polym. Sci.* **2003**, *28*, 521–581.

(20) Tabuchi, M.; Kawauchi, T.; Kitayama, T.; Hatada, K. *Polymer* **2002**, *43*, 7185–7190.

(21) Jacobs, C.; Varshney, S. K.; Hautekeer, J.-P.; Fayt, R.; Jérôme, R.; Teyssié, P. *Macromolcules* **1990**, *23*, 4024–4025.

(22) Schmitt, B.; Müller, A. H. E. *Macromolecules* **2001**, *34*, 2115–2120.

(23) Bordwell, F. G. *Acc. Chem. Res.* **1988**, *21*, 456–463.

(24) Lian, B.; Lehmann, C. W.; Navarro, C.; Carpentier, J.-F. *Organometallics* **2005**, *24*, 2466–2472.

(25) Nodono, M.; Tokimitsu, T.; Tone, S.; Makino, T.; Yanagase, A. *Macromol. Chem. Phys.* **2000**, *201*, 2282–2288.

CHAPTER V

ACTIVATION OF TANTALOCENE(V) ALKYL AND ALKYLIDENE COMPLEXES WITH STRONG ORGANO-LEWIS ACIDS AND APPLICATION TO POLYMERIZATION CATALYSIS

This dissertation chapter contains the manuscript of a full paper in press in *Organometallics* [Mariott, W. R.; Gustafson, L. O.; Chen, E. Y.-X *Organometallics* **2006**, *25*, 3721–3729] and describes investigations into the activation of group(V) metallocene complexes. This chapter addresses a long standing goal of developing an active group(V) metallocene-based system for the polymerization of functionalized alkenes such as alkyl methacrylates and acrylamides. This work on the activation of tantalocene(V) alkyl and alkylidene complexes by strong organo-Lewis acids has resulted in the isolation and structural characterization of three new cationic and zwitterionic tantalocene complexes. Further studies into the polymerization of methyl methacrylate (MMA) and *N*,*N*-dimethylacrylamide (DMAA) by Schrock's tantalocene alkylidene complex $Cp_2Ta(=CH_2)Me$ with 2 equiv of $Al(C_6F_5)_3$ afforded highly active polymerization systems.

L.O.G. (an R.E.U. student working under the supervision of W.R.M.) performed the initial survey experiments in activation of tantalocene alkyl and alkylidene complexes as well as the use of the derived activated species for the polymerization of MMA.

Abstract

This work reexamines the reaction of the tantalocene trialkyl complex Cp_2TaMe_3 with strong organo-Lewis acids (LAs) $E(C_6F_5)_3$ (E = B, Al) under various reaction conditions, investigates activation of Schrock's alkylidene complex $Cp_2Ta(=CH_2)Me$ with $Al(C_6F_5)_3$, and employs the alkylidene complex for the polymerization of functionalized alkenes such as methyl methacrylate (MMA) and *N*,*N*-dimethyl acrylamide (DMAA). Three cationic and zwitterionic tantalocene complexes have been isolated and structurally characterized, including cationic $[Cp_2TaMe_2]^+[MeB(C_6F_5)_3]^-$ (**1**), zwitterionic $Cp_2Ta^+[CH_2Al(C_6F_5)_3^-]Me$ (**2**), as well as cationic $[Cp_2Ta(CH_2)MeAl(C_6F_5)_2]^+[Al(C_6F_5)_4]^-$ (**3**). Complex **3**, which is formed by unusual nucleophilic attack of a C_6F_5 group within the aluminate moiety in **2** on $Al(C_6F_5)_3$ present in excess, consists of the cation portion that can be viewed as a hybrid of two extreme structures: $Cp_2Ta^+[CH_2Al(C_6F_5)_2]Me$ and cationic tantalocene alkylidene-LA adduct $[Cp_2Ta(=CH_2)MeAl(C_6F_5)_2]^+$; the investigation into the scope of such a unique reaction type shows to be specific to the aluminate/alane (Al^-/Al) pair. All three isolated complexes are inactive for polymerization of MMA and DMAA; however, the combination of $Cp_2Ta(=CH_2)Me$ with 2 equiv of $Al(C_6F_5)_3$ is highly active, producing high molecular weight polymers presumably via an Al^-/Al bimolecular propagation process.

Introduction

Polymerization of functionalized alkenes such as methacrylates[1], acrylates,[2] and acrylamides[3] catalyzed by group 4 metallocene and related complexes has attracted

increasing attention due to the demonstrated remarkable versatility and control of most of these polymerization systems in terms of both catalyst structure and polymer architecture. In contrast, applications of group 5 metallocene and related complexes, especially tantalocenes(V), to the polymerization of these functionalized alkenes are scarce. Half-sandwich tantalum bis(diene) complexes, upon activation with suitable activators, are active for the polymerization of methyl methacrylate (MMA);[4] tantalocene trimethyl Cp_2TaMe_3, in combination with 2 equiv of $Al(C_6F_5)_3$ is active and highly active for MMA polymerization in toluene and 1,2-dichlorobenzene, respectively, whereas other tantalocene/cocatalyst combinations, such as $Cp_2TaMe_3/Al(C_6F_5)_3$, $Cp_2TaMe_3/xB(C_6F_5)_3$ (x = 1, 2), and $Cp_2TaMe_3/[Ph_3C][B(C_6F_5)_4]$, exhibit no activity for MMA polymerization in both types of solvents.[5]

Our earlier investigations into how these cocatalysts activate Cp_2TaMe_3 provided knowledge for the understanding of the activity or inactivity of the above tantalocene(V)/LA systems. The 1:1 ratio reaction of Cp_2TaMe_3 and $E(C_6F_5)_3$ (E = B, Al) in polar, halogenated solvents such as C_6D_5Br and CD_2Cl_2 leads to clean formation of the corresponding ion pair $[Cp_2TaMe_2]^+[MeE(C_6F_5)_3]^-$,[5b] whereas the reaction of Cp_2TaMe_3 with 2 equiv of $Al(C_6F_5)_3$ in either arene (benzene and toluene) or polar chlorinated (bromobenzene) solvents affords a unique cationic tantalocene μ-Me dialuminate complex, $[Cp_2TaMe_2]^+[(C_6F_5)_3Al–Me–Al(C_6F_5)_3]^-$, which was structurally characterized.[6] Since the other above combinations produce the same tantalocene cation $[Cp_2TaMe_2]^+$ paired with non-dialuminate anions and are inactive for the MMA polymerization, the polymerization activity of the $Cp_2TaMe_3/2Al(C_6F_5)_3$ system was thus attributed not to the cation, but to the μ-Me dialuminate anion-mediated bimolecular

propagating process.[5a] We earlier invoked the formation of the analogous μ-Me diborate anion based on ^{1}H and ^{19}F NMR data of the resulting phase-separated mixture derived from the reaction of Cp_2TaMe_3 with $B(C_6F_5)_3$ in C_6D_6 or C_7D_8 and the structure of the aluminate analogue.[6] One might wonder, however, why the combination of Cp_2TaMe_3 with excess $B(C_6F_5)_3$ is ineffective for MMA polymerization if the species formed are analogous to the μ-Me dialuminate. Recent reports by Collins and Piers that such a diborate anion was not detected by NMR from either the reaction of $B(C_6F_5)_3$ with $[Bu_4N]^+[MeBC_6F_5)_3]^-$ in C_6D_6/CD_2Cl_2 (5/1 v/v)[7] or the reaction of $[(Me_3Si)_2N]_3ZrMe$ (or Cp_2ZrMe_2) with the chelating diborane 1,2-$[B(C_6F_5)_2]_2C_6F_4$[8] cast further doubt on the original report of the diborate species. Most recently, Royo and co-workers showed that the reaction of the half-sandwich tantalum tetramethyl complex Cp^*TaMe_4 with 1 equiv of $B(C_6F_5)_3$ forms the corresponding cation $[Cp^*TaMe_3]^+$ paired with methyl borate anion $[MeBC_6F_5)_3]^-$.[9] These questions and observations prompted our current reinvestigation of the reaction of Cp_2TaMe_3 with $E(C_6F_5)_3$ under varied reaction conditions including concentration, solvent, temperature, ratio, and scale, as well as by isolation and structural characterization.

Another readily available tantalocene(V) complex that could potentially lead to an active system for the MMA polymerization, upon appropriate activation, is Schrock's methyl methylidene complex $Cp_2Ta(=CH_2)Me$[10] that contains both alkyl and nucleophilic alkylidene ligands. Piers et al.[11] investigated the reactions of this methylidene complex with $HB(C_6F_5)_2$ and $B(C_6F_5)_3$ as well as isolated and structurally characterized the reaction products arising from attack of the borane by the methylidene ligand, the latter reaction of which produces the zwitterionic tantalocene complex

$Cp_2Ta^+[CH_2B(C_6F_5)_3^-]Me$. In our continued quest for active group 5 metallocene systems for the polymerization of functionalized alkenes, we found that $Cp_2Ta(=CH_2)Me/xE(C_6F_5)_3$ (E = B, x = 1, 2; E = Al, x = 1) systems are inactive for MMA polymerization but a combination of $Cp_2Ta(=CH_2)Me$ with 2 equiv of $Al(C_6F_5)_3$ is highly active. Prompted by this observation, we investigated the reaction of $Cp_2Ta(=CH_2)Me$ with $Al(C_6F_5)_3$ and discovered that the reaction product depends on stoichiometry; while the 1:1 ratio reaction gives analogous zwitterionic complex $Cp_2Ta^+[CH_2Al(C_6F_5)_3^-]Me$ (**2**), the reaction with excess $Al(C_6F_5)_3$ affords cationic complex $[Cp_2Ta(CH_2)MeAl(C_6F_5)_2]^+[Al(C_6F_5)_4]^-$ (**3**), involving unusual nucleophilic attack of a C_6F_5 group within the aluminate moiety in **2** at $Al(C_6F_5)_3$.

Experimental Section

Materials and Methods. All syntheses and manipulations of air- and moisture-sensitive materials were carried out in flamed Schlenk-type glassware on a dual-manifold Schlenk line, a high-vacuum line (typically 10^{-5} to 10^{-7} Torr), or in an argon or nitrogen-filled glovebox (typically <1.0 ppm oxygen and moisture). NMR-scale reactions (typically in a 0.02 mmol scale in ~0.7 mL of an NMR solvent) were conducted in Teflon-valve-sealed J. Young-type NMR tubes. HPLC grade organic solvents were sparged extensively with nitrogen during filling of the solvent reservoir and then dried by passage through activated alumina (for THF, Et_2O, and CH_2Cl_2) followed by passage through Q-5-supported copper catalyst (for toluene and hexanes) stainless steel columns. Benzene-d_6 and toluene-d_8 were degassed, dried over sodium/potassium alloy, and filtered before use, whereas $CDCl_3$, C_6D_5Br, CD_2Cl_2, and 1,2-dichlorobenzene (DCB)

were degassed and dried over activated Davison 4 Å molecular sieves. NMR spectra were recorded on either a Varian Inova 300 (FT 300 MHz, ^{1}H; 75 MHz, ^{13}C; 282 MHz, ^{19}F) or a Varian Inova 400 spectrometer. Chemical shifts for ^{1}H and ^{13}C spectra were referenced to internal solvent resonances and are reported as parts per million relative to tetramethylsilane, whereas ^{19}F NMR spectra were referenced to external $CFCl_3$. Elemental analyses were performed by Desert Analytics, Tucson, Arizona.

Reagents $TaCl_5$, CpTl, Ph_3CBF_4, and $NaNH_2$ were purchased from Alfa Aesar, while $ZnMe_2$ (10 wt% in hexanes), Me_4PBr, and $AlMe_3$ (neat) were purchased from Strem Chemical Co.; they were used as received. Methyl methacrylate (MMA) and *N,N*-dimethylacrylamide (DMAA) were purchased from Aldrich Chemical Co. and TCI America, respectively; they were purified by first degassing and drying over CaH_2 overnight, followed by vacuum distillation; final purification of MMA involved titration with neat tri(*n*-octyl)aluminum to a yellow end point[12] followed by a second vacuum distillation. The purified monomers were stored in brown bottles over activated Davison 4Å molecular sieves (for DMAA) in a –30 °C freezer inside the glovebox.

Tris(pentafluorophenyl)borane $B(C_6F_5)_3$ was obtained as a research gift from Boulder Scientific Co. and further purified by recrystallization from hexanes at –30 °C. Tris(pentafluorophenyl)alane $Al(C_6F_5)_3$, as a 0.5 toluene adduct $Al(C_6F_5)_3 \cdot (C_7H_8)_{0.5}$ based on the elemental analysis for the vacuum-dried sample, was prepared by the ligand exchange reaction of $B(C_6F_5)_3$ and $AlMe_3$ in a 1:3 toluene/hexanes solvent mixture in quantitative yield;[5b] this is the modified synthesis based on literature procedures.[13] *Extra caution should be exercised when handling this material, especially the unsolvated form, because of its thermal and shock sensitivity.* Literature procedures were employed for the

preparation of the following compounds or metallocene complexes: $[Ph_3C][B(C_6F_5)_4]$,[14] Cp_2TaMe_3 ($Cp = \eta^5$-C_5H_5),[10] $Cp_2Ta(=CH_2)Me$, [10] and $Cp_2TaMe^+CH_2B(C_6F_5)_3^-$.[11b]

Isolation of $[Cp_2TaMe_2]^+[MeB(C_6F_5)_3]^-$ (1). In an argon-filled glovebox, a 30-mL glass reactor was equipped with a stir bar and charged with Cp_2TaMe_3 (53.4 mg, 0.150 mmol), $B(C_6F_5)_3$ (76.8 mg, 0.150 mmol), and 15 mL of CH_2Cl_2. The resulting clear yellow reaction mixture was allowed to stir for 30 min at ambient temperature, after which all volatiles were removed in vacuo to give a pale yellow microcrystalline solid. This solid was washed with 3 × 2 mL of hexanes and dried under vacuum for 2 h, yielding 116 mg (89%) of the pure title complex as a pale yellow microcrystalline solid. Anal. Calcd. for $C_{31}H_{19}BF_{15}Ta$: C, 42.88; H, 2.21. Found: C, 43.14; H, 2.28.

^{1}H NMR (CD_2Cl_2, 23 °C): δ 6.44 (s, 10H, C_5H_5), 0.64 (s, 6H, Ta-*Me*), 0.47 (s, br, 3H, B-*Me*). ^{19}F NMR (CD_2Cl_2, 23°C): δ –131.50 (d, $^3J_{FF}$ = 20.6 Hz, 6F, *o*-F), –163.37 (t, $^3J_{FF}$ = 20.6 Hz, 3F, *p*-F), –166.00 (m, 6F, *m*-F). ^{13}C NMR (CD_2Cl_2, 23 °C): δ 148.81 (d, $^1J_{CF}$ = 241.5 Hz, C_6F_5), 138.03 (d, $^1J_{CF}$ = 243.5 Hz, C_6F_5), 136.97 (d, $^1J_{CF}$ = 242.8 Hz, C_6F_5), and 129.52 (s, br) for C_6F_5 carbons, 112.92 (C_5H_5), 57.13 (Ta-*Me*), 10.49 (B-*Me*).

Isolation of $Cp_2Ta^+[CH_2Al(C_6F_5)_3^-]Me$ (2). In an argon-filled glovebox, a 30-mL glass reactor was equipped with a stir bar and charged with $Cp_2Ta(=CH_2)Me$ (34.0 mg, 0.100 mmol), $Al(C_6F_5)_3$•$(C_7H_8)_{0.5}$ (57.4 mg, 0.100 mmol), and 5 mL of toluene. The resulting clear dark green solution was allowed to stir for 30 min at ambient temperature, after which all volatiles were removed in vacuo affording a dark green sticky residue. This residue was washed with 5 × 2 mL hexanes and dried under vacuum to yield 81.9 mg (94%) of the pure title complex as a dark green solid. Anal. Calcd. for $C_{30}H_{15}AlF_{15}Ta$: C, 41.50; H, 1.74. Found: C, 41.56; H, 1.59.

^{1}H NMR (C_6D_5Br, 23 °C): δ 5.76 (s, 10H, C_5H_5), 3.77 (s, br, 2H, CH_2), 0.09 (s, 3H, CH_3). ^{19}F NMR (C_6D_5Br, 23°C): δ –121.17 (d, $^3J_{FF}$ = 19.6 Hz, 6F, *o*-F), –154.71 (t, $^3J_{FF}$ = 20.3 Hz, 3F, *p*-F), –161.45 (m, 6F, *m*-F). ^{13}C NMR (C_6D_5Br, 23 °C): δ 150.34 (d, $^1J_{CF}$ = 231.1 Hz, C_6F_5), 141.18 (d, $^1J_{CF}$ = 251.0 Hz, C_6F_5), 137.25 (d, $^1J_{CF}$ = 254.0 Hz, C_6F_5), 109.89 (C_5H_5), 31.51 (CH_3). The CH_2 carbon and *ipso*-carbon of the C_6F_5 group could not be assigned with confidence due to their aluminum-broadened peaks and overlapping with the NMR solvent peaks; the HMQC experiment gave $^1J_{CH}$ of 126.0 Hz for the CH_2 group.

Synthesis of $[Cp_2Ta(CH_2)MeAl(C_6F_5)_2]^+[Al(C_6F_5)_4]^-$ (3). In an argon-filled glovebox, a 25-mL Schlenk flask was equipped with a stir bar and charged with $Cp_2Ta(=CH_2)Me$ (34.0 mg, 0.100 mmol) and $Al(C_6F_5)_3•(C_7H_8)_{0.5}$ (0.230 g, 0.400 mmol). The flask was sealed, removed from the glovebox, and interfaced to a Schlenk line in a 23 °C water bath, after which 5 mL of bromobenzene was added via gastight syringe. The reaction mixture was allowed to stir at 23 °C for 24 h, during which time the solution gradually changed from light green to dark green. All volatiles were removed in vacuo, and the resulting sticky green residue was dried for additional 2 h before being taken into a glovebox and washed with 3 × 1 mL of cold (–30 °C) toluene followed by 3 × 2 mL of hexanes. The residue was dried extensively under vacuum affording 115.5 mg (83%) of the pure title complex as a dark green solid. Anal. Calcd. for $C_{48}H_{15}Al_2F_{30}Ta$: C, 41.28; H, 1.08. Found: C, 41.02; H, 1.09.

^{1}H NMR (C_6D_5Br, 23 °C): δ 8.96 (s, br, 2H, CH_2), 5.85 (s, 10H, C_5H_5), 0.47 (s, 3H, CH_3). ^{19}F NMR (C_6D_5Br, 23°C): δ –120.51 [d, $^3J_{FF}$ = 21.1 Hz, 4F, *o*-F, $Al(C_6F_5)_2$], –121.87 [d, $^3J_{FF}$ = 18.8 Hz, 8F, *o*-F, $Al(C_6F_5)_4$], –147.02 [s, br, 2F, *p*-F, $Al(C_6F_5)_2$], –

156.41 [t, $^3J_{FF}$ = 20.0 Hz, 4F, *p*-F, $Al(C_6F_5)_4$], –157.42 (m, 4F, *m*-F), –162.78 [m, 8F, *m*-F, $Al(C_6F_5)_4$].

General Polymerization Procedures. Polymerizations were carried out in 30-mL glass reactors at ambient temperature (~25 °C) inside an argon-filled glovebox in either toluene or DCB. For activated complex polymerizations, $Cp_2Ta(=CH_2)Me$ (8.0 mg, 23.4 μmol) and $Al(C_6F_5)_3•(C_7H_8)_{0.5}$ (26.9 mg, 46.8 μmol) were dissolved in 5 mL solvent and stirred for 10 min at ambient temperature before the addition of MMA (1.00 mL, 9.35 mmol) to the vigorously stirred solution. The solution was stirred for 30 min, after which the reaction was quenched by the addition of 5 mL 5% HCl-acidified methanol. The quenched mixture was precipitated into 100 mL of methanol, stirred for 30 min, filtered, and washed with methanol. The polymer product was collected and dried in a vacuum oven at 50 °C overnight to a constant weight. Activated monomer polymerizations were performed in a similar manner, but for these runs a solution of $Al(C_6F_5)_3$ in MMA was added via pipette to a vigorously stirred solution of $Cp_2Ta(=CH_2)Me$ in 5 mL of solvent. Polymerizations of DMAA were carried out in a similar manner to the MMA polymerizations, except for different work-up procedures. Upon quenching a DMAA polymerization by the addition of 5 mL 5% HCl-acidified methanol, the quenched mixture was precipitated into 100 mL of diethyl ether, stirred for 30 min, and the solvent was decanted off. An additional 75 mL of diethyl ether was used to wash the polymer product and then decanted. The product was dried in a vacuum oven at 50 °C overnight, dissolved in minimum CH_2Cl_2 or methanol, precipitated into a 10-fold excess of diethyl ether, stirred for 30 min, filtered, washed with diethyl ether, and dried in a vacuum oven at 50 °C overnight to a constant weight.

Polymer Characterizations. Gel permeation chromatography (GPC) analyses of the polymers were carried out at 40 °C and a flow rate of 1.0 mL/min, with $CHCl_3$ as the eluent, on a Waters University 1500 GPC instrument equipped with four 5 μm PL gel columns (Polymer Laboratories) and calibrated using 10 PMMA standards. Chromatograms were processed with Waters Empower software (version 2002); number-average molecular weight and polydispersity of polymers are given relative to PMMA standards. NMR spectra of the resulting polymers were recorded in $CDCl_3$ and analyzed according to literature procedures.[15]

X-Ray Crystallographic Analyses of 1, 2, and 3. Single crystals of complexes **1**, **2**, and **3** suitable for X-ray diffraction were grown from a CH_2Cl_2 solution layered with hexanes, a 1:1 toluene:hexanes solvent mixture, and a 10:1 toluene:CH_2Cl_2 solvent mixture, respectively, all at –30 °C inside the freezer of a glovebox. The crystals were quickly covered with a layer of Paratone-N oil (Exxon, dried and degassed at 120 °C/10^{-6} Torr for 24 h) after the mother liquors were decanted and then mounted on a thin glass fiber and transferred into the cold nitrogen stream of a Bruker SMART CCD diffractometer. The structures were solved by direct methods and refined using the Bruker SHELXTL program library by full-matrix least-squares on F^2 for all reflections.[16] All non-hydrogen atoms were refined with anisotropic displacement parameters, whereas hydrogen atoms were included in the structure factor calculations at idealized positions, except for the bridging methylene and methyl hydrogen atoms in **2** and **3** which were located by the difference Fourier synthesis and refined. There are a CH_2Cl_2, a toluene, and two CH_2Cl_2 crystallization solvent molecules in the lattice in complexes **1**, **2**, and **3**,

respectively. Selected crystal data and structural refinement parameters are collected in Table 1.

Table 1. Crystal Data and Structure Refinements for **1**•CH_2Cl_2, **2**•C_7H_8, and **3**•$2CH_2Cl_2$.

	1•CH_2Cl_2	**2**•C_7H_8	**3**•$2CH_2Cl_2$
empirical formula	$C_{32}H_{21}BCl_2F_{15}Ta$	$C_{37}H_{23}AlF_{15}Ta$	$C_{50}H_{19}Al_2Cl_4F_{30}Ta$
formula weight	953.15	960.48	1566.36
temperature/K	173(2)	100(2)	173(2)
wavelength/Å	0.71073	0.71073	0.71073
crystal system	orthorhombic	orthorhombic	triclinic
space group	$P2_12_12_1$	*Pbca*	$P\bar{1}$
a/Å	12.6003(10)	19.9908(11)	12.2991(10)
b/Å	15.4046(12)	16.7232(9)	14.0265(11)
c/Å	16.4304(13)	20.0723(11)	16.5511(13)
α/deg	90	90	87.396(2)
β/deg	90	90	78.182(2)
γ/deg	90	90	68.632(20
volume/Å^3	3189.2(4)	6710.4(6)	2601.3(4)
Z	4	8	2
density (calcd)/ Mg/m^3	1.985	1.901	2.000
abs coeff/mm^{-1}	3.727	3.415	2.499
F(000)	1840	3728	1512
crystal size/mm^3	0.30 × 0.20 × 0.08	0.54 × 0.24 × 0.11	0.19 × 0.14 × 0.06
θ range for data collection/°	1.81 to 28.44	1.88 to 28.33	2.79 to 38.07
index ranges	-16≤h≤16, -20≤k≤20	-26≤h≤25, -22≤k≤22	-21≤h≤21, -24≤k≤24
	-21≤l≤21	-26≤l≤26	-28≤l≤28
reflections collected	30175	61163	254589
independent reflections	7807[R_{int} = 0.0328]	8313[R_{int} = 0.0304]	28325[R_{int} = 0.0412]
completeness to θ	98.3%	99.4%	99.5%
data /restraints/parameters	7807/0/460	8313/0/495	28325/1/796
goodness-of-fit on F^2	1.022	1.059	1.011
final R indices [$I>2\sigma(I)$]	R_1 = 0.0236	R_1 = 0.0251	R_1 = 0.0337
	wR_2 = 0.0495	wR_2 = 0.0587	wR_2 = 0.0928
R indices (all data)	R_1 = 0.0280	R_1 = 0.0398	R_1 = 0.0408
	wR_2 = 0.0509	wR_2 = 0.0679	wR_2 = 0.0972
largest diff. Peak and hole/eÅ^{-3}	1.311 and –0.583	1.065 and –0.460	2.304 and –2.919

Results and Discussion

Reaction of Cp_2TaMe_3 with $E(C_6F_5)_3$ (E = B, Al): Reexamination. Mixing of Cp_2TaMe_3 with 1 equiv of $B(C_6F_5)_3$ in nonpolar, hydrocarbon solvents such as C_6D_6 and C_7D_8 (28.6 mM) at ambient temperature initially formed a light yellow suspension which turned gradually to yellow oily precipitates in about 15 min. The resulting phase-separated mixture showed two sets of signals in ^1H and ^{19}F NMR spectra at ambient temperature, both assignable to the $[MeB(C_6F_5)_3]^-$ anion or a closely related anion moiety. In the ^1H NMR (C_6D_6, 23 °C) spectrum, the separation between the two broad singlet *Me*B peaks is 0.38 ppm (δ 1.33 vs 0.95 ppm), whereas the separations between two Cp (δ 5.04 and 5.01 ppm) and *Me*Ta (δ –0.38 and –0.40 ppm) peaks are only marginal. The diagnostic *ortho*, *para*-, and *meta*-fluorine patterns and chemical shifts for a typical free $[MeB(C_6F_5)_3]^-$ type anion in the ^{19}F NMR spectrum are also seen as sharp peaks in pairs with only marginal separations: δ –131.99 vs. –132.36 (d, $^3J_{FF}$ = 21.2 Hz, *o*-F), –163.98 vs. –164.05 (t, $^3J_{FF}$ = 21.4 Hz, *p*-F), and –166.57 vs. –166.64 (m, *m*-F). The ratio of these two sets of peaks changes with time when monitored over a period of 15 min to 18 h and also with varied concentration (28.6, 14.3, and 7.15 mM). The 1:2 ratio with $B(C_6F_5)_3$ and the 1:1 ratio with $Al(C_6F_5)_3$ reactions also gave phase-separated mixtures exhibiting similar doubling of the peaks in ^1H and ^{19}F NMR spectra. An exception is the 1:2 ratio reaction with $Al(C_6F_5)_3$, which cleanly generates in either benzene or toluene the μ-Me dialuminate complex, $[Cp_2TaMe_2]^+[(C_6F_5)_3Al–Me–Al(C_6F_5)_3]^-$, as colorless crystals.[6]

When the 1:1 ratio reaction of Cp_2TaMe_3 and $B(C_6F_5)_3$ was carried out in polar, halogenated solvents such as C_6D_5Br and CD_2Cl_2, a homogeneous solution was obtained,

the NMR spectra of which indicated clean formation of the corresponding ion pair $[Cp_2TaMe_2]^+[MeB(C_6F_5)_3]^-$ (**1**).[5b] The noncoordinating nature of the anion $[MeB(C_6F_5)_3]^-$ in **1** is inferred by the observation of diagnostically a small chemical shift difference of < 3 ppm [$\Delta(m,p\text{-F})$ = 2.6 ppm in **1**] between the *para*- and *meta*-fluorines.[17] The preparative scale reaction in CH_2Cl_2 afforded the analytically pure **1** in 89% isolated yield, and its molecular structure is confirmed by X-ray diffraction analysis, featuring unassociated

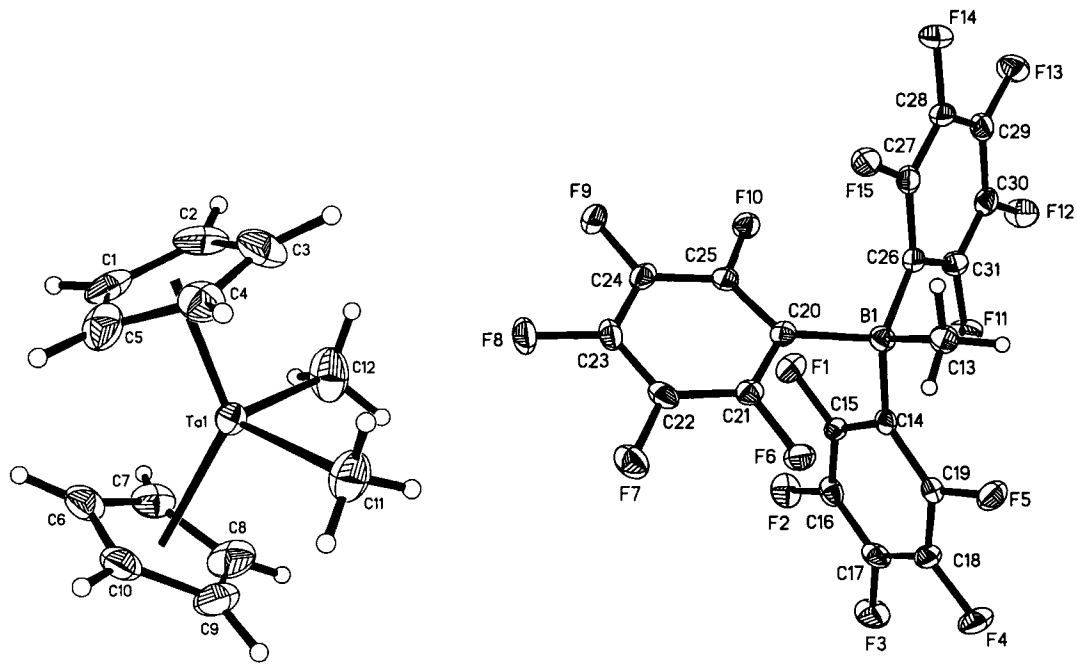

Figure 1. Molecular structure of complex **1**. Selected bond lengths (Å): Ta–C(11) = 2.178(3), Ta–C(12) = 2.170(4), B–C(13) = 1.634(5), B–C(14) = 1.658(5), B–C(20) = 1.659(5), B–C(26) = 1.661(5); selected bond angles (deg): C(11)–Ta–C(12) = 97.0 (1), C(13)–B–C(14) = 114.8(3), C(13)–B–C(20) = 109.0(3), C(13)–B–C(26) = 103.9(3), C(14)–B–C(20) = 103.7(3), C(14)–B–C(26) = 111.7(3), C(20)–B–C(26) = 114.1(3).

cation $[Cp_2TaMe_2]^+$ and anion $[MeB(C_6F_5)_3]^-$ pairs (Figure 1). The 1:1 ratio reaction with $Al(C_6F_5)_3$ in C_6D_5Br occurs analogously to generate cleanly the aluminate derivative $[Cp_2TaMe_2]^+[MeAl(C_6F_5)_3]^-$.[5b] [The use of C_6D_5Br, instead of CD_2Cl_2, for this reaction is noteworthy; CD_2Cl_2 is not suitable for the reaction involving the unsolvated $Al(C_6F_5)_3$ or

$Al(C_6F_5)_3•(C_7H_8)_{0.5}$ as CH_2Cl_2 decomposes $Al(C_6F_5)_3$ via facile chloride abstraction to form $(C_6F_5)_2AlCl$, which has been structurally characterized as a dimer in the solid state.[18] Conversely, CH_2Cl_2 presents no problems for reactions involving base adducts such as $THF•Al(C_6F_5)_3$ and $MMA•Al(C_6F_5)_3$.] The 1:2 ratio reactions with $E(C_6F_5)_3$ are drastically different, however, depending on E; while the reaction of Cp_2TaMe_3 with 2 equiv of $Al(C_6F_5)_3$ cleanly produces the crystalline μ-Me dialuminate complex, the reaction with 2 equiv of $B(C_6F_5)_3$ affords the same product **1** as the 1:1 ratio reaction, along with the excess $B(C_6F_5)_3$ and a small amount of $MeB(C_6F_5)_2$. Additionally, the reaction of Cp_2TaMe_3 with 1 equiv of $B(C_6F_5)_3$ and 1 equiv of $Al(C_6F_5)_3$ did not produce the plausible μ-Me bridged borate-aluminate mixed anion $[(C_6F_5)_3B–Me–Al(C_6F_5)_3]^-$.

With the fully characterized **1** on hand, the nature of the second set of NMR signals appearing in arene solvents can be understood. Redissolving the crystals of **1** or the isolated liquid clathrate phase, obtained from a preparative scale reaction of Cp_2TaMe_3 with $B(C_6F_5)_3$ in toluene, back in C_6D_6 gave identical NMR spectra exhibiting a doubling of NMR signals similar to that observed in the reaction carried out in arene solvents; the switch to CD_2Cl_2 afforded cleanly only one set of peaks identical to those for the isolated **1** in CD_2Cl_2. Variable temperature ^1H NMR experiments of **1** in C_7D_8 (28.6 mM) also showed only one set of peaks at temperature $\geq$ 60 °C (Figure 2); VT ^{19}F NMR spectra corresponded to the same trend. It is clear from these results that the observation of the second set of peaks from the reaction in arene solvents at ambient temperature is not due to the formation of the plausible μ-Me diborate species, but rather simply the clathrate phase of ionic aggregates that are in slow exchange and can also give rise to decent NMR signals with different chemical shifts than those of the monomeric form in solution. Thus,

we previously erred when attributing the second set of NMR signals to the plausible μ-Me diborate species.[6] Consequently, the stability of such μ-alkyl diborate anions must be questioned. The larger covalent radius of aluminum compared to that of boron, reflected by considerably longer distances of typical Al–C bonds (with electrostatic character) than B–C bonds (more covalent in nature), likely better accommodates the steric crowding of two $Al(C_6F_5)_3$ moieties connected by the small Me group for the facile formation of $[(C_6F_5)_3Al–Me–Al(C_6F_5)_3]^-$; on the other hand, isolation, or even detection, of μ-Me boron-containing dinuclear anions, such as $[(C_6F_5)_3B–Me–Al(C_6F_5)_3]^-$ and $[(C_6F_5)_3B–Me–B(C_6F_5)_3]^-$, still remains elusive.

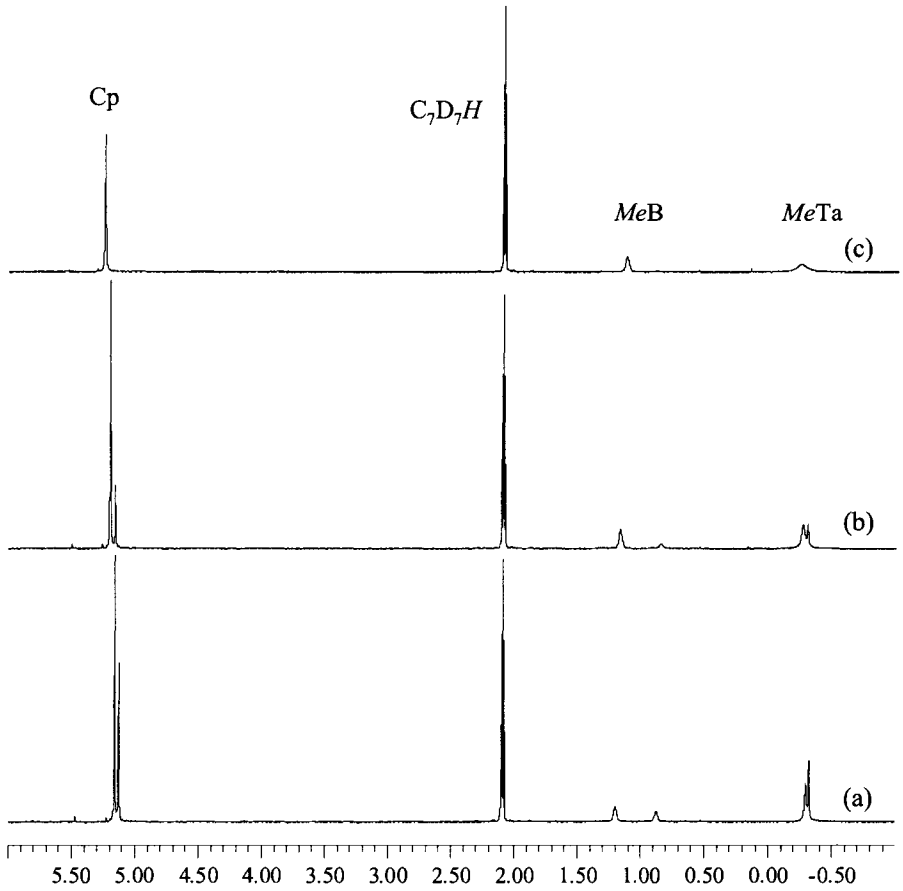

Figure 2. ^1H NMR spectra of **1** in C_7D_8 at 25 °C (a), 40 °C (b), and 60 °C (c).

Reaction of $Cp_2Ta(=CH_2)Me$ with 1 Equiv of $Al(C_6F_5)_3$. Piers and co-workers[11b] showed that the reaction of $Cp_2Ta(=CH_2)Me$ with $B(C_6F_5)_3$ in toluene rapidly produces the zwitterionic tantalocene complex $Cp_2Ta^+[CH_2B(C_6F_5)_3^-]Me$ in which the cationic Ta center is stabilized by a strong α-agostic interaction involving one of the C–H bonds of the electron-rich methylene unit (Scheme 1). We found that the reaction with 1 equiv of $Al(C_6F_5)_3$ in toluene occurs analogously affording the zwitterionic tantalocene aluminate derivative $Cp_2Ta^+[CH_2Al(C_6F_5)_3^-]Me$ (**2**, Scheme 1); treatment of the borate derivative with 1 equiv of $Al(C_6F_5)_3$ in C_6D_5Br also leads to complex **2** as the major product (vide infra). As in the reaction with $B(C_6F_5)_3$, electrophilic attack of $Al(C_6F_5)_3$ at the methylidene carbon causes a drastic high-field shift of the sharp peak at 10.14 ppm (C_6D_6) for the methylidene protons in $Cp_2Ta(=CH_2)Me$ to a now aluminum-broadened peak at 3.77 ppm in C_6D_5Br (3.64 ppm in CD_2Cl_2 or 3.63 ppm in C_7D_8) for the methylene protons in **2**; furthermore, the ^{19}F NMR chemical shifts of the resulting product are consistent with the alkyl tris(pentafluorophenyl)aluminate formation.[19] However, unlike the structure of the borate derivative, there is no solution NMR evidence ($^1J_{CH}$ of the CH_2 group is 126.0 Hz) for the presence of an α-agostic interaction in this aluminate derivative, arguing that the charge separation in **2** is less extensive than the borate analog. The molecular structure of **2** has been confirmed by X-ray diffraction (Figure 3), in which both CH_2 hydrogens were located and refined.

Scheme 1

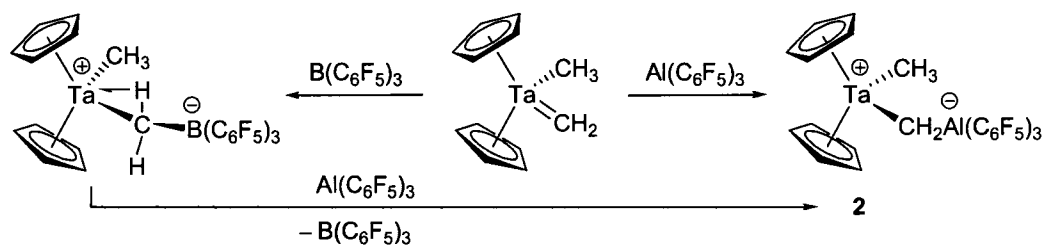

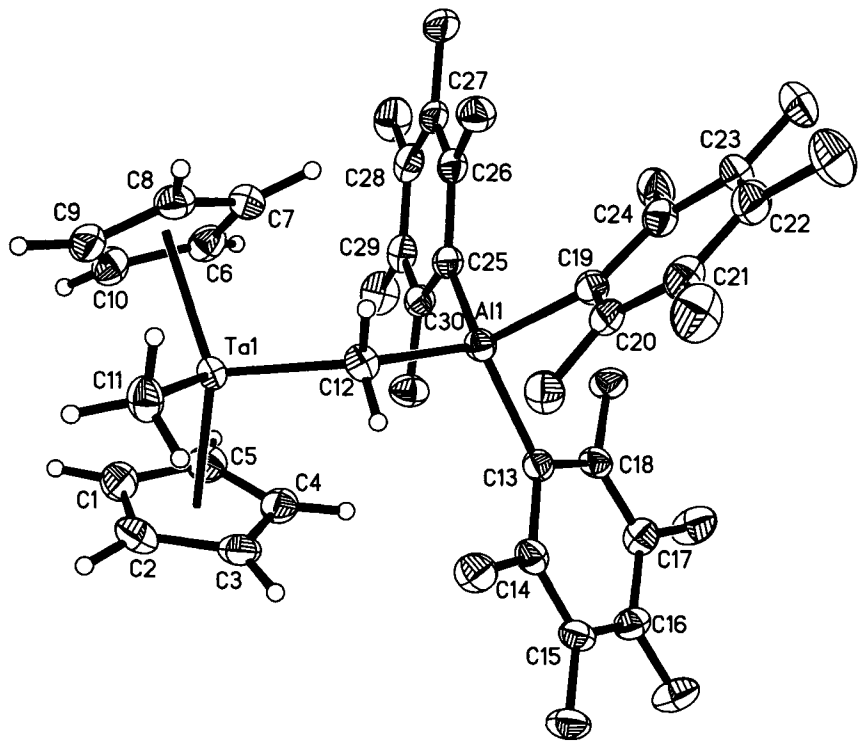

Figure 3. Molecular structure of complex **2**. Selected bond lengths (Å): Ta–C(11) = 2.202(3), Ta–C(12) = 2.106(3), Al–C(12) = 2.008(3), Al–C(13) = 2.035(3), Al–C(19) = 2.033(3), Al–C(25) = 2.025(3); selected bond angles (deg): Ta–C(12)–Al = 133.2 (1), C(11)–Ta–C(12) = 95.5(1), C(12)–Al–C(13) = 115.0(1), C(12)–Al–C(19) = 107.9(1), C(12)–Al–C(25) = 110.0(1), C(13)–Al–C(19) = 102.2(1), C(13)–Al–C(25) = 109.3(1), C(19)–Al–C(25) = 112.3(1).

The absence of an α-agostic interaction in the solid state structure of **2** is evident by the observation of the normal, similar C–H distances for both H(12) hydrogens [C(12)–H(12a) = 0.973(3) Å, C(12)–H(12b) = 0.929(3) Å], normal, similar angles for both Ta–C(12)–H(12) vectors [Ta–C(12)–H(12a) = 105.0 (17)°, Ta–C(12)–H(12b) = 105.6 (17)°], and large, nonbonding Ta–H distances for both H(12) hydrogens [Ta–H(12a) = 2.538(3) Å, Ta–H(12b) = 2.520 Å)]. As in the borate derivative, the Ta–CH_2 distance is notably shorter than the Ta–CH_3 distance by ~0.1 Å [Ta–C(11) = 2.202(3) Å, Ta–C(12) = 2.106(3) Å]. The metric parameters of the –$CH_2Al(C_6F_5)_3$ aluminate moiety compares well with those of the μ-Me-aluminate –$MeAl(C_6F_5)_3$ moiety observed in group 4 metallocene cationic complexes.[19] Considerably larger distances of Al–C bonds in **2** than

the corresponding B–C bonds in the borate derivative [e.g., Al–CH_2(bridging) = 2.008(3) Å, B–CH_2 = 1.661(7) Å] presumably alleviate the steric interactions between the –$Al(C_6F_5)_3$ moiety and Cp rings, resulting in an approximately 12° smaller Ta–C(12)–E vector angle in **2** than that in the borate derivative; these results are consistent with the conclusion that the degree of charge separation in **2** is less than the borate derivative.

Reaction of $Cp_2Ta(=CH_2)Me$ with Excess $Al(C_6F_5)_3$. The outcome of the reaction of $Cp_2Ta(=CH_2)Me$ with excess (2 to 4 equiv) $E(C_6F_5)_3$ depends on E. Thus, the reaction with excess $B(C_6F_5)_3$ in C_6D_6 or CD_2Cl_2 gave the same adduct $Cp_2Ta^+[CH_2B(C_6F_5)_3^-]Me$ as in the 1:1 ratio reaction, along with the unreacted excess borane. However, the reaction with excess $Al(C_6F_5)_3$ in C_6D_5Br slowly but cleanly converted the rapidly formed adduct **2** to a new species over a 24 h period. The ^1H NMR spectrum of this new species exhibits a broad signal at 8.96 ppm for the CH_2 moiety attached to an Al center, reflecting a 5.2 ppm down-field shift as compared with **2**, while the Me protons were also down-field shifted although only by ~0.4 ppm. Interestingly, its ^{19}F NMR spectrum exhibits two sets of Al-C_6F_5 peaks corresponding to a neutral alane-like structure [δ –120.51 (d, 4F, o-F), –147.02 (s, br, 2F, p-F), –157.42 (m, 4F, m-F)] and an anionic aluminate-like structure [δ –121.87 (d, 8F, o-F), –156.41 (t, 4F, p-F), –162.78 (m, 8F, m-F)], the integrals of which show two C_6F_5 groups for the neutral species and four C_6F_5 groups for the aluminate anion. The spectroscopic data of this new species are consistent with the structure $[Cp_2Ta(CH_2)MeAl(C_6F_5)_2]^+[Al(C_6F_5)_4]^-$ (**3**) depicted in Scheme 2, and its formation is proposed to resemble the established nucleophilic attack of the Me group within the free $[MeAl(C_6F_5)_3]^-$ anion at $Al(C_6F_5)_3$ to form the μ-Me dialuminate complex.[6] Specifically, when nucleophilic moieties such as Me(Al) are absent within the aluminate moiety in **2**, a

commonly regarded as chemically robust, resistant-to-electrophilic-attack C_6F_5 group attacks $Al(C_6F_5)_3$ to form the tetrakis(pentafluorophenyl) aluminate anion $[Al(C_6F_5)_4]^-$, followed by nucleophilic linking of Me(Ta) to the resulting neutral alane, producing an μ-(Me)(CH_2)-doubly bridged tantalocene cation. Direct abstraction of either the Me(Ta) or the anionic $-CH_2Al(C_6F_5)_3$ moiety in **2** by excess $Al(C_6F_5)_3$ would generate a 14-electron tantalocene dication; however, this reaction produced no evidence for the formation of such a species, presumably due to either instability of such a dication or steric inaccessibility of $Al(C_6F_5)_3$ to the Me(Ta) or (Ta)CH_2(Al), or a combination of both factors.

Scheme 2

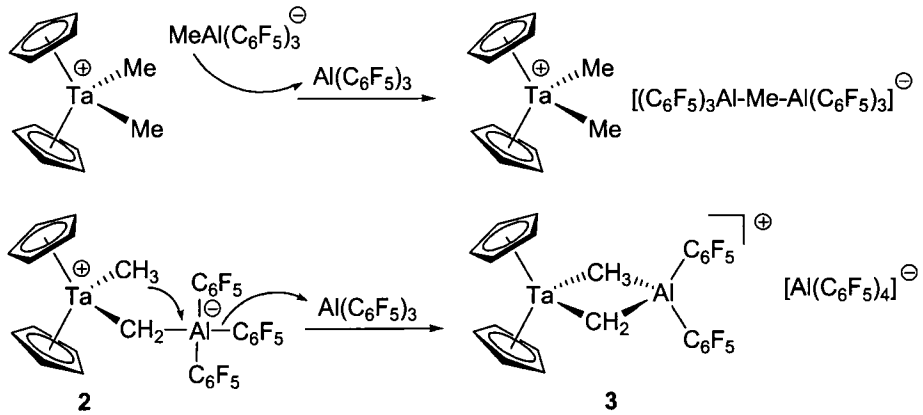

The solid state structure (Figure 4) determined by X-ray diffraction confirmed the molecular structure of **3** shown in Scheme 2. There are two CH_2Cl_2 (crystallization solvent) molecules in the crystal lattice, and the cation $[Cp_2Ta(CH_2)MeAl(C_6F_5)_2]^+$ and tetrakis anion $[Al(C_6F_5)_4]^-$ exist as unassociated ion pairs. The metric parameters based on the located and refined hydrogens attached to the bridging carbons show no evidence for any α-agostic interaction. The Ta–CH_2 distance is notably shorter than the Ta–CH_3 distance by ~0.16 Å [Ta–C(11) = 2.129(2) Å, Ta–C(12) = 2.290(2) Å]; this difference is more pronounced than that found in the zwitterionic tantalocene aluminate **2**, but the Ta–

CH_2 distance in **3** is still longer than that in the parent complex $Cp_2Ta(=CH_2)Me$[20] by ~0.1 Å. On going from **2** to **3** which is accompanied by the heterometalacycle formation, the Ta–CH_2 and Ta–CH_3 distances are shortened and lengthened by ~0.07 Å and 0.18 Å, respectively, while the Al–CH_2 distance is lengthened by ~0.1 Å. The Al–CH_3 distance in **3** [Al(1)–C(12) = 2.149(2) Å] compares well to some of the Al–CH_3 (bridging) distances found in $(C_6F_5)_3Al_2(CH_3)_3$.[17a] Overall, these structural data argue that the cation portion of **3** could be viewed as a hybrid of two extreme structures: $Cp_2Ta^+[CH_2Al(C_6F_5)_2]Me$ and $[Cp_2Ta(=CH_2)MeAl(C_6F_5)_2]^+$; the latter structure, formally an adduct of the neutral Lewis acid $MeAl(C_6F_5)_2$ with the tantalocene methylidene cation $[Cp_2Ta(=CH_2)]^+$ that is isoelectronic with neutral titanocenes methylidene complex $[Cp_2Ti(=CH_2)]$, is particularly interesting because it resembles the Tebbe's reagent $Cp_2Ti(CH_2)ClAlR_2$,[21] being considered an adduct of $[Cp_2Ti(=CH_2)]$ with $ClAlR_2$.

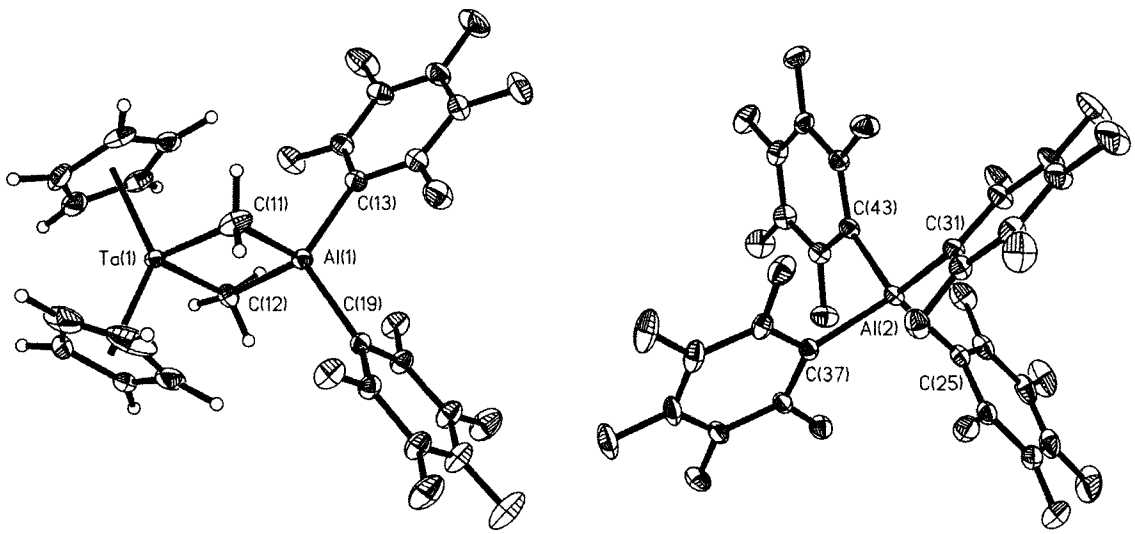

Figure 4. Molecular structure of complex **3**. Selected bond lengths (Å): Ta–C(11) = 2.129(2), Ta–C(12) = 2.290(2), Al(1)–C(11) = 2.111(2), Al(1)–C(12) = 2.149(2), Al(1)–C(13) = 1.981(2), Al(1)–C(19) = 1.979(2), Al(2)–C(25) = 2.021(2), Al(2)–C(31) = 2.008(2), Al(2)–C(37) = 2.025(2), Al(2)–C(43) = 2.011(2); selected bond angles (deg): C(11)–Ta–C(12) = 96.51(7), Ta–C(11)–Al(1) = 83.30 (7), Ta–C(12)–Al(1) = 78.72 (6), C(11)–Al(1)–C(12) = 101.47(9), C(11)–Al(1)–C(13) = 108.64(9), C(11)–Al(1)–C(19) = 116.22(8), C(12)–Al(1)–C(13) = 114.03(8), C(12)–Al(1)–C(19) = 103.46(8), C(13)–

Al(1)–C(19) = 112.58(8), C(25)–Al(2)–C(31) = 115.66(8), C(25)–Al(2)–C(37) = 99.60(7), C(25)–Al(2)–C(43) = 111.72(8), C(31)–Al(2)–C(37) = 112.67(8), C(31)–Al(2)–C(43) = 103.86(8), C(37)–Al(2)–C(43) = 113.77(8).

The scope of the reaction of the zwitterionic adducts $Cp_2Ta^+[CH_2E(C_6F_5)_3^-]Me$ with $E(C_6F_5)_3$ and $[Ph_3C][B(C_6F_5)_4]$ has also been investigated. As mentioned earlier, there is no further reaction between $Cp_2Ta^+[CH_2B(C_6F_5)_3^-]Me$ and $B(C_6F_5)_3$. Treatment of $Cp_2Ta^+[CH_2Al(C_6F_5)_3^-]Me$ (**2**) with $[Ph_3C][B(C_6F_5)_4]$ in CD_2Cl_2 resulted no reaction over 24 h, neither did mixing of **2** with $B(C_6F_5)_3$. Interestingly, when $Cp_2Ta^+[CH_2B(C_6F_5)_3^-]Me$ was treated with $Al(C_6F_5)_3$ in C_6D_5Br, the aluminate adduct **2** was gradually generated as a major product via apparent B/Al exchange within the $-CH_2B(C_6F_5)_3^-$ moiety (Scheme 1), with concomitant formation of $B(C_6F_5)_3$ and a minor amount of $[Al(C_6F_5)_4]^-$. Overall, the reaction type depicted in Scheme 2 seems to be specific to the aluminate/alane (Al^-/Al) pair, for example, the reaction of **2** with $Al(C_6F_5)_3$.

Polymerization of MMA and DMAA. Only the species derived from the alkylidene complex $Cp_2Ta(=CH_2)Me$ were examined for the polymerization of MMA and DMAA in this study, whereas the MMA polymerization by the species derived from the alkyl complex Cp_2TaMe_3 had been previously investigated.[5] First, control runs with either $Cp_2Ta(=CH_2)Me$ or $E(C_6F_5)_3$ (E = B, Al) alone under the polymerization conditions employed in this study (see Table 2) yielded no polymer products. Second, the following complexes or systems also exhibited no activity for polymerization of MMA: adduct **2** [either isolated or readily generated by in situ mixing of $Cp_2Ta(=CH_2)Me$ with 1 equiv of $Al(C_6F_5)_3$], complex **3** (with or without 1 equiv of $Al(C_6F_5)_3$], and the complex or mixture derived from the mixing of $Cp_2Ta(=CH_2)Me$ with 1 or 2 equiv of $B(C_6F_5)_3$

[which generates $Cp_2Ta^+[CH_2E(C_6F_5)_3^-]Me$ or this complex plus the unreacted borane]. Third, the system based on $Cp_2Ta(=CH_2)Me$ and 2 equiv of $Al(C_6F_5)_3$ is, however, uniquely active for MMA polymerization, the results of which are summarized in Table 2 and discussed below.

Table 2. MMA Polymerization Results by $Cp_2Ta(=CH_2)Me/2Al(C_6F_5)_3$ [a]

entry	temp (°C)	activation mode	reaction solvent	yield (%)	$10^4 M_n$ [b] (g/mol)	PDI [b] (M_w/M_n)	[rr] [c] (%)	[mr] [c] (%)	[mm] [c] (%)
1	25	monomer	toluene	93	68.5	1.43	72.9	25.4	1.7
2	25	monomer	DCB	13	8.95	1.50	72.8	25.6	1.6
3	25	complex	toluene	0					
4	25	complex	DCB	>99	41.5	1.65	72.0	26.2	1.8
5	0	complex	DCB	>99	49.7	1.67	74.9	22.8	2.3

[a]Conditions: solvent, 5.0 mL; reaction time, 30 min; $[M]_0//[Al]_0/[Ta]_0$ = 400/2/1; monomer activation mode: addition of the premixed M + Al (5 min) to a Ta solution; complex activation mode: addition of M to the premixed Ta + Al solution (10 min); DCB = 1,2-dichlorobenzene. [b]Number average molecular weight (M_n) and polydispersity index (PDI) determined by GPC relative to PMMA standards. [c]Methyl triad distribution determined by ^1H NMR spectroscopy in $CDCl_3$.

The polymerization by the $Cp_2Ta(=CH_2)Me/2Al(C_6F_5)_3$ system is highly sensitive to the reaction medium and addition sequence of the reagents involved. When the monomer activation mode (monomer is premixed with the alane followed by its addition to a Ta solution) is executed, the polymerization is highly active in toluene, producing high molecular weight (M_n = 6.85 × 10^5, M_w/M_n = 1.43) polymer of moderate syndiotacticity ([rr] = 72.9%) in 93% isolated yield within 30 min (run 1, Table 2). Interestingly, the polymer yield was significantly dropped to only 13% for the same reaction time period when the solvent was changed from toluene to DCB (run 2 vs. 1). In contrast, when the complex activation mode (complex is premixed with the alane followed by addition of monomer) is employed, the polymerization in toluene is inactive, while the polymerization in DCB is highly active, giving quantitative polymer yield (run 4 vs. 3). Lowering the temperature of the polymerization in DCB from ambient temperature to 0 °C apparently did not affect the activity but notably increased the

resulting polymer molecular weight and syndiotacticity (run 5 vs. 4). Polymerization of DMAA in DCB follows the same trend, with high activity (>99% yield in 30 min) for the complex activation mode and no activity for the monomer activation mode.

The observation that neither $Cp_2Ta(=CH_2)Me$ nor complexes **2** and **3** is active for MMA polymerization clearly points to a critical role of $Al(C_6F_5)_3$ that renders the high activity of the $Cp_2Ta(=CH_2)Me/2Al(C_6F_5)_3$ system. In the activated monomer polymerization, chain initiation presumably involves nucleophilic attack of the electron-rich methylidene moiety at the activated monomer $Al(C_6F_5)_3$•MMA to generate an active enolaluminate species[22] (**A**) that participates in the aluminate/alane bimolecular propagation steps as depicted in Scheme 3. Attempts to acquire MALDI-TOF MS spectra of low-molecular-weight polymer samples for chain-end group analysis were unsuccessful because the molecular weights were still too high even with low [monomer]/[initiator] ratios of 50 and 20, indicative of the currently ill-controlled polymerization system. On the other hand, NMR-monitoring of the reaction of $Cp_2Ta(=CH_2)Me$ and $2Al(C_6F_5)_3$ premixed with 10 equiv of MMA in C_7D_8 showed the rapid formation of PMMA by ^1H NMR and three C_6F_5-group-containing aluminum species by ^{19}F NMR, including the neutral $Al(C_6F_5)_3$•MMA (or •PMMA) adduct [δ –122.66 (o-F), –151.62 (p-F), –160.83 (m-F)] and two anionic aluminate species **A** [δ –122.04 (o-F), –153.66 (p-F), –161.84 (m-F)] and **B** [δ –119.98 (o-F), –154.40 (p-F), –162.20 (m-F)]. The ^{19}F NMR chemical shifts of **A** are consistent with an enolaluminate moiety, whereas those of **B** are consistent with its decomposition product $[(C_6F_5)_3Al–OMe–Al(C_6F_5)_3]^-$. The reaction of $Cp_2Ta(=CH_2)Me$ with 2 equiv of $Al(C_6F_5)_3$•MMA in C_7D_8 formed the same three alane and aluminate species by ^{19}F NMR, while the reaction

in CD_2Cl_2 gave the majority of species **B**. Thus, the instability of such enolaluminate active species, especially in polar chlorinated solvents, explains low initiator efficiency for the polymerization in toluene and low monomer conversion for the reaction in DCB. On the other hand, in the activated complex polymerization, the relevant species of interest are in situ generated **2** and excess (1 equiv) $Al(C_6F_5)_3$ as the reaction of $Cp_2Ta(=CH_2)Me$ with 2 equiv $Al(C_6F_5)_3$ in $\leq$10 min produced these two species, plus a trace amount of **3**, which is inactive (as is the **3**/$Al(C_6F_5)_3$ system, vide supra). NMR-monitoring of the reaction of $Cp_2Ta(=CH_2)Me/2Al(C_6F_5)_3$ [i.e., **2**/$Al(C_6F_5)_3$] with 1 or 10 MMA in C_6D_5Br indicated the formation of, in addition to **2**, the same aluminate species **A** and **B** as those observed in the reaction by the monomer activation sequence in C_7D_8, suggesting the same propagating species involved. However, the key difference is that in the activated complex polymerization the initiator $Cp_2Ta(=CH_2)$ is "stored or trapped" as transient adduct **2**, which can reactivate (reinitiate) the system in DCB when the enolaluminate active species is rapidly depleted by decomposition, thereby driving to a quantitative monomer conversion. Apparently, the initiation by the **2**/$Al(C_6F_5)_3$ system is incompetent in toluene, as this system is inactive in this solvent.

Scheme 3

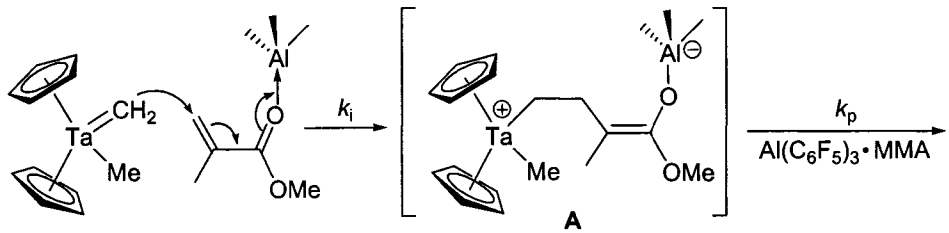

Conclusions

We have isolated and structurally characterized three cationic and zwitterionic tantalocene complexes, including $[Cp_2TaMe_2]^+[MeB(C_6F_5)_3]^-$ (**1**), $Cp_2Ta^+[CH_2Al(C_6F_5)_3^-]Me$ (**2**), and $[Cp_2Ta(CH_2)MeAl(C_6F_5)_2]^+[Al(C_6F_5)_4]^-$ (**3**), over the course of our reexamination of the reaction of Cp_2TaMe_3 with $E(C_6F_5)_3$ under various reaction conditions and investigation into the activation of the alkylidene complex $Cp_2Ta(=CH_2)Me$ with $Al(C_6F_5)_3$. The combination of $Cp_2Ta(=CH_2)Me$ with 2 equiv of $Al(C_6F_5)_3$ has been shown to be highly active for the polymerizations of MMA and DMAA, producing high molecular weight polymers via the proposed aluminate/alane bimolecular propagating process. The current investigation also corrected the previous erroneous attribution of the NMR signals derived from the liquid clathrate phase of ionic aggregates to the formation of the μ-Me diborate species and presented a cautionary note when analyzing NMR spectra of ion pairs as phase-separated mixtures in certain NMR solvents. Perhaps the most interesting finding of this work is that complex **3** is formed apparently by unusual nucleophilic attack of a C_6F_5 group, commonly regarded as chemically robust, resistant-to-electrophilic-attack, within the aluminate moiety in **2** at $Al(C_6F_5)_3$ present in excess to give the tetrakis aluminate anion $[Al(C_6F_5)_4]^-$, which somewhat resembles the formation of the μ-Me dialuminate anion $[(C_6F_5)_3Al–Me–Al(C_6F_5)_3]^-$ by nucleophilic attack of the Me group within the free $[MeAl(C_6F_5)_3]^-$ anion at $Al(C_6F_5)_3$. The investigation into the scope of this unique reaction shows that it is specific to the aluminate/alane (Al^-/Al) pair; such anion reactivity may also apply to olefin polymerization systems where aluminum-containing anions are ubiquitous and aluminum LAs are typically present in excess with respect to the cation and anion.

Acknowledgements. Funding for this work was provided by the National Science Foundation and Colorado State University. We thank Prof. Scott Collins of the University of Akron for sharing the results and insightful discussions with us, as well as Boulder Scientific Co. for the gift of $B(C_6F_5)_3$. W.R.M. and L.O.G. gratefully acknowledge an ARCS/Hach Graduate Fellowship and the NSF-REU program, respectively.

References

(1) For leading examples since 2000, see: (a) Rodriguez-Delgado, A.; Chen, E. Y.-X. *Macromolecules* **2005**, *38*, 2587–2594. (b) Kostakis, K.; Mourmouris, S.; Kotakis, K.; Nikogeorgos, N.; Pitsikalis, M.; Hadjichristidis, N. *J. Polym. Sci. Part A: Polym. Chem.* **2005**, *43*, 3305–3314. (c) Lian, B.; Lehmann, C. W.; Navarro, C.; Carpentier, J.-F. *Organometallics* **2005**, *24*, 2466–2472. (d) Bolig, A. D.; Chen, E. Y.-X. *J. Am. Chem. Soc.* **2004**, *126*, 4897–4906. (e) Stojcevic, G.; Kim, H.; Taylor, N. J.; Marder, T. B.; Collins, S. *Angew. Chem. Int. Ed.* **2004**, *43*, 5523–5526. (f) Strauch, J. W.; Fauré, J.-L.; Bredeau, S.; Wang, C.; Kehr, G.; Fröhlich, R.; Luftmann, H.; Erker, G. *J. Am. Chem. Soc.* **2004**, *126*, 2089–2104. (g) Chen, E. Y.-X. *J. Polym. Sci. Part A: Polym. Chem.* **2004**, *42*, 3395–3403. (h) Karanikolopoulos, G.; Batis, C.; Pitsikalis, M.; Hadjichristidis, N. *J. Polym. Sci. Part A: Polym. Chem.* **2004**, *42*, 3761–3774. (i) Ferenz, M.; Bandermann, F.; Sustmann, R.; Sicking, W. *Macromol. Chem. Phys.* **2004**, *205*, 1196–1205. (j) Rodriguez-Delgado, A.; Mariott, W. R.; Chen, E. Y.-X. *Macromolecules* **2004**, *37*, 3092–3100. (k) Jensen, T. R.; Yoon, S. C.; Dash, A. K.; Luo, L.; Marks, T. J. *J. Am. Chem. Soc.* **2003**, *125*, 14482–14494. (l) Chen, E. Y.-X.; Cooney, M. J. *J. Am. Chem. Soc.* **2003**, *125*, 7150–7151. (m) Mariott, W. R. Chen, E. Y.-X. *J. Am. Chem. Soc.* **2003**, *125*, 15726–15727. (n) Jin, J.; Mariott, W. R.; Chen, E. Y.-X. *J. Polym. Chem. Part A: Polym. Chem.* **2003**, *41*, 3132–3142. (o) Batis, C.; Karanikolopoulos, G.; Batis, C.; Pitsikalis, M.; Hadjichristidis, N. *Macromolecules* **2003**, *36*, 9763–9774. (p) Karanikolopoulos, G.; Batis, C.; Pitsikalis, M.;

Hadjichristidis, N. *Macromol. Chem. Phys.* **2003**, *204*, 831–840. (q) Bolig, A. D.; Chen, E. Y.-X. *J. Am. Chem. Soc.* **2002**, *124*, 5612–5613. (r) Jin, J.; Chen, E. Y.-X. *Organometallics* **2002**, *21*, 13–15 (s) Bandermann, F.; Ferenz, M.; Sustmann, R.; Sicking, W. *Macromol. Symp.* **2001**, *174*, 247–253. (t) Karanikolopoulos, G.; Batis, C.; Pitsikalis, M.; Hadjichristidis, N. *Macromolecules* **2001**, *34*, 4697–4705. (u) Bolig, A. D.; Chen, E. Y.-X. *J. Am. Chem. Soc.* **2001**, *123*, 7943–7944. (v) Frauenrath, H.; Keul, H.; Höcker, H. *Macromolecules* **2001**, *34*, 14–19. (w) Nguyen, H.; Jarvis, A. P.; Lesley, M. J. G.; Kelly, W. M.; Reddy, S. S.; Taylor, N. J.; Collins, S. *Macromolecules* **2000**, *33*, 1508–1510. (x) Bandermann, F.; Ferenz, M.; Sustmann, R.; Sicking, W. *Macromol. Symp.* **2000**, *161*, 127–134. (y) Cameron, P. A.; Gibson, V.; Graham, A. J. *Macromolecules* **2000**, *33*, 4329–4335. (z) Stuhldreier, T.; Keul, H.; Höcker, H. *Macromol. Rapid Commun.* **2000**, *21*, 1093–1098.

(2) (a) Mariott, W. R.; Rodriguez-Delgado, A.; Chen, E. Y.-X. *Macromolecules* **2006**, *39*, 1318–1327. (b) Kostakis, K.; Mourmouris, S.; Pitsikalis, M.; Hadjichristidis, N. *J. Polym. Sci. Part A: Polym. Chem.* **2005**, *43*, 3337–3348. (c) Li, Y.; Ward, D. G.; Reddy, S. S.; Collins, S. *Macromolecules* **1997**, *30*, 1875–1883. (d) Deng, H.; Soga, K. *Macromolecules* **1996**, *29*, 1847–1848.

(3) (a) Mariott, W. R.; Chen, E. Y.-X. *Macromolecules* **2005**, *38*, 6822–6832. (b) Mariott, W. R.; Chen, E. Y.-X. *Macromolecules* **2004**, *37*, 4741–4743.

(4) (a) Matsuo, Y.; Mashima, K.; Tani, K. *Angew. Chem., Int. Ed. Engl.* **2001**, *40*, 960–962. (b) Mashima, K. *Macromol. Symp.* **2000**, *159*, 69–76.

(5) (a) Mariott, W. R.; Hayden, L. M.; Chen, E. Y.-X. *ACS Symp. Ser.* **2003**, *857*, 101–111. (b) Feng, S.; Roof, G. R.; Chen, E. Y.-X. *Organometallics* **2002**, *21*, 832–839.

(6) Chen, E. Y.-X.; Abboud, K. A. *Organometallics* **2000**, *19*, 5541–5543.

(7) Al-Humydi, A.; Garrison, J. C.; Youngs, W. J.; Collins, S. *Organometallics* **2005**, *24*, 193–196.

(8) Williams, V. C.; Dai, C.; Li, Z.; Collins, S.; Piers, W.; Clegg, W.; Elsegood, M. R. J.; Marder, T. B. *Angew. Chem. Int. Ed.* **1999**, *38*, 3695–3698.

(9) While revising our manuscript the following paper appeared: Sánchez-Nieves, J.; Royo, P.; Mosquera, M. E. G. *Organometallics* **2006**, *25*, 2331–2336.

(10) Schrock, R. R.; Sharp, P. R. *J. Am. Chem. Soc.* **1978**, *100*, 2389–2399.

(11) (a) Cook, K. S.; Piers, W. E.; Patrick, B. O.; McDonald, R. *Can. J. Chem.* **2003**, *81*, 1137–1148. (b) Cook, K. S.; Piers, W. E.; Rettig, S. J.; McDonald, R. *Organometallics* **2000**, *19*, 2243–2245. (c) Cook, K. S.; Piers, W. E.; Rettig, S. J. *Organometallics* **1999**, *18*, 1575–1577.

(12) Allen, R. D.; Long, T. E.; McGrath, J. E. *Polym. Bull.* **1986**, *15*, 127–134.

(13) (a) Lee, C. H.; Lee, S. J.; Park, J. W.; Kim, K. H.; Lee, B. Y.; Oh, J. S. *J. Mol. Cat., A: Chem.* **1998**, *132*, 231–239. (b) Biagini, P.; Lugli, G.; Abis, L.; Andreussi, P. U.S. Pat. 5,602269, 1997.

(14) (a) Chien, J. C. W.; Tsai, W.-M.; Rausch, M. D. *J. Am. Chem. Soc.* **1991**, *113*, 8570–8571. (b) Ewen, J. A.; Elder, M. J. Eur. Pat. Appl. EP 0,426,637, 1991.

(15) (a) Bulai, A.; Jimeno, M. L.; de Queiroz, A.-A. A.; Gallardo, A.; Roman, J. S. *Macromolecules* **1996**, *29*, 3240–3246. (b) Ferguson, R. C.; Ovenall, D. W.

Macromolecules **1987**, *20*, 1245–1248. (c) Subramanian, R.; Allen, R. D.; McGrath, J. E.; Ward, T. C. *Polym. Prepr.* **1985**, *26*, 238–240.

(16) *SHELXTL*, Version 6.12; Bruker Analytical X-ray Solutions: Madison, WI, 2001.

(17) (a) Klosin, J.; Roof, G.; Chen, E. Y.-X.; Abboud, K. A. *Organometallics* **2000**, *19*, 4684–4686. (b) Horton, A. D.; de With, J.; van der Linder, A. J.; van de Weg, H. *Organometallics* **1996**, *15*, 2672–2674.

(18) Chakraborty, D.; Chen, E. Y.-X. *Inorg. Chem. Commun.* **2002**, *5*, 698–701.

(19) (a) Stahl, N. G.; Salata, M. R.; Marks, T. J. *J. Am. Chem. Soc.* **2005**, *127*, 10898–10909. (b) Liu, Z.; Somsook, E.; Landis, C. R. *J. Am. Chem. Soc.* **2001**, *123*, 2915–2916. (c) Chen, E. Y.-X.; Kruper, W. J.; Roof, G.; Wilson, D. R. *J. Am. Chem. Soc.* **2001**, *123*, 745–746.

(20) Guggenberger, L. J.; Schrock, R. R. *J. Am. Chem. Soc.* **1975**, *97*, 6578–6579.

(21) Tebbe, F. N.; Parshall, G. W.; Reddy, G. S. *J. Am. Chem. Soc.* **1978**, *100*, 3611–3613.

(22) Rodriguez-Delgado, A.; Chen, E. Y.-X. *J. Am. Chem. Soc.* **2005**, *127*, 961–974.

CHAPTER VI

SUMMARY

The work described within this dissertation has focused on the polymerization of functionalized alkenes catalyzed by early transition metallocenium complexes both within silicate nanogalleries and in solution. The development of intergallery-anchored metallocenium cations of varied ligand symmetries led to the first demonstration of exfoliated P(MMA)-silicate nanocomposites with stereocontrolled matrices, while the use of alane-intercalated silicate in combination with metallocene dimethyls of varied symmetries allowed for the production of intercalated P(MMA)-silicate nanocomposites. The dilute solution crystallization of *it*- and *st*- P(MMA)-silicate nanocomposites afforded predominantly exfoliated supramolecular stereocomplex P(MMA)-silicate nanocomposites with T_m >200 °C. Investigations into the solution polymerization of acrylamides, such as *N,N*-dimethylacrylamide (DMAA), catalyzed by C_2-ligated zirconocenium enolates provided strong evidence for a living and stereospecific process that proceeds via a monometallic, intramolecular coordinative-conjugate-addition mechanism. Conversely, the polymerization of *n*-butyl acrylate by the same catalyst systems proceeds in an uncontrolled fashion due to the presence of chain transfer and

termination reactions that take place on the polymerization time scale, preventing the formation of high molecular weight polymer. Expanding the scope of our studies to group 5 metallocenes, investigations into the activation of tantalocene(V) alkylidene complexes with strong organo Lewis acids have resulted in the isolation and structural characterization of three new cationic and zwitterionic tantalocene complexes as well as the elucidation of a highly active catalyst system for the polymerization of MMA and DMAA.

While this work has focused mainly on the mechanistic aspects of the polymerization of polar vinyl monomers by the highly active, electro-deficient early transition metallocene catalysts, the study has also yielded several novel and potentially useful polymeric materials, including exfoliated stereoregular P(MMA)-silicate nanocomposites, stereo-defect free and high T_m isotactic P(DMAA), as well as the amphiphilic stereodiblock copolymer P(MMA)-*b*-P(DMAA).

APPENDIX A

LIST OF REFEREED PUBLICATIONS BY W. R. M.

1. Mariott, W. R.; Gustafson, L. O.; Chen, E. Y.-X.* "Activation of Tantalocene(V) Alkyl and Alkylidene Complexes with Strong Organo-Lewis Acids and Application to Polymerization Catalysis," *Organometallics* **2006**, *25*, 3765–3773.

2. Rodriguez-Delgado, A.; Mariott, W. R.; Chen, E. Y.-X.* "Synthesis and MMA Polymerization of Chiral *ansa*-Zirconocene Ester Enolate Complexes with C_2- and C_s-Ligation," *J. Organomet. Chem.* **2006**, *691*, 3490–3497.

3. Mariott, W. R.; Rodriguez-Delgado, A.; Chen, E. Y.-X.* "Chain Termination and Transfer Reactions in the Acrylate Polymerization by a Monometallic Chiral Zirconocenium Catalyst System," *Macromolecules* **2006**, *39*, 1318–1327.

4. Mariott, W. R.; Chen, E. Y.-X.* "Mechanism and Scope of Stereospecific, Coordinative-Anionic Polymerization of Acrylamides by Chiral Zirconocenium Ester and Amide Enolates," *Macromolecules* **2005**, *38*, 6822–6832.

5. Mariott, W. R.; Chen, E. Y.-X.* "Stereospecific, Coordination Polymerization of Acrylamides by Chiral *ansa*-Metallocenium Alkyl and Ester Enolate Cations," *Macromolecules* **2004**, *37*, 4741–4743.

6. Rodriguez-Delgado, A.; Mariott, W. R.; Chen, E. Y.-X.* "Living and Syndioselective Polymerization of Methacrylates by Constrained Geometry Titanium Alkyl and Enolate Complexes," *Macromolecules* **2004**, *37*, 3092–3100.

7. Mariott, W. R.; Chen, E. Y.-X.* "Stereochemically Controlled PMMA-Exfoliated Silicate Nanocomposites Using Intergallery-Anchored Metallocenium Cations," *J. Am. Chem. Soc.* **2003**, *125*, 15726–15727.

8. Jin, J.; Mariott, W. R.; Chen, E. Y.-X.* "Polymerization of Methyl Methacrylate by Metallocene Imido Complexes and Tris(pentafluorophenyl)alane," *J. Polym. Sci. Part A: Polym. Chem.* **2003**, *41*, 3132–3142.

9. Mariott, W. R.; Hayden, L. M.; Chen, E. Y.-X.* "Olefin Copolymerization and Polymerization of Methyl Methacrylate Catalyzed by Tantalum(V)-Based Complexes," in *Beyond Metallocenes. Next-Generation Polymerization Catalysts*; Patil, A. O.; Hlatky, G. G. Eds.; *ACS Symp. Ser.* **2003**, *857*, 101–111.